

1976

Excitation temperature and electron number density distributions experienced by analyte species in an inductively coupled argon plasma

Dennis James Kalnicky
Iowa State University

Follow this and additional works at: <https://lib.dr.iastate.edu/rtd>

 Part of the [Physical Chemistry Commons](#)

Recommended Citation

Kalnicky, Dennis James, "Excitation temperature and electron number density distributions experienced by analyte species in an inductively coupled argon plasma " (1976). *Retrospective Theses and Dissertations*. 5752.
<https://lib.dr.iastate.edu/rtd/5752>

This Dissertation is brought to you for free and open access by the Iowa State University Capstones, Theses and Dissertations at Iowa State University Digital Repository. It has been accepted for inclusion in Retrospective Theses and Dissertations by an authorized administrator of Iowa State University Digital Repository. For more information, please contact digirep@iastate.edu.

INFORMATION TO USERS

This material was produced from a microfilm copy of the original document. While the most advanced technological means to photograph and reproduce this document have been used, the quality is heavily dependent upon the quality of the original submitted.

The following explanation of techniques is provided to help you understand markings or patterns which may appear on this reproduction.

1. The sign or "target" for pages apparently lacking from the document photographed is "Missing Page(s)". If it was possible to obtain the missing page(s) or section, they are spliced into the film along with adjacent pages. This may have necessitated cutting thru an image and duplicating adjacent pages to insure you complete continuity.
2. When an image on the film is obliterated with a large round black mark, it is an indication that the photographer suspected that the copy may have moved during exposure and thus cause a blurred image. You will find a good image of the page in the adjacent frame.
3. When a map, drawing or chart, etc., was part of the material being photographed the photographer followed a definite method in "sectioning" the material. It is customary to begin photoing at the upper left hand corner of a large sheet and to continue photoing from left to right in equal sections with a small overlap. If necessary, sectioning is continued again — beginning below the first row and continuing on until complete.
4. The majority of users indicate that the textual content is of greatest value, however, a somewhat higher quality reproduction could be made from "photographs" if essential to the understanding of the dissertation. Silver prints of "photographs" may be ordered at additional charge by writing the Order Department, giving the catalog number, title, author and specific pages you wish reproduced.
5. PLEASE NOTE: Some pages may have indistinct print. Filmed as received.

University Microfilms International

300 North Zeeb Road
Ann Arbor, Michigan 48106 USA
St. John's Road, Tyler's Green
High Wycombe, Bucks, England HP10 8HR

77-10,324

KALNICKY, Dennis James, 1949-
EXCITATION TEMPERATURE AND ELECTRON
NUMBER DENSITY DISTRIBUTIONS EXPERIENCED
BY ANALYTE SPECIES IN AN INDUCTIVELY
COUPLED ARGON PLASMA.

Iowa State University, Ph.D., 1976
Chemistry, physical

Xerox University Microfilms, Ann Arbor, Michigan 48106

Excitation temperature and electron number density
distributions experienced by analyte species
in an inductively coupled argon plasma

by

Dennis James Kalnicky

A Dissertation Submitted to the
Graduate Faculty in Partial Fulfillment of
The Requirements for the Degree of
DOCTOR OF PHILOSOPHY

Department: Chemistry
Major: Physical Chemistry

Approved:

Signature was redacted for privacy.

In Charge of Major Work

Signature was redacted for privacy.

For the Major ~~Department~~

Signature was redacted for privacy.

For the Graduate College

Iowa State University
Ames, Iowa

1976

TABLE OF CONTENTS

	Page
CHAPTER I: INTRODUCTION	1
CHAPTER II: DIAGNOSTIC TECHNIQUES	4
LTE in Analytical Inductively Coupled Plasmas	4
Temperature Calculations, Thermometric Species, and Transition Probabilities	6
Abel Inversion Calculations and Source Symmetry	14
Electron Number Density Measurements	20
Saha-Eggert's ionization equilibria methods	20
Stark broadening methods	23
H $_{\beta}$ line	24
Ar I lines	25
CHAPTER III: FACILITIES	28
Experimental Facilities	28
Computer Facilities	34
CHAPTER IV. EXPERIMENTAL PROCEDURES	37
Intensity Measurements, Lateral Profiling, and Abel Inversions	37
Temperature Calculations	38
Electron Number Density from Saha-Eggert's Ionization Calculations	39
Electron Number Density from Stark Broadening Calculations	39
H $_{\beta}$ line	39
Ar I lines	43

CHAPTER V: RESULTS AND DISCUSSION	47
Symmetry	47
Intensity Distributions of Analyte Lines	47
Intensity Distributions of Ar Lines	54
Temperature Profiles	56
Electron Number Density Profiles	65
Analyte Excitation	75
CHAPTER VI: SUGGESTIONS FOR FUTURE WORK	81
BIBLIOGRAPHY	84
ACKNOWLEDGEMENTS	94
APPENDIX A: ABEL INVERSION AND TEMPERATURE PROGRAM	95
APPENDIX B: ABEL INVERSION CALCULATIONS	146
General Considerations and the Abel Integral Equation	146
Numerical Methods	150
Data Approximation Methods	155
Method of integration for zones 2-5	159
Method of integration for zone 1	162
Error analysis	163
APPENDIX C: ATOMIC PARTITION FUNCTION AND SAHA-EGGERT'S ELECTRON DENSITY CALCULATIONS	166
Use of the Saha-Eggert's Electron Density Program	172
APPENDIX D: CONVOLUTION AND H_{β} ELECTRON DENSITY CALCULATIONS	178
H_{β} Electron Density Program	184

LIST OF TABLES

	Page
Table I. Fe I emission line data (four-line set)	13
Table II. Fe I emission line data (ten-line set)	15
Table III. Ar I emission line data	16
Table IV. Emission line data for Saha-Eggert's electron number density calculations	22
Table V. Experimental facilities and operating conditions	29
Table VI. Intensities, intensity ratios, and two- line temperatures for Fe I lines in peak and valley regions with 60 Hz modulation on the forward power	35
Table VII. Ion to neutral atom lateral intensity ratios for lines of Zn, Cd, Fe, Mg and Ca with and without added Na	51
Table VIII. Radial ion to atom number density ratios, $n_{X^+}(R)/n_{X^0}(R)$, for Zn, Cd, Fe and Ca with and without added Na at 1000W, 1.0 l/min, and 15 mm height	74
Table IX. Effective half-widths of H β and Ar I lines measured at the plasma axis for 1000W forward power and 1.0 l/min aerosol carrier gas flow	76
Table A-1. Data card requirements for C337TEM2	98
Table C-1. Data card requirements for C337EDNS	173
Table D-1. Data card requirements for C337CONV	186
Table D-2. Data card requirements for C337BROD	206

LIST OF FIGURES

	Page
Figure 1. Oscilloscope tracings showing emission intensity modulation with a 60 Hz ripple on the forward power to the plasma: (A) dark current, (B) Fe I 382.444 nm, (C) Fe I 381.584 nm	33
Figure 2. Reduced Stark profile half-widths, $\alpha'_{1/2}$, corrected for Doppler and instrument broadening plotted <u>vs.</u> $\log_{10} T$ for electron densities from 10^{12} to 10^{16} cm^{-3} for the H_β 486.13 nm line	42
Figure 3. Doppler and instrument profile corrected Stark half-widths for Ar I lines, $\Delta\lambda_{1/2}$ <u>vs.</u> $\log_{10} T$ for electron density from $10^{13.5}$ to 10^{16} cm^{-3}	45
Figure 4. Lateral profiles for Saha species at 15 mm, 1000W and 1.0 ℓ/min aerosol carrier gas flow	49
	with
	without
	Na
	6900 μg
	Na/ml
10 μg Zn/ml: Zn II 206.19 nm (—○—)	(—□—)
Zn I 213.88 nm (—X—)	(—+—)
150 μg Fe/ml: Fe II 258.588 nm (—○—)	(—□—)
Fe I 252.285 nm (—X—)	(—+—)
10 μg Ca/ml: Ca II 396.847 nm (—○—)	(—□—)
Ca I 422.673 nm (—X—)	(—+—)
Figure 5. Radial intensity distributions for the Fe I 382.043 nm line at 1000W for three observation heights and two aerosol carrier gas flows; 150 μg Fe/ml (—○—) and 150 μg Fe/ml + 6900 μg Na/ml (—△—).	53

	Page
Figure 6. Toroidal lateral and radial relative intensity distributions for the Ar I 425.936 nm line at 15 mm, 1000W and 1.0 l/min aerosol carrier gas flow	55
Figure 7. Radial excitation temperatures at 15 mm, 1000W and 1.0 l/min aerosol carrier gas flow. Ar I eight-line with Corliss and Shumaker (77) transition probability data (—●—); Fe I ten-line with Huber and Parkinson (67) data (—X—) and with Reif (30) and Banfield and Huber (66) data (—○—); Fe I three-line with Reif data (—△—) and with Banfield and Huber data (—□—)	58
Figure 8. Percent uncertainty in temperature as a function of percent uncertainty of intensity for typical Fe I and Ar I lines employed in temperature calculations	61
Figure 9. Radial Fe I excitation temperatures at 1000W for three observation heights and two aerosol carrier gas flows; 150 µg Fe/ml (—○—), 150 µg Fe/ml + 6900 µg Na/ml (—●—)	63
Figure 10. Radial electron density distributions at 1000W, 15 mm and 1.0 l/min aerosol carrier gas flow for H _β Stark broadening (—X—) and Saha calculations; 10 µg Ca/ml (—○—), 150 µg Fe/ml (—□—), 10 µg Mg/ml (—△—), 10 µg Cd/ml (—+—), 10 µg Zn/ml (—●—)	67
Figure 11. Radial Saha-Eggert's electron density distributions at 15, 20, and 25 mm for Mg atom/ion line combinations; 10 µg Mg/ml (—○—, —□—, —△—), 10 µg Mg/ml + 6900 µg Na/ml (—●—, —■—, —▲—)	70

- Figure 12. Radial number density ratios, $n_{\text{Mg}}/n_{\text{MgO}}$, at 1000W and 1.0 l/min aerosol carrier gas flow for Mg lines employed in electron density calculations; 10 $\mu\text{g Mg/ml}$ at 15 mm (—○—), 20 mm (—□—), and 25 mm (—△—); 10 $\mu\text{g Mg/ml}$ + 6900 $\mu\text{g Na/ml}$ at 15 mm (—●—), 20 mm (—X—), and 25 mm (—▲—) 72b
- Figure 13. Effective electron density at 1000W and 1.0 l/min aerosol carrier gas flow for several observation heights. Stark broadening with deionized water nebulized; $\text{H}\beta$ 486.13 nm (—○—), Ar I 542.14 nm (—□—), Ar I 549.59 nm (—△—). Stark broadening with 6900 $\mu\text{g Na/ml}$ nebulized; $\text{H}\beta$ 486.13 nm (—●—), Ar I 542.14 nm (—*—), Ar I 549.59 nm (—+—). Saha-Eggert's ionization; 10 $\mu\text{g Mg/ml}$ (—◇—), 10 $\mu\text{g Mg/ml}$ + 6900 $\mu\text{g Na/ml}$ (—◆—) 77b
- Figure B-1. Spatial relationship between the measured lateral intensity, $I(X)$, at displacement X ; and, the radial intensity, $J(R)$, at radius R from the center of a circularly symmetric source employing side-on observation. R_B is the boundary radius at which no lateral intensity is detected 148
- Figure B-2. Two-dimensional representation of a circularly symmetric source divided into N zones of equal width, a 152
- Figure B-3. Schematic representation of five zone subdivision of the $I(X)$ profile (bell-type curve case) 158

CHAPTER I: INTRODUCTION

Inductively coupled, argon-supported plasmas (ICP's) possess properties that make them useful atomization-ionization-excitation sources for analytical atomic emission spectroscopy (1). Among the several fundamental ICP properties that have not been adequately characterized are the excitation temperature distributions and the electron number densities (hereafter denoted by n_e) that are experienced by the analyte species and the argon support gas. Most measurements reported to date have primarily characterized the temperature and n_e environment of the support gas in plasmas that have not been extensively used for analytical purposes (2-14). Recently, several experimental studies of the excitation temperature and n_e distributions experienced by analyte species have been reported (15-20) and theoretical treatments of these and other relevant ICP properties have been discussed (21-23). Despite these efforts significant discrepancies and inconsistencies still exist among the reported results. The following typical examples may be cited. First, effective (spatially integrated) temperatures and number densities were reported by Boumans and de Boer (19) who concluded that their data could not be used for explaining interelement effects because it was useless to "speculate on what precisely happens without detailed knowledge of the complex changes in the spatial structure of

the ICP." Second, some preliminary radial (spatially resolved) temperatures reported by Kornblum and de Galan (16) exhibited large scatter and peculiarly steep off-axis peak behavior. Third, the n_e values determined by Jaroz et al. (2b) and Mermet (17a) from Stark broadening measurements were two orders of magnitude greater than those obtained from Saha ionization equilibrium calculations based on Mg atom/ion emission line intensity ratios. Fourth, Kalnicky et al. (18) recently reported spatially resolved, radial excitation temperatures experienced by the Fe I thermometric species that were essentially in agreement with the values reported by Mermet and Robin (2a) and Alder and Mermet (15) and with the Doppler temperatures reported by Human and Scott (20) but disagreed significantly with excitation temperatures reported by Kornblum and de Galan (16), who cautioned that "only the overall shapes of the distributions and the order of magnitude of the quantities" could be concluded from their data. Fifth, recognized differences still exist between computer simulation and experimental studies of ICP's used for spectrochemical analysis (21,22). Finally, even the temperature measurements themselves are rendered inconsistent by the lack of accuracy and agreement in published transition probability data (15,17,18).

The large discrepancies between the n_e values calculated by line broadening methods and those obtained from Saha

ionization calculations, which were reported by Jaroz et al. (2b) and Mermet (17a) led these investigators to question the validity of the local thermodynamic equilibrium (LTE) assumption for the operating conditions of their plasma. Clearly, more investigations on temperature and n_e distributions are required to interpret discrepancies in reported values and to lead to a more definitive understanding of the atomization, ionization, and excitation processes occurring in analytically useful ICP's. The purpose of this investigation is, therefore, to examine the spatially resolved, radial excitation temperatures and radial n_e distributions experienced by the analyte species. These examinations include observations at several sites in the plasma and, with and without the presence of an easily ionized element (EIE).

CHAPTER II. DIAGNOSTIC TECHNIQUES

LTE in Analytical Inductively Coupled Plasmas

In a rigorous sense, temperature is a physically meaningful concept only when a system is in complete thermodynamic equilibrium (TE). In such a system a unique value of temperature describes: (1) a Maxwellian velocity distribution for all particles; (2) excitation according to Boltzmann's distribution law; (3) ionization according to the Saha-Eggert relationship; (4) dissociation-recombination according to the Guldberg-Waage mass action law; and (5) the distribution of the electromagnetic radiation according to Planck's law (24-31). However, the strong temperature and density gradients which exist in almost all laboratory plasmas prevent the establishment of TE and it follows that the radiation collected from these plasmas strongly deviates from the Planck function distribution (29). Despite these deviations from TE, conditions may exist for which the useful concept of local thermodynamic equilibrium can be employed in these plasmas. The latter applies when radiation equilibrium is not established but all other TE relationships remain valid and are governed by the "local temperature" even though different temperatures are allowed at different points in the plasma. The LTE state is reached when the local rate of equipartition of energy over the different degrees of freedom

is much faster than the net rate of transport of heat, mass, and radiation through the plasma.

When the various degrees of freedom are not equilibrated it is useful to designate "temperatures" which are named after the special process to which they apply, e.g., translation temperature, excitation temperature, etc. The better the agreement between these temperatures, the closer the approach to equilibrium, and the more physically meaningful the temperature concept. The conditions necessary to assure the validity of the LTE assumption for common laboratory plasmas have been discussed in detail elsewhere (29,31) and will not be reiterated here. Likewise, many excellent theoretical treatments related to plasma diagnostics are available (3,11,24,29,32-48). Therefore, the following discussions will be limited to those techniques relevant to temperature and n_e measurements.

Spectroscopic methods of temperature measurement are generally considered superior to probe techniques because the former do not disturb the microscopic system and, in fact, may be the only feasible approach for high temperature sources or for those sources which are inaccessible to probes (3b,47,48).

The LTE state is generally assumed to exist in the central portions of argon-supported, inductively coupled plasmas sustained at atmospheric pressure (18). If this

assumption is accepted, spectroscopic techniques may be combined with the Boltzmann energy distribution and the Saha-Eggert ionization equilibrium relationships to yield temperature and n_e distributions. The limitations and physical significance of the temperature values so obtained have been adequately reviewed (30,36,40). In particular, caution must be exercised in interpreting the physical significance of the temperatures and n_e values determined unless appropriate mathematical treatments, such as Abel inversion techniques (49-58), are used to transform the experimentally measured lateral (average) distributions of spectral line radiances to their corresponding spatially resolved radial (local) distributions. The requirements of the Abel inversion techniques employed in this investigation are discussed in a later section of this Chapter.

The observations of Jaroz et al. (2b) and Mermet (17) and the results of this investigation suggest that the LTE assumption may be invalid for some operating conditions employed in the spectrochemical applications of these plasmas. Indeed, the assumption of LTE has been questioned for other plasmas as well (45,59-63).

Temperature Calculations, Thermometric Species, and Transition Probabilities

The relative lateral intensity of an emission line radiating from a source in LTE with negligible self-absorption

and homogeneous analyte distribution is given by (29,30,40)

$$I_{qp}(X) = \frac{d}{4\pi} A_{qp} h \nu_{qp} n_q(X) \quad (1)$$

where, d = optical depth of the plasma within the viewing field of the spectrometer,

A_{qp} = relative transition probability of spontaneous emission for the transition $q \longrightarrow p$,

h = Planck's constant,

ν_{qp} = frequency of the emission transition,

$n_q(X)$ = number density of the emitting level at lateral displacement X .

This equation describes the space-integrated (averaged) emission over the depth of the plasma and, accordingly, represents the power radiated per unit solid angle per unit area, which is collected within the viewing field of the spectrometer (29,40). Equation 1 may be combined with the Boltzmann expression for n_q to yield

$$I_{qp}(X) = \frac{d}{4\pi} A_{qp} h \nu_{qp} \frac{g_q}{g_o} n_o(X) \exp \left\{ -\frac{E_q}{k T(X)} \right\} \quad (2)$$

where, g_q, g_o = statistical weights of the emitting and ground level, respectively,

$n_o(X)$ = number density of the ground level at lateral displacement X ,

E_q = energy of the emitting level,

k = Boltzmann's constant,
 $T(X)$ = temperature at lateral displacement X .

The desired relative radial (local) intensities (J_{qp}) are obtained from Abel inversion of the measured lateral (averaged) intensity profiles and represent spatially resolved, per-unit-volume quantities.

With consideration of radial quantities and by rearrangement of Equation 2, the radial "slope" temperature is given by (29,33,36,40)

$$\ln \left(\frac{g_q A_{qp} v_{qp}}{J_{qp}(R)} \right) = \frac{E_q}{kT(R)} + \ln \left(\frac{4\pi g_o}{h n_o(R)} \right) \quad (3)$$

where R denotes the radial position in the plasma. For emission lines originating from the same ionization stage a plot of $\ln \frac{g_q A_{qp} v_{qp}}{J_{qp}}$ vs. E_q should yield a straight line with slope equal to $1/kT(R)$ where, $T(R)$ is the "slope" temperature at radius R . Equation (3) may be solved simultaneously for two spectral emission lines ($q \rightarrow p$ and $t \rightarrow s$) to yield the radial "two-line" temperature defined by the following expression:

$$T(R) = 0.6247(E_q - E_t) / \left[\log_{10} \left(\frac{g_q A_{qp} v_{qp} J_{ts}(R)}{g_t A_{ts} v_{ts} J_{qp}(R)} \right) \right] \quad (4)$$

when E_q and E_t are expressed in reciprocal centimeters (cm^{-1}).

Certain conditions must be satisfied before Equations 3 and 4 may be used for temperature determinations, namely, relative radial emission intensities must be directly proportional to integrated line radiances and they must not be affected by self-absorption (30). The importance of employing quantities strictly proportional to integrated line radiances for calculations based on spectroscopic measurements where slit effects are important has been extensively treated for molecular (64) as well as atomic lines (24,30,65), therefore, only a brief summary will be presented here.

When emission from a spectral transition is monitored by a spectrometer, the true profile is distorted by the instrument with the distortion being proportional to the reciprocal of the resolving power of the monochromator. These distortions are of electrical and optical origin and it is convenient to treat them separately. Accurate intensities can be obtained only if instrumental distortions are properly accounted in the measurement. When a spectrometer is set at a single value, a discrete wavelength is not transmitted but, rather, a range of wavelengths are collected each of which contributes to the recorded line profile. This wavelength interval is referred to as the bandpass of the instrument. The weight of each contribution can be expressed as a function of displacement from the line center and determines a curve called the slit function. Accurate intensity measurements are made only when the bandpass of the instrument is

negligible in comparison to the halfwidth of the line intensity profile. The exit slit distribution is predominantly determined by diffraction effects for slits narrow in comparison to the wavelength of the impinging radiation. When the slits are sufficiently wide, the contributions to the geometrical image from diffraction and optical distortions are rendered negligible. Thus, if the width of the exit slit is much wider than the entrance slit, the geometrical image of the latter falls entirely within the band pass of the spectrometer and the measured intensity is proportional to integrated line radiance (30). A trapezoidal line shape should be obtained. Aberration and diffraction effects tend to round off the top and base of the profile.

The lateral emission intensities obtained here were measured with the entrance and exit slits of the monochromator set at the same width (15 μm). Time integrated intensities were obtained at the maximum of the respective emission line profiles when the monochromator was "peaked" on a line. Under these conditions, the measurements did not represent the integrated area (radiance) under the line profiles. However, the peak intensities for Fe I thermometric lines were proportional to integrated radiances when the latter were obtained with the exit slit much wider than the entrance slit (30). Consequently, peak intensities were employed in this study because: (1) these intensities were

proportional to integrated line radiances, (2) the resolution of the monochromator deteriorated rapidly as the exit slit was opened wider than the entrance slit, and (3) more elaborate measurement procedures were required to obtain the integrated radiances.

Neutral iron was selected as the thermometric species because its emission lines possess desirable characteristics for spectroscopic temperature determinations (30,40). Among the factors considered in the line selection process were: (a) maximal spread in excitation potentials to minimize relative error in calculated temperatures, (b) freedom of spectral interference from plasma components, (c) availability of accurate transition probabilities, and (d) wavelength proximity precluding the necessity of calibrating the detector response with respect to wavelength. So that the measurements and Abel inversion operations would not be too unwieldy, the number of lines initially employed was restricted to four.

A number of Fe I transition probability tabulations were examined for these lines (30,66-73a); of the most recent compilations, only the Reif (30), and the Banfield and Huber (66) collections provided transition probability data on all of the four lines, and Huber and Parkinson (67) on only two of the lines. These lines, their wavelengths, excitation energies and the statistical weights of the emitting levels (74), and relevant transition probability

data are summarized in Table I.¹ The relative transition probabilities for the useful sets of data were normalized to the Fe I 371.994 nm line because the lifetime of this transition is well known (66,67). It is evident that there is good agreement among the Fe 382.043, 382.444, and 382.588 nm lines for the Reif and Banfield and Huber data. Thus, a priori, good agreement in the temperature profiles should be obtained for calculations based on these lines, but a lack of consistency should be evident if the Fe 381.584 nm line were included. Indeed, temperatures obtained with various combinations of transition probabilities involving the Fe I 381.584 nm line showed this lack of consistency particularly for those calculated from two-line combinations (18). Because virtually identical temperature profiles resulted from three-line slope temperature calculations (18) for transition probability data from references 30 and 66, the three-line set excluding the Fe I 381.584 nm line was considered acceptable for inclusion in studies for this dissertation research.

¹After this dissertation research was completed an additional transition probability tabulation (73b) was found which provided data on three of the four lines in Table I. Consideration of these values revealed good agreement with the Fe I 382.043 nm and 382.588 nm line data but not for the 381.584 nm line. Inclusion of these data would neither change the conclusions drawn about these lines nor affect the temperature results obtained with the lines employed from this table.

Table I. Fe I emission line data (four-line set)

$\lambda(\text{nm})^a$	$E_q(\text{cm}^{-1})^b$	g_q^c	Relative Transition Probabilities ^d		
			R	BH	HP
381.584	38175	7	0.948	1.540	1.530
382.043	33096	9	0.638	0.656	0.882
382.444	26140	7	0.0283	0.0292	---
382.588	33507	7	0.567	0.610	---

^a λ = wavelength of the transition $q \rightarrow p$, and for subsequent tables.

^b E_q = excitation energy of the emitting level, and for subsequent tables.

^c g_q = statistical weight of the emitting level, and for subsequent tables.

^dRelative transition probabilities normalized to the Fe I 371.994 nm line by $A_{371.994} = 0.163$: R = Reif (30); BH = Banfield and Huber (66); HP = Huber and Parkinson (67).

An additional Fe I ten-line set was selected for temperature measurements; the relevant data for these lines are summarized in Table II.¹ In selecting these lines, the criteria discussed previously as well as consistency among the transition probability data were emphasized. An Ar I eight-line set was also selected for determination of the excitation temperature environment experienced by the support gas. The relevant data for these lines are given in Table III (74-80).

The operation of the temperature and Abel inversion computer program for slope temperature calculations employed in this dissertation research is discussed in Appendix A. A listing of the source statements of this program is also included in this appendix.

Abel Inversion Calculations and Source Symmetry

Excellent discussions of the basic principles of the Abel inversion calculation and the various methods of solution are found in references 49 and 50. Preliminary

¹The Bridges and Kornblith tabulation (73b) also provided transition probability data on these lines which were in excellent agreement with the values listed in Table II. As before, inclusion of these data would neither significantly change the conclusions drawn about these lines nor the temperatures obtained with them.

Table II. Fe I emission line data (ten-line set)

$\lambda(\text{nm})$	$E_q(\text{cm}^{-1})$	g_q	Relative Transition Probabilities		
			R	BH	HP
367.992	27167	9	0.0138	0.0151	0.0169
370.557	27395	7	0.0328	0.0341	0.0372
371.994	26875	11	0.163	0.163	0.163
372.256	27560	5	0.0505	0.0531	0.0580
373.487	33695	11	0.886	0.776	0.867
373.713	27167	9	0.143	0.140	0.143
374.826	27560	5	0.0904	0.0870	0.0994
374.949	34040	9	0.744	0.681	0.798
375.824	34329	7	0.611	0.611	0.674
376.379	34547	5	0.523	0.610	0.622

Table III. Ar I emission line data

λ (nm)	E_q (cm^{-1})	g_q	$A_{qp} \times 10^{-7}$ (sec^{-1}) ^a					
			AP	MC	CS	BTW	G	BW
425.118	116,660	3	0.0085	0.0089	0.0132	0.0075	0.0079	0.0076
425.936	118,871	1	0.360	0.3665	0.450	0.3643	0.360	0.320
426.629	117,184	5	0.028	0.0265	0.036	0.0294	0.028	0.023
427.217	117,151	3	0.071	0.0688	0.090	0.0769	0.071	0.063
430.010	116,999	5	0.034	0.0318	0.042	0.0366	0.034	0.031
433.356	118,469	5	0.049	0.0506	0.074	0.0551	0.049	0.048
433.535	118,459	3	0.0333	0.0308	0.044	0.0385	0.040	0.029
434.545	118,408	3	0.028	0.0273	0.041	0.0278	0.028	0.022

^aAbsolute transition probabilities: AP = Adcock and Plumtree (75); MC = Malone and Corcoran (76); CS = Corliss and Shumaker (77); BTW = B. T. Wujec (78); G = Gericke (79); BW = B. Wende (80).

calculations indicated that the Cremers and Birkebak data approximation method (50) was superior to the numerical method of Nestor and Olsen (49). The Cremers and Birkebak method provided: (a) better agreement of calculated radial coefficients with known values ($\sim 1-2\%$) when integrable test functions were employed (53) and, (b) less scatter in calculated radial intensities when real data were employed. The computational procedures and error analyses for these methods are discussed in Appendix B. An F-test for best fit (81) from the linear to the maximum allowed 4-th degree fit and polynomials of the type of Equations B20 and B36 in Appendix B were applied to smoothed lateral intensity profiles when the Cremers and Birkebak method was employed. Second degree polynomials with ~ 20 points per profile were generally found to provide adequate fits for bell-type lateral profiles but higher degree fits were required for toroidal distributions.

The optical system employed and the emission symmetry of the radiating source must meet several requirements if lateral emission profiles are to be reliably transformed by Abel inversion techniques. Figure B-1 (Appendix B) illustrates the spatial relationship between the measured lateral intensity, $I(X)$, at displacement X ; and, the radial intensity, $J(R)$, at radius R from the center of a circularly symmetric source when normal side-on observation is employed. Examination of

this diagram reveals that the following conditions are necessary prerequisites for reliable radial intensity calculations:

- 1) The depth-of-field (DOF) of the optical transfer system (OTS) must extend beyond the source boundaries.
- 2) The analyte emission intensity distribution must be circularly symmetric about the plasma axis.

In addition to these requirements, the plasma source must be optically thin, i.e., there must be negligible self-absorption of the emission lines of interest.

For the ideal case the OTS would have infinite DOF so that all emission points within the source volume along the optical axis would be transferred with exactly the same efficiency. However, the DOF of any real OTS is not infinite so that defocussing along the optical axis is an important consideration (82) when relative intensity measurements are made. For radial intensity calculations a DOF extending beyond the plasma boundaries is sufficient. This is accomplished with a low aperture optical system ($f/40$ to $f/50$) in which the lens and monochromator entrance slit are stopped to a diameter so that the plasma volume observed is essentially cylindrical. When the latter condition prevails the observed solid angle is chosen so that any two lines $Y_1 = X$ and $Y_2 = X + \Delta X$ (Figure B-1) defining the lateral

sampling zone for an $I(X)$ value can be considered parallel. For the wavelength range employed in the present investigation, the focal length of the lens was about 150 mm so that a 3 mm diaphragm produced an approximate $f/50$ system. Hence, at a plasma radius of 10 mm, the $f/50$ system sampled radiation over a cross section of 0.2 mm diameter. With the above conditions the DOF extended beyond the plasma boundaries and, defocussing problems were minimized. The large aperture optical systems normally employed in analytical investigations cannot be used if precise lateral intensities are to be measured. The enlarged acceptance cone of such systems introduces defocussing problems into lateral intensity measurements, leading to distorted lateral intensity profiles, and, subsequently, erroneous radial intensity and temperature distributions.

The second condition necessary for reliable radial intensity determination was verified when profiles across the entire emission zone showed circular symmetry about the plasma axis. Experimental verification of this symmetry criterion is presented later in the RESULTS section (Chapter V) of this thesis. The requirement of negligible self-absorption was verified for the analyte thermometric lines of interest when plots of $\log I(X)$ vs. $\log C$ showed linearity over several orders of magnitude 'n concentration.

Electron Number Density Measurements

Saha-Eggert's ionization equilibria methods

The theory and application of n_e determinations from Saha-Eggert ionization equilibrium calculations has been discussed elsewhere (29,36,40,83). This method requires the measurement of relative emission line intensities from successive ionization stages, generally for the neutral atom and singly ionized species. When these intensities are combined with the known equilibrium relationships between spectral emission and temperature and with the Saha-Eggert's expression, the n_e may be calculated. The n_e values so obtained are dependent upon the assumption that the plasma is in the LTE state, which may not be the case.

Five elements with neutral atom ionization potentials ranging from 6.11 eV (Ca I) to 9.39 eV (Zn I) were selected for atom/ion emission line intensity measurements. The factors considered in the selection process were: (a) availability of sufficiently intense atom/ion line pairs; (b) availability of transition probability data for the atom and ion lines; (c) closely matched excitation energies for the atom and ion lines so that the exponential temperature effect would be minimized; (d) freedom from spectral interferences; and (e) wavelength proximity precluding the necessity of calibrating the detector response with respect to wavelength. The line wavelengths, their excitation

energies, statistical weights of emitting levels (74,84) and transition probability data (66,85-92) for the species selected are given in Table IV. The last column of this table gives the averages and \pm limits of the $gA\lambda$ ratios listed. The relative \pm limits range from about $\pm 2\%$ for Ca to $\pm 12\%$ for Cd.

For the emission lines of the neutral atom and first ionized species the radial n_e is given by (29,36,40)

$$n_e(R) = 4.83 \times 10^{15} \frac{J^{\circ}(R)}{J^{+}(R)} \cdot \frac{g^{+}A^{+}\lambda^{\circ}}{g^{\circ}A^{\circ}\lambda^{+}} T(R)^{3/2} \quad (5)$$

$$\times \exp \left\{ \frac{E^{+} - E^{\circ} - E_1^{\circ} + \Delta E_1^{\circ}}{k T(R)} \right\}$$

where, $(^{\circ}), (^{+})$ denote the neutral atom and singly ionized species, respectively,

λ = wavelength of the emission transition,

E_1° = ionization energy of the neutral atom species,

ΔE_1° = lowering of the ionization energy.

A ΔE_1° correction was applied to the ionization energy to account for the interaction of free atom states with the electric microfield, which is produced by the charged plasma particles (31,36). A number of methods for calculating ΔE_1° have been reported (31,36,59). When the Unsöld formula (31) was applied, a value of $\Delta E_1^{\circ} = 403 \text{ cm}^{-1}$ (0.05 eV) was found

Table IV. Emission line data for Saha-Eggert's electron number density calculations

Species	λ (nm)	E_q (cm^{-1})	g_q	$\frac{g^{\circ} A^{\circ} \lambda^+}{g^+ A^+ \lambda^{\circ}}$	Ratios ^a	Average Ratio
Ca I	422.673	23652	3			
Ca II	396.847	25192	2		2.1738(SL), 2.0488(SG), 2.1029(NBS) ^b	2.0911 ± 0.0379
Mg I	285.213	35087	3			
Mg II	279.553	35732	4		1.4317(SL), 1.504(ADJS), 1.333(SG), 1.3578(NBS)	1.4066 ± 0.0773
Mg II	280.270	35652	2		2.8708(SL), 3.0161(ADJS), 2.6649(SG), 2.743(NBS)	2.8273 ± 0.154
Fe I	252.285	39626	9			
Fe II	258.588	38660	8		3.4050(AS 1), 2.8658(BH/H)	3.1354 ± 0.270
Cd I	228.802	43692	3			
Cd II	226.502	44136	2		2.6575(AS 2), 3.3949(BS)	3.0262 ± 0.369
Zn I	213.86	46745	3			
Zn II	206.19	48481	2		3.0290(AS 2), 2.5203(BS)	2.7747 ± 0.254

^aNumerals I,II and superscripts (^o),(⁺) denote neutral atom and first ion species, respectively.

^bTransition probability sources: ADJS = Andersen, *et al.* (85); AS 1 = Assousa and Smith (86); AS 2 = Andersen and Sorensen (87); BH/H = Banfield and Huber (66) and Huber (88); BS = Bauman and Smith (89); NBS = National Bureau of Standards (90); SG = Smith and Gallagher (91); SL = Smith and Liszt (92).

to be compatible with the temperatures and densities considered in this study.

The ratio of the ion number density to that of the neutral atoms is given by (40)

$$\frac{n_{X^+}(R)}{n_{X^0}(R)} = \frac{J^+(R)}{J^0(R)} \cdot \frac{g_{A^0\lambda^+}^0}{g_{A^+\lambda^0}^+} \cdot \frac{Z^+[T(R)]}{Z^0[T(R)]} \cdot \exp \left\{ \frac{E^+ - E^0}{kT(R)} \right\} \quad (6)$$

where, $Z[T(R)]$ is the partition function for the radial temperature $T(R)$. Partition functions for neutral atom and singly ionized species were calculated from the method suggested by Griem (36), which included a correction for the lowering of the ionization energy. The details of the partition function calculations and the Saha n_e computer program employed in this investigation are discussed in Appendix C.

Stark broadening methods

The theory and application of Stark broadening methods for the determination of n_e in plasmas has been discussed extensively (36,93-98). Atomic hydrogen lines are most frequently employed for these calculations because of the availability of extensive tabulations of Stark broadening parameters for the complete line profiles (36,96,98) and because the theory is somewhat simpler to apply and more accurate than that for multielectron atomic species. Griem (36,96) has also tabulated Stark broadening parameters for

the emission lines of a number of other neutral atom and singly ionized species.

H_β line The H_β line (486.13 nm) was selected for n_e calculations because: (a) it is free from spectral interference by plasma components; (b) the range of half-widths anticipated (~1.0 to 5.0 Å) and the relative intensities observed were of sufficient magnitude to allow accurate measurement at various observation heights in the plasma; (c) extensive Stark data were available for the complete line profile (96,98) encompassing a broad range of n_e values and temperatures; and (d) greater accuracy is generally associated with Stark calculations for the H_β line than for other atomic hydrogen lines. The theory developed by Griem (36), Kepple and Griem (95) and Griem (96) and the tabulated Stark parameters from Videl et al. (98) were employed in these calculations.

The Stark width for the H_β line is related to n_e by (94-96,98)

$$n_e(R) = \left\{ \frac{\Delta\lambda_{\frac{1}{2}}^S(R)}{2\alpha_{\frac{1}{2}}(2.61 e)} \right\}^{3/2} \quad (7)$$

where $\Delta\lambda_{\frac{1}{2}}^S(R)$ = Stark half-width at radius R,

$\alpha_{\frac{1}{2}}$ = reduced Stark profile half-width parameter,

e = electrostatic unit of charge.

Equation 7 cannot be used directly unless experimental line

profiles have been deconvoluted to account for Doppler and instrument broadening. This correction, on a half-width basis, is not a straightforward procedure. A simpler alternative is to use pure Stark reduced profiles, $S(\alpha)$, at various n_e and temperature combinations (98) as base values and then apply convolution calculations to account for other broadening contributions. These calculations were accomplished as follows: (a) Doppler profiles were convoluted with the $S(\alpha)$ profiles (98) to yield Doppler corrected profiles, $S^D(\alpha)$ and (b) the instrument profile was measured (99) and then convoluted with the $S^D(\alpha)$ profiles to yield the desired instrument and Doppler corrected Stark profiles, $S(\alpha')$. This convolution procedure yielded a set of reduced half-widths, $\alpha'_{\frac{1}{2}}$, which could be compared directly with experimentally observed H_β half-widths, $\Delta\lambda^O_{\frac{1}{2}}(R)$. When these quantities were substituted for $\Delta\lambda^S_{\frac{1}{2}}(R)$ and $\alpha_{\frac{1}{2}}$ in Equation 7 and the constants were evaluated, the radial n_e was given by

$$n_e(R) = 7.9658 \times 10^{12} \left\{ \frac{\Delta\lambda^O_{\frac{1}{2}}(R)}{\alpha'_{\frac{1}{2}}} \right\}^{3/2} \quad (8)$$

A discussion of the details and accuracy of the convolution procedure and of the H_β n_e computer program employed in this study is given in Appendix D.

Ar I lines The Ar I 542.135 and 549.588 nm lines were also employed for effective n_e determinations; the Stark parameters given by Griem (36,96) were used in these

calculations. The parameters for n_e values and temperatures not listed were obtained by using the scaling procedure indicated in the description of these parameters (36,96).

For neutral atom emitters the Stark half-widths are given approximately by (36,96)

$$\Delta\lambda_{\frac{1}{2}}^S \approx 2w[1 + 1.75 A (1 - 0.75 R')] \quad (9)$$

where w = electron impact width, proportional to n_e ,
 A = ion broadening parameter, proportional to $(n_e)^{\frac{1}{4}}$,
 R' = ratio of the mean distance between ions, r_1 , to the Debye radius ρ_D .

The R' term in Equation 9, which is a measure of ion-ion correlations and Debye shielding, is given by (36,96)

$$R' = r_1/\rho_D = 1.82 \pi^{1/6} \frac{e}{(kT)^{\frac{1}{2}}} (n_e)^{1/6} \quad (10)$$

where, k is the Boltzmann constant and other symbols have their usual meaning. Values of w and A are tabulated for Ar I lines by Griem (36,96) for $n_e = 10^{16} \text{ cm}^{-3}$ and temperatures of 2,500; 5,000; 10,000; 20,000; and 40,000 K. Stark half-widths were calculated from the w and A parameters given for the Ar I 542.135 nm line and for the 549.588 nm line in references 36 and 96, respectively. These $\Delta\lambda_{\frac{1}{2}}^S$ values were obtained for each line at the temperatures listed and for

n_e from $10^{13.5}$ to 10^{16} cm^{-3} in half-order steps by appropriate scaling of the tabulated w and A values (36,96). The Gaussian contribution to Ar I line half-widths, $\Delta\lambda_{\frac{1}{2}}^G$, was calculated from the Doppler and instrument profile contributions (99); a value of $\Delta\lambda_{\frac{1}{2}}^G = 0.22 \text{ \AA}$ was employed for temperatures of $T = 2,500 \text{ K}$ to $10,000 \text{ K}$.

CHAPTER III: FACILITIES

Experimental Facilities

The experimental facilities, except as modified for this study, were adapted from those previously described by Scott et al. (100). The principal components of the equipment employed here are outlined in Table V and the modifications incorporated for this study are described below.

The mechanism for positioning the impedance matching network was altered to provide for adjustment along the optical axis as well as providing the capability of precise horizontal and vertical positioning of the plasma torch. To achieve the latter the impedance matching network and plasma torch were mounted on a stand which allowed movement of the torch vertically, horizontally (laterally), and parallel to the monochromator optical axis. The vertical and horizontal movements could be read to ± 0.05 mm on a vernier scale. The parallel torch movement and lens positioning along the optical axis were accurate to ± 0.5 mm. A He-Ne laser ($\lambda = 632.8$ nm, C. W. Radiation Inc., Mountain View, CA) was employed for optical alignment and to check the validity of the horizontal and parallel movements of the torch. The lens aperture and the monochromator entrance slit were limited to 3 mm openings to achieve compliance with the criteria necessary for Abel inversion calculations.

Table V. Experimental facilities and operating conditions

<u>Plasma Generation</u>	
Radiofrequency generator	Fixed frequency (27.12 MHz), 1.5 kW crystal controlled oscillator and air-cooled amplifier (International Plasma Corporation, Hayward, CA). A feedback circuit was added to this facility to maintain constant forward power in the transmission line (type RG-8U coaxial cable) to the impedance matching network by controlling the screen voltage of the oscillator. Forward power in the transmission line was measured with a Thru-line Wattmeter (Model 43, 2500-H Element, Bird Electronics Corp., Cleveland, OH).
Impedence matching network	Variable (30-turn) vacuum capacitor coupling circuit (International Plasma Corporation, Hayward, CA) as described in reference 100. Copper, two-turn, water-cooled load coil, 5 mm o.d.
Plasma torch	Concentric quartz tube arrangement similar to that described previously (101). Inner and outer tubes were clear precision quartz tubing (Wilmad Glass Co., Buena, NJ). Spacing between inner and outer tubes and, position of aerosol injector tube accurately set with a machined brass alignment plug during torch construction.
coolant tube	Outer tube, 20 ± 0.025 mm o.d., 18.05 ± 0.025 mm i.d.
plasma tube	Inner tube, 15 ± 0.025 mm o.d., 13 ± 0.025 mm i.d.

Table V. (Continued)

aerosol tube	Clear fused quartz, 6 mm o.d., 4 mm i.d., tapered orifice, 1.5 mm i.d.
Argon flow rates	Coolant; 12.5 l/min. Plasma; Optional, used when igniting the plasma to prevent "burning" the plasma and aerosol tubes. Aerosol; 1.0 l/min and 1.3 l/ min.
Ignition	Tesla coil ignition with no aerosol flow and coolant-plasma flow of approximately 15 l/min. After the plasma was formed the tesla coil was shut off and flow rates were adjusted to operating values.

Aerosol Generation

Nebulizer	Right-angle pneumatic, uptake approximately 2.5 ml/min at 1.0 l/min aerosol flow, construction details given in reference 102.
Aerosol chamber	Dual tube aerosol chamber (100) and (later) a simpler Teflon and glass chamber (103). The simpler chamber reduced the clear-out time between sample- background readings.

Table V. (Continued)

<u>Spectroscopic Equipment</u>	
Spectrometer	0.5 meter, Ebert mount, scanning monochromator (Jarrell-Ash Division, Fisher Scientific Co., Waltham, MA, Model No. 82000).
Grating	1180 rulings/mm, blazed at 2500 Å, first order.
Slits	Fixed, 15 μm entrance and exit, entrance slit height masked to 3 mm.
Reciprocal linear dispersion	16 Å/mm, first order.
Detector	EMI 6256B photomultiplier, S-13 response (Gencom Division, Emitronics, Inc., Plainview, NY)
Optical transfer system	Plasma emission focussed by 16 cm focal length x 5 cm diameter plano-convex, fused quartz lens with aperture limited to 3 mm by adjustable iris diaphragm concentrically mounted on the lens holder. Lens positioned at twice the focal length (2f) from the entrance slit and plasma central axis for each wavelength region studied.
Amplifier	Linear picoammeter with zero suppression (Keithly Instruments, Cleveland, OH, Model 417)
Integrator	Digital readout system, hard copy only (Infotronics, Houston, TX, Model CRS-80).
Recorder	X-Y recorder (Moseley Division, Hewlett-Packard, Pasadena, CA, Model 7001-A).

The power supply to the filament of the RF generator power tube was modified to accommodate time-independent relative intensity measurements. With reference to this modification it is worth noting that many high frequency generators produce a sinusoidal 60 Hz modulation on the forward power high voltage envelope; this was found to be true for the radio-frequency (RF) generator employed in this investigation. Consequently, emission from analyte and Ar I lines observed in the plasma displayed similar 60 Hz modulations; the peak-to-peak magnitudes of these modulations were a sensitive function of the excitation energies. Subsequently, the relative intensities obtained represented time-averages over the integration period employed for the intensity measurements; these intensities yielded erroneous time-averaged excitation temperature values.

Experimental verification of this effect is provided by the oscilloscope tracings shown in Figure 1 for the Fe I 381.584 nm and 382.444 nm lines; these neutral atom lines possessed excitation energies of $38,175 \text{ cm}^{-1}$ and $26,140 \text{ cm}^{-1}$, respectively. The tracings shown in Figure 1 were obtained by filtering the signal current taken directly from the photomultiplier tube output. Trace C for the higher excitation potential line clearly displays greater intensity sensitivity to forward power modulation than does the lower excitation potential line shown in trace B. Consequently,

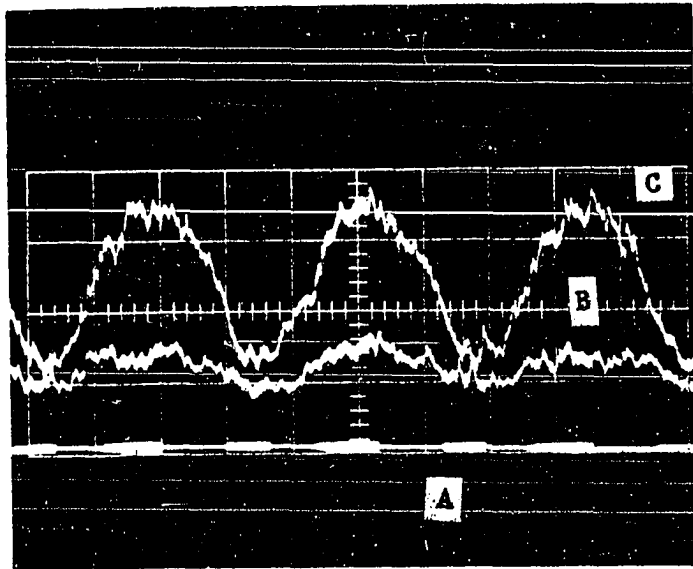


Figure 1. Oscilloscope tracings showing emission intensity modulation with a 60 Hz ripple on the forward power to the plasma:
(A) dark current, (B) Fe I 382.444 nm,
(C) Fe I 381.584 nm

the intensity ratio of the two lines was significantly different in the peak and valley regions of the oscilloscope tracings. The peak and valley relative intensities (above dark current), intensity ratios, and the corresponding two-line temperatures calculated from these ratios with two sets of transition probabilities are summarized in Table VI. Because peak values were clearly $\sim 15\%$ higher than the valley temperatures, erroneous time-averaged excitation temperatures were obtained under these conditions. These temperatures were biased by the excitation energy range of the lines employed. The actual time-independent temperatures were obtained when the 60 Hz ripple was eliminated from the generator power tube filament. This was accomplished with the DC power supply which by-passed the generator ac supply, the source of the 60 Hz modulation. With the elimination of the 60 Hz ripple on the RF forward power, a smaller 120 Hz sawtooth ripple of $\sim 9\%$ peak-to-peak magnitude, remained. The 120 Hz ripple was reduced to $\sim 3\%$ near maximum power and to $< 1\%$ at 900 W by increasing the generator high voltage filtering network capacitance from $4\mu\text{F}$ to $12\mu\text{F}$. For the latter the reflected power was reduced from ~ 10 W to ~ 1 W when the 60 Hz ripple was eliminated.

Computer Facilities

Off-line computer calculations were handled by PL1 and FORTRAN IV programs which were processed on the IBM 370/158

Table VI. Intensities, intensity ratios, and two-line temperatures for Fe I lines in peak and valley regions with 60 Hz modulation on the forward power

Region	Relative Intensity		Ratio ^a	Temperature (K)	
	Fe I 381.584	Fe I 382.444		R ^b	BH
peak	3.3	1.4	0.42	6500	5600
valley	1.3	0.85	0.65	5600	4900

^aIntensity ratio, $I_{382.444}/I_{381.584}$.

^bTransition probability data: BH = Banfield and Huber (66); R = Reif (30).

and M/65 facilities at the Iowa State University Computations Center. Remote processing was accomplished with the facilities located at the Ames Laboratory Computer Garage. The expert assistance provided by the staff of the Ames Laboratory Computer Service Group was invaluable during the writing and debugging of a number of the programs employed in this investigation. The ASR 35 teletype in B28 Spedding Hall was employed to process CPS/PL1 jobs which were mainly used for disk data file management. A Digital Equipment Corporation (DEC) PDP 8/e minicomputer with 8K of core was employed for some preliminary on-line profiling experiments on a different plasma facility than the one used in this study. The characteristics and potential of this DEC PDP 8/e plasma system will be briefly discussed in a later chapter of this thesis.

CHAPTER IV: EXPERIMENTAL PROCEDURES

Intensity Measurements, Lateral Profiling,
and Abel Inversions

The analyte thermometric species (Fe I) was nebulized into the plasma (100,102,103) as a 150 $\mu\text{g Fe/m}\ell$ solution. The relative intensities of the Fe I emission lines listed in Table II and those for the three-line set from Table I were measured at increasing lateral displacements (0.4-1.0 mm intervals) from the axial channel of the plasma until the signals could no longer be detected. Three to four data points on the opposite side of center were also collected to assure accurate location of the vertical symmetry axis of the plasma. The latter was taken at the position of the peak of the symmetric bell-type lateral distributions after a smooth curve was drawn through the original data points. Spectral backgrounds at each emission line of interest were measured while deionized water was aspirated into the plasma. The signals and spectral backgrounds were integrated over an 8-second period. The net relative intensities used in the final calculations were the averages of three to five background corrected values. These relative intensities were plotted vs. displacement to construct a lateral profile for each Fe I line of interest. Relative intensity measurements were taken for all lines at a given displacement before proceeding to the next lateral observation zone.

Complete lateral profiles from one edge of the plasma through the geometric center to the opposite edge were obtained in a similar fashion for the neutral atom and first ion lines listed in Table IV. The center of the bell-type profiles so obtained was taken at the peak of the distribution. Complete lateral profiles with water nebulized into the plasma at an aerosol carrier gas flow of 1.0 l/min were also obtained for the Ar I spectral lines listed in Table III. The spectral backgrounds for these Ar I lines were obtained from the continuum emission adjacent to the lines. The center of the toroidally-shaped lateral distributions obtained for these Ar I lines was taken as the midpoint between the off-axis peaks.

The Cremers and Birkebak Abel inversion method described previously was used to obtain spatially resolved radial intensity distributions from the corresponding lateral profiles. The right and left portions of the complete lateral intensity profiles discussed above were inverted separately for comparative purposes.

Temperature Calculations

The slope method described previously (Equation 3) was used to calculate radial excitation temperature distributions from the corresponding radial intensity profiles. The temperature profiles so obtained for the different thermometric

species, Fe I and Ar I, and for different Fe I line sets and transition probabilities are compared later in Chapter V of this thesis.

Electron Number Density from Saha-Eggert's Ionization Calculations

Equation 5 was used to calculate radial n_e values from the corresponding radial intensities for the atom/ion line combinations and average $(g^0 A^0 \lambda^+ / g^+ A^+ \lambda^0)$ ratios given in Table IV. Radial number density ratios $(n_{X^+}(R)/n_{X^0}(R))$ were obtained from Equation 6 for the atom/ion line combinations listed in this table. A listing of the source statements of the computer program employed in these calculations is given in Appendix C.

Electron Number Density from Stark Broadening Calculations

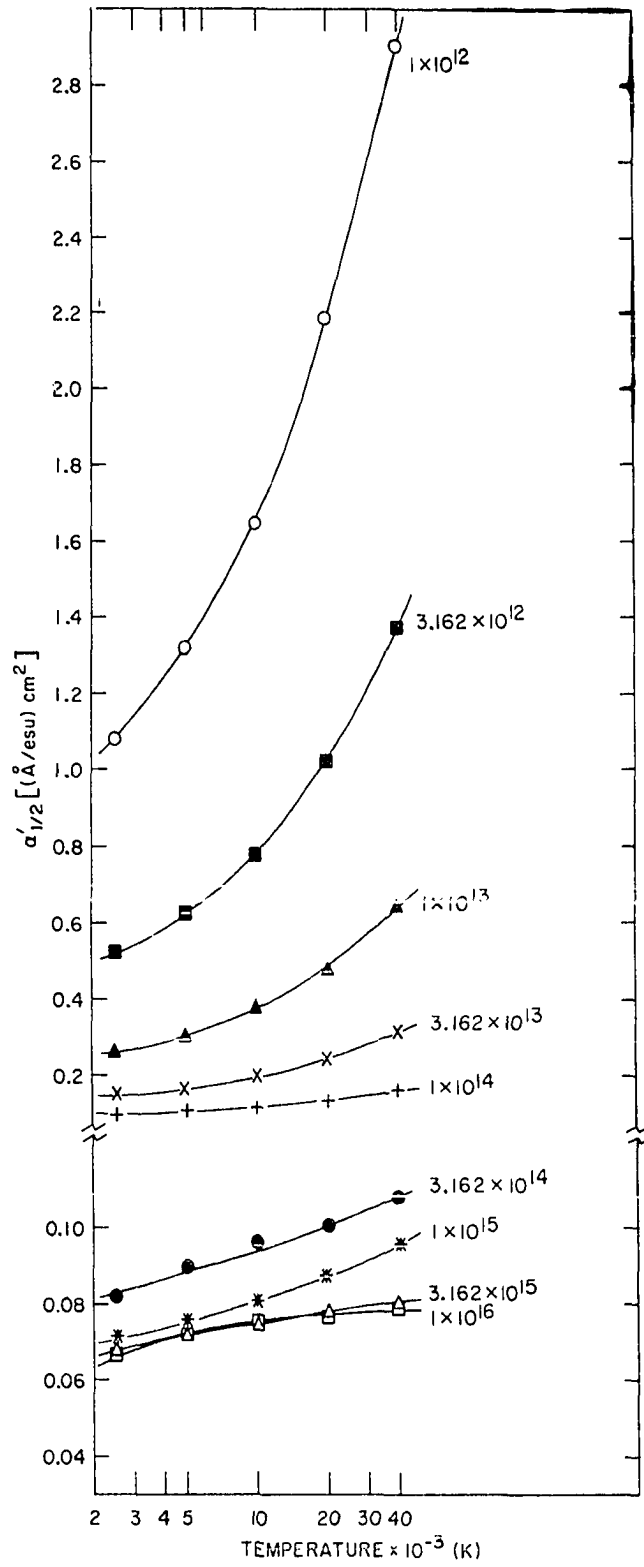
H _{β} line

Wavelength scans over the H _{β} line profile were obtained at successive lateral displacements across the plasma discharge. First, each scan was divided into ~ 25 constituent wavelengths spanning the entire interval of the H _{β} line profile. Second, lateral profiles were constructed for each constituent wavelength and the spectral background was interpolated from the continuum emission beyond the H _{β} line

wings. Third, radial intensity profiles were obtained from the corresponding lateral profiles for each constituent wavelength by employing the Abel inversion method described previously. Finally, the H_{β} profile at each radial position was reconstructed from the radial intensity data; the radial half-widths, $\Delta\lambda^{\circ}_{\frac{1}{2}}(R)$, were measured from these H_{β} profiles.

A FORTRAN IV computer program was written to perform the n_e calculations. The details of this program are discussed and a listing of the source statements is given in Appendix D. The computer calculations were performed as follows. First, a matrix of $\alpha'_{\frac{1}{2}}$ vs. $\log_{10} T$ values was constructed from the instrument and Doppler corrected reduced Stark half-width data (98) for n_e from 10^{12} to 10^{16} cm^{-3} in half-order steps, and for temperatures of 2,500; 5,000; 10,000; 20,000; and 40,000 K. The values obtained are shown in Figure 2. Second, the value of $\Delta\lambda^{\circ}_{\frac{1}{2}}(R)$ obtained as described above was inserted into Equation 8 to evaluate the $[\Delta\lambda^{\circ}_{\frac{1}{2}}(R)]^{3/2}$ term. Third, $[\alpha'_{\frac{1}{2}}, n_e(R)]$ pairs were calculated by appropriate interpolation methods (98) for the Fe I excitation temperature, $T(R)$, at radius R . Fourth, an approximate $[\alpha'_{\frac{1}{2}}]_0$ was selected and inserted into Equation 8 to calculate a zero-order approximation to the electron density, $[n_e(R)]_0$. Fifth, a first-order $[\alpha'_{\frac{1}{2}}]_1$ value was interpolated from the $\alpha'_{\frac{1}{2}}$ vs. $n_e(R)$ relationship and from the value of $[n_e(R)]_0$. This value for $[\alpha'_{\frac{1}{2}}]_1$ was used in Equation 8 to give a

Figure 2. Reduced Stark profile half-widths, $\alpha'_{\frac{1}{2}}$, corrected for Doppler and instrument broadening plotted vs. $\log_{10} T$ for electron densities from 10^{12} to 10^{16} cm^{-3} for the H_{β} 486.13 nm line

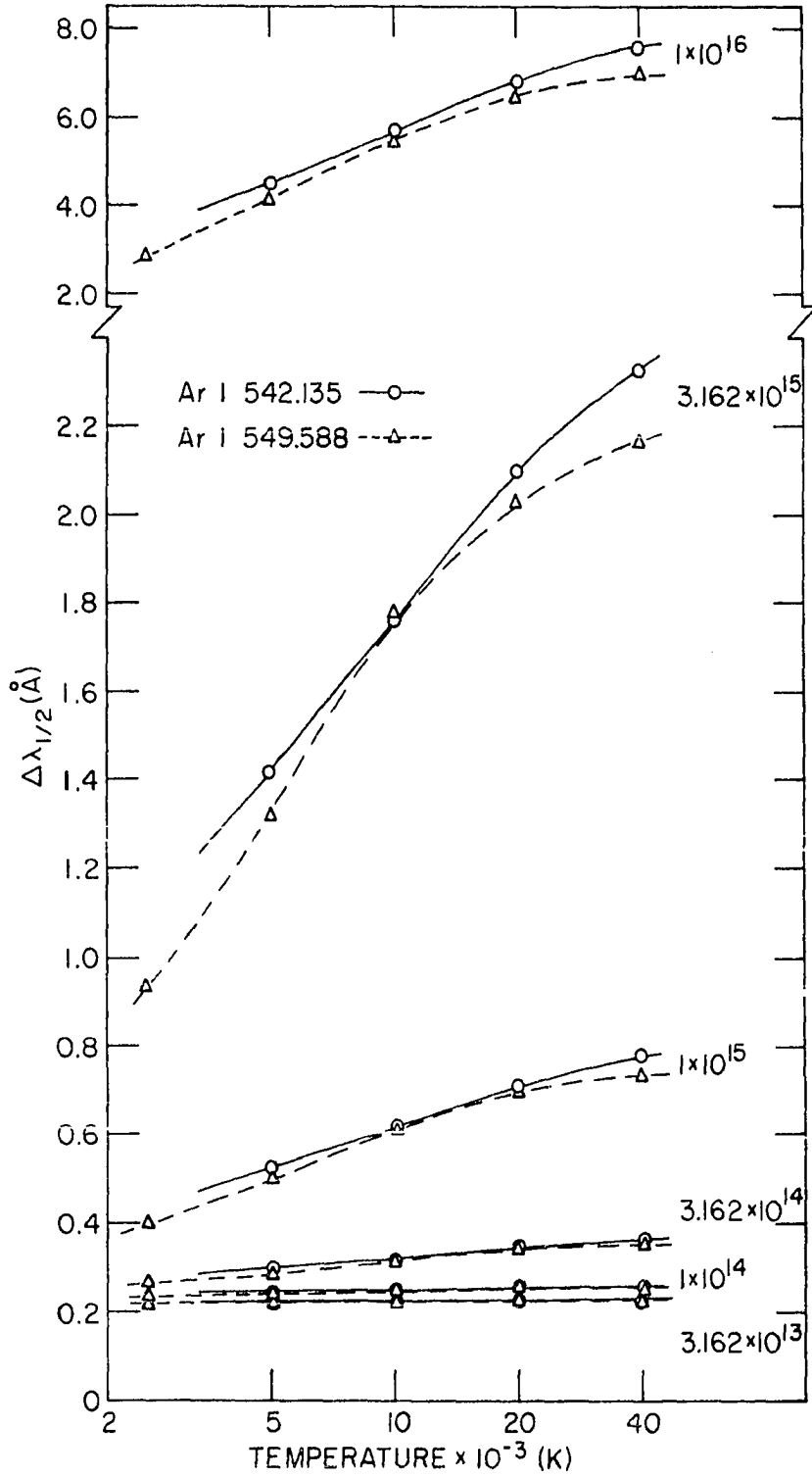


first-order electron density, $[n_e(R)]_1$. Finally, this procedure was repeated iteratively until a self-consistent pair of $[\alpha'_{\frac{1}{2}}, n_e(R)]$ values was obtained to the desired accuracy.

Ar I lines

Wavelength scans over the lateral (effective) Ar I line profiles were obtained at the central axis of the plasma discharge. The Ar I lines were assumed to have Voigt profiles so that the tabulated half-width ratios (93); i.e., $\Delta\lambda_{\frac{1}{2}}^S/\Delta\lambda_{\frac{1}{2}}^G$ and $\Delta\lambda_{\frac{1}{2}}^S/\Delta\lambda_{\frac{1}{2}}$, could be used to calculate the expected experimental half-width, $\Delta\lambda_{\frac{1}{2}}$, at the appropriate n_e and temperature combinations. The $\Delta\lambda_{\frac{1}{2}}^S/\Delta\lambda_{\frac{1}{2}}$ ratios were plotted as a function of the $\Delta\lambda_{\frac{1}{2}}^S/\Delta\lambda_{\frac{1}{2}}^G$ ratios for the values given in reference 93. Equation 9 was used to calculate the $\Delta\lambda_{\frac{1}{2}}^S$ values and the $\Delta\lambda_{\frac{1}{2}}^S/\Delta\lambda_{\frac{1}{2}}^G$ ratio was obtained from the Stark half-width and the known value for $\Delta\lambda_{\frac{1}{2}}^G$. The corresponding $\Delta\lambda_{\frac{1}{2}}^S/\Delta\lambda_{\frac{1}{2}}$ ratio was interpolated from the plot and the $\Delta\lambda_{\frac{1}{2}}$ value was calculated from this ratio. This procedure was used to obtain $\Delta\lambda_{\frac{1}{2}}$ values for each Ar I line at each n_e and temperature combination considered. The semi-log plots of $\Delta\lambda_{\frac{1}{2}}$ vs. $\log_{10} T$ which were constructed for each line in half-order steps for n_e from $10^{13.5}$ to 10^{16} cm^{-3} are shown in Figure 3. The n_e corresponding to an experimentally measured Ar I line half-width was then obtained by linear interpolation between

Figure 3. Doppler and instrument profile corrected
Stark half-widths for Ar I lines,
 $\Delta\lambda_{\frac{1}{2}}$ vs. $\log_{10} T$ for electron density
from $10^{13.5}$ to 10^{16} cm^{-3}



the values plotted in this figure. Effective temperatures were estimated for observation heights at which no measurements were obtained, i.e., below 15 mm.

CHAPTER V: RESULTS AND DISCUSSION

Symmetry

The bell-type lateral intensity distributions which were obtained for Fe I thermometric emission lines complied well with the circular symmetry requirement discussed in Chapter II. The bell-type profiles of the emission lines given in Table IV for Saha-Eggert's n_e calculations were also in compliance with this symmetry criterion. In contrast, the toroidally shaped Ar I lateral intensity distributions for the thermometric lines given in Table III showed deviations from symmetry primarily in the off-axis regions. The lateral intensity distributions for the wavelength constituents of the H_β line profile displayed similar toroidal shapes and similar deviations from circular symmetry. The different lateral distributions are discussed in the following sections.

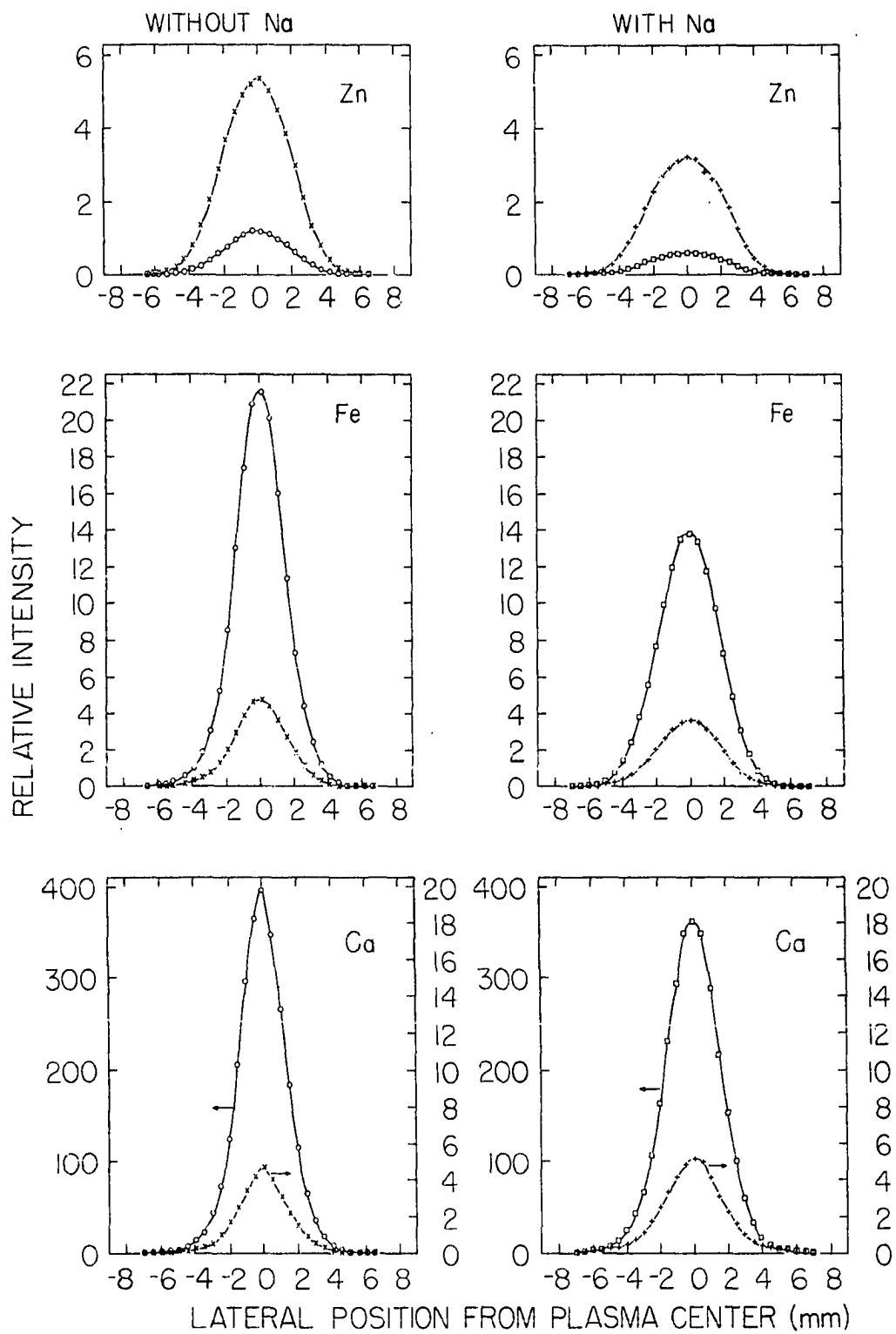
Intensity Distributions of

Analyte Lines

Figure 4 shows typical lateral intensity profiles for the Zn, Fe, and Ca atomic and ionic emission lines listed in Table IV. It is seen that bell-type intensity distributions were obtained for the wide range of excitation and ionization energies represented by the spectral lines of these species. Similar profiles were obtained for the Mg and Cd atomic and

Figure 4. Lateral profiles for Saha species at 15 mm,
1000 W and 1.0 l/min aerosol carrier gas flow

			without Na	with 6900 $\mu\text{g Na/ml}$
10 $\mu\text{g Zn/ml}$:	Zn II	206.19 nm	(—○—)	(—□—)
	Zn I	213.88 nm	(—X—)	(—+—)
150 $\mu\text{g Fe/ml}$:	Fe II	258.588 nm	(—○—)	(—□—)
	Fe I	252.285 nm	(—X—)	(—+—)
10 $\mu\text{g Ca/ml}$:	Ca II	396.847 nm	(—○—)	(—□—)
	Ca I	422.673 nm	(—X—)	(—+—)



ionic lines from Table IV. The corresponding Abel inverted radial intensity profiles showed similar bell-type behavior.

The addition of a large excess of an EIE should, under equilibrium conditions, suppress ionization of the analyte species. The trends of the Ca profiles in Figure 4 tend to support this interpretation, i.e., the atomic line is slightly enhanced while the ionic line is relatively more depressed. However, the axial depressions in the atomic line profiles of Fe and Zn suggest ionization suppression is not the dominating process. This suggestion is supported by the data in Table VII which lists ion/atom lateral or "averaged" intensity ratios at the plasma central axis for the line profiles shown in Figure 4 and for the Mg and Cd lines listed in Table IV. Again, the existence of some analyte ionization suppression is indicated by the decrease in these ratios upon the addition of Na to the plasma but, in comparison to flames, the suppression is surprisingly small (104). These unusually small interference effects were first reported by Larson et al. (103) and confirmed later by Mermet and associates (105) and by Boumans and de Boer (1c).

Further evidence that ionization suppression plays only a minor role at least under some combinations of experimental conditions is found in the radial relative intensity profiles shown in Figure 5 for the Fe I 382.043 nm emission line. These profiles clearly show that Fe I radial intensity

Table VII. Ion to neutral atom lateral intensity ratios for lines of Zn, Cd, Fe, Mg and Ca with and without added Na

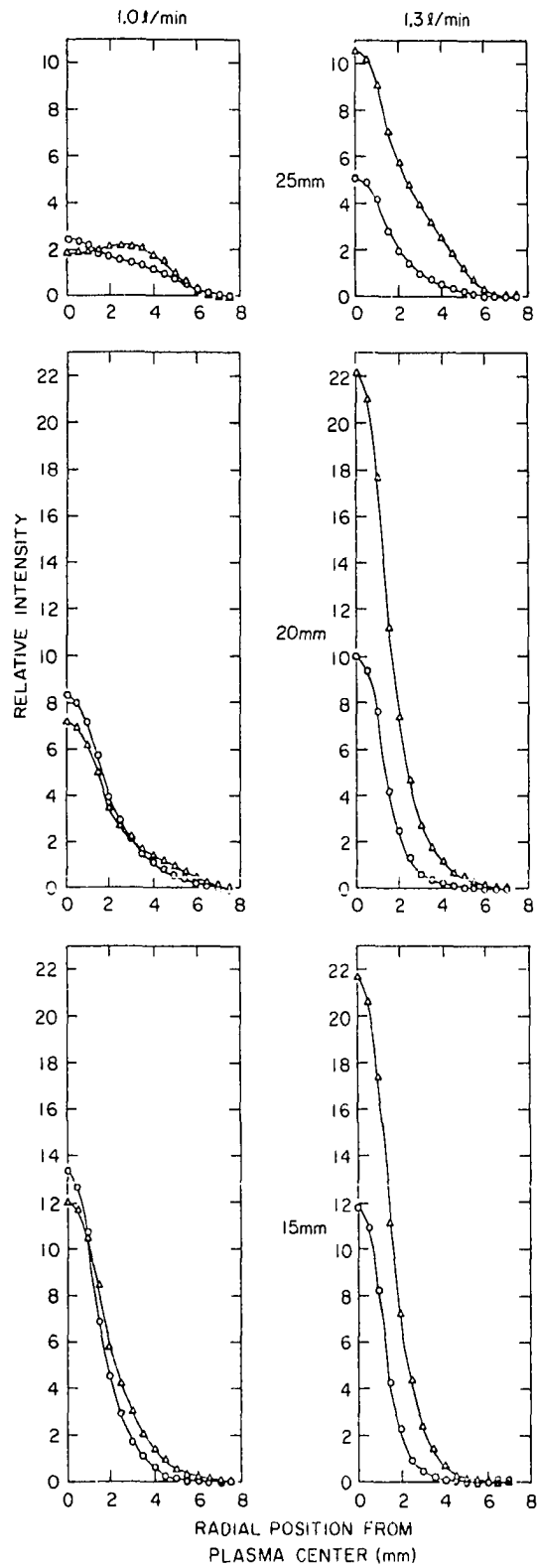
Species	I^+/I^0 Ratios ^a		$\frac{(I^+/I^0)_{Na}}{(I^+/I^0)}$
	Without Na	With 6900 $\mu\text{g Na/ml}$	
Zn	0.22	0.18	0.82
Cd	0.88	0.67	0.76
Fe	4.6	3.8	0.83
Mg ^b	10.4	9.9	0.95
Mg ^c	5.3	5.1	0.96
Ca	85	70	0.82

^aRelative intensity ratio, ion line intensity/atom line intensity.

^bIon line, Mg II 279.553 nm.

^cIon line, Mg II 280.270 nm.

Figure 5. Radial intensity distributions for the Fe I 382.043 nm line at 1000W for three observation heights and two aerosol carrier gas flows; 150 $\mu\text{g Fe/ml}$ (—○—) and 150 $\mu\text{g Fe/ml}$ + 6900 $\mu\text{g Na/ml}$ (—△—)



distributions are essentially unchanged upon addition of Na as an EIE at the lower aerosol carrier gas flow but, are enhanced about two-fold at the higher flow.

These observations imply that greater interferences due to the presence of an EIE would be expected to occur at higher aerosol carrier gas flows when lateral intensities are measured under analytical experimental conditions. Indeed, Larson et al. (103) and Boumans and de Boer (1c) have established that this is so. It is important to note that the combination of argon carrier gas flow of ~ 1.0 l/min and an observation height of ~ 15 -20 mm corresponds to the values of these parameters that lead to excellent powers of detection and a low degree of ionization and other interelement interactions (1b,1c,103).

Intensity Distributions of Ar Lines

The typical toroidal lateral and radial relative intensity distributions for the Ar I 425.936 nm line reproduced in Figure 6 clearly show that both the lateral and radial profiles are asymmetric, as evidenced by the larger left side peak in the lateral profile and by the disagreement between right and left side intensities in the central region of the radial profile. These observations are typical for Ar I profiles, even though elaborate precautions were taken in order to assure symmetry in the construction of the plasma

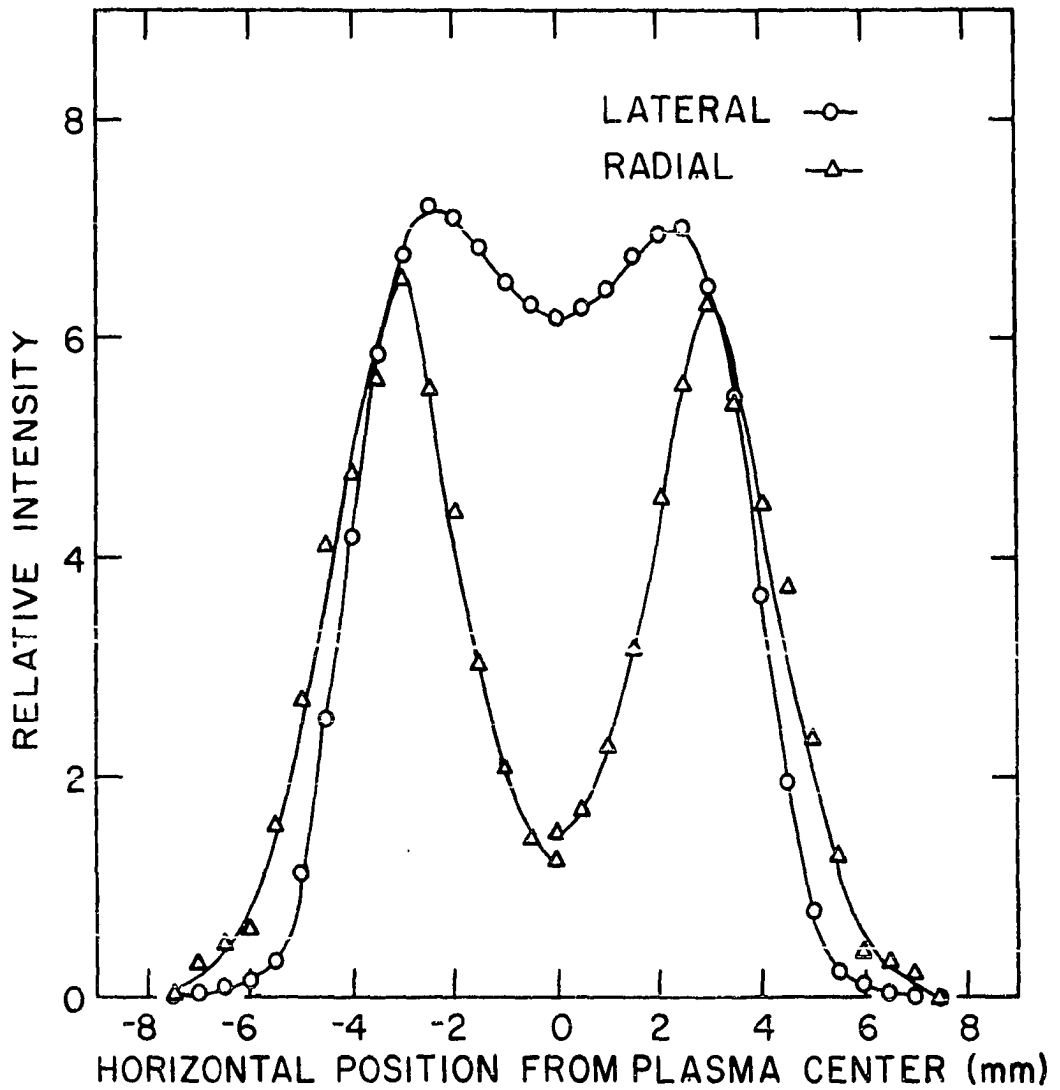


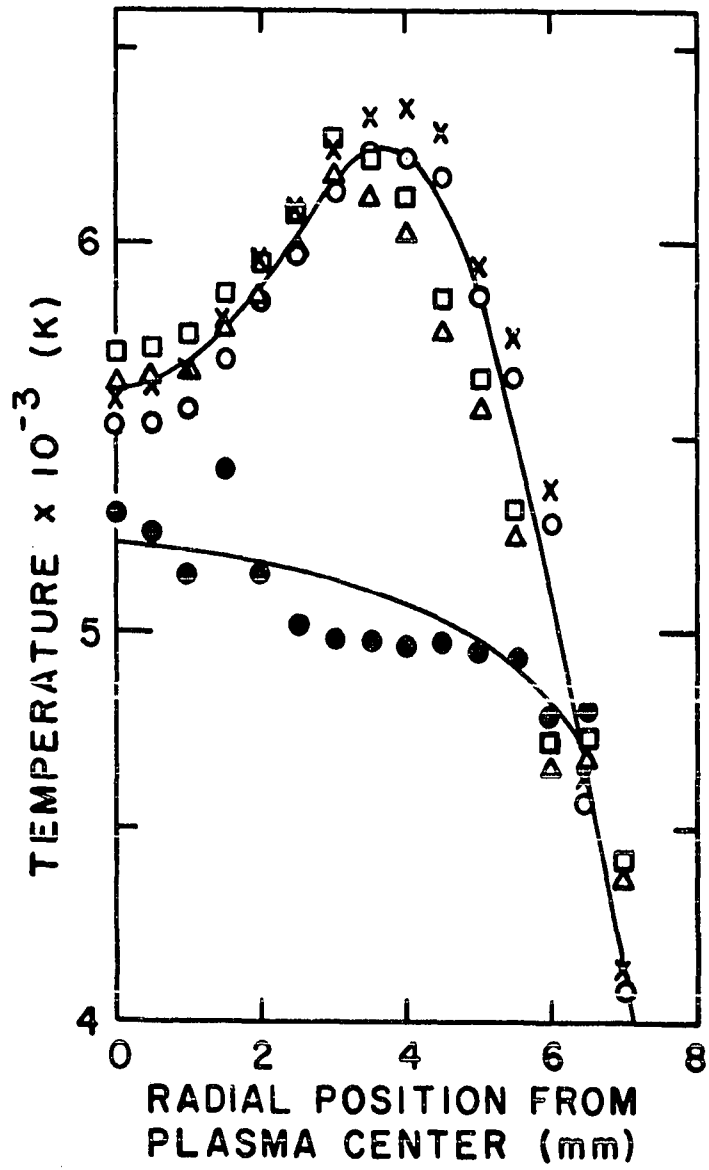
Figure 6. Toroidal lateral and radial relative intensity distributions for the Ar I 425.936 nm line at 15 mm, 1000W and 1.0 l/min aerosol carrier gas flow

torch. Evidently very critical adjustments beyond present fabrication technology are required for precise control of Ar flow patterns. Asymmetry in the magnetic and electric fields induced by the load coil and in the interaction of these fields with the Ar plasma support gas may also contribute to asymmetry in the Ar I lateral profiles. The toroidal lateral and radial relative intensity distributions which were obtained for the constituents of the H_{β} line profile displayed similar asymmetric characteristics. Other investigators have also reported similar problems with asymmetric toroidal lateral intensity distributions when Abel inversion methods have been applied to these profiles (2a,15,16,45). These results suggest that further refinements in torch and coil design should be explored ultimately; these studies were not considered important enough to justify their inclusion in the present context.

Temperature Profiles

The excitation temperatures obtained from Equation 3 for analyte (Fe I) and support gas (Ar I) thermometric lines are plotted in Figure 7. It is seen that the excitation temperatures calculated from different sets of transition probabilities (30,66,67) for the Fe I three-line set (From Table I) and for the expanded ten-line set (given in Table II) agree to within $\sim 3\%$ in the axial channel region and within $\pm 10\%$

Figure 7. Radial excitation temperatures at 15 mm, 1000W and 1.0 l/min aerosol carrier gas flow. Ar I eight-line with Corliss and Shumaker (77) transition probability data (—●—); Fe I ten-line with Huber and Parkinson (67) data (—X—) and with Reif (30) and Banfield and Huber (66) data (—○—); Fe I three-line with Reif data (—△—) and with Banfield and Huber data (—□—)



in the wings. The temperature data obtained from the Ar I eight-line set (listed in Table IV) are not that encouraging, even though the temperatures obtained with the transition probability data given in references 75-77, and 80 agreed to within $\pm 3\%$. The uncertainty in the Ar I data as represented by the scatter of the points in the radial temperature profile, and the disagreement with the Fe I temperatures, are reconcilable. First, the asymmetric character of the toroidal Ar I lateral intensity distributions (see Figure 6) introduces large uncertainties into Abel inversion calculations, especially for the axial region (2a,15,16,18,45). Second, errors in relative intensity measurements are amplified considerably when the selected lines possess a limited range of excitation energies, as shown by the data plotted in Figure 8. These plots, which were calculated by methods discussed elsewhere (2a,81,106), clearly show that the Ar I temperature calculations are subject to an approximate five-fold larger uncertainty than the Fe I values for the same $\Delta I/I$ measurement error.

In view of the good agreement between the Fe I temperatures and the large uncertainties associated with the Ar I temperatures henceforth, only the temperatures calculated for the Fe I three-line set from Table I will be considered. These temperatures, which were obtained at two aerosol carrier gas flows and with and without the presence of relatively high concentrations of an EIE, are shown in Figure 9.

Figure 8. Percent uncertainty in temperature as a function of percent uncertainty of intensity for typical Fe I and Ar I lines employed in temperature calculations

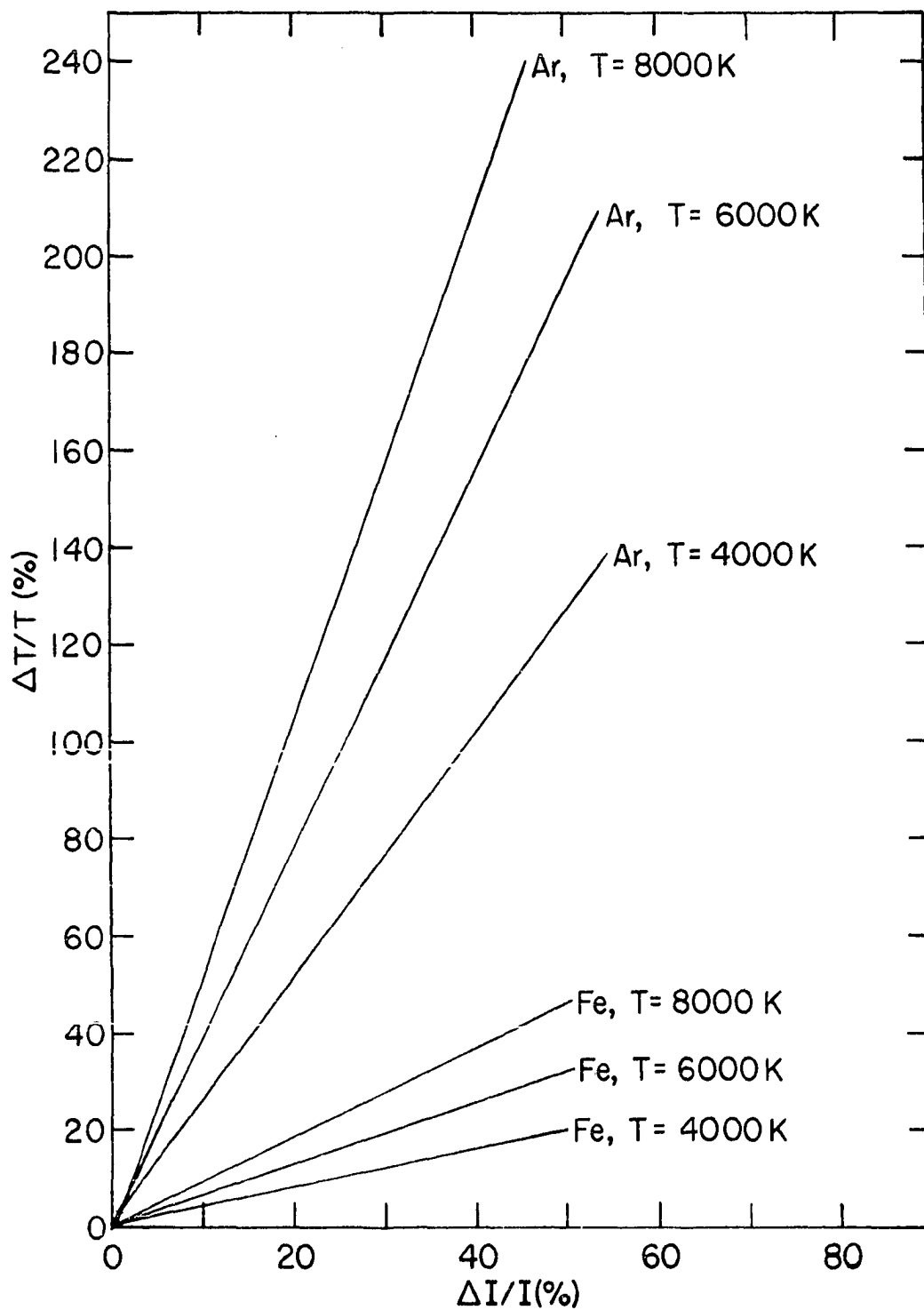
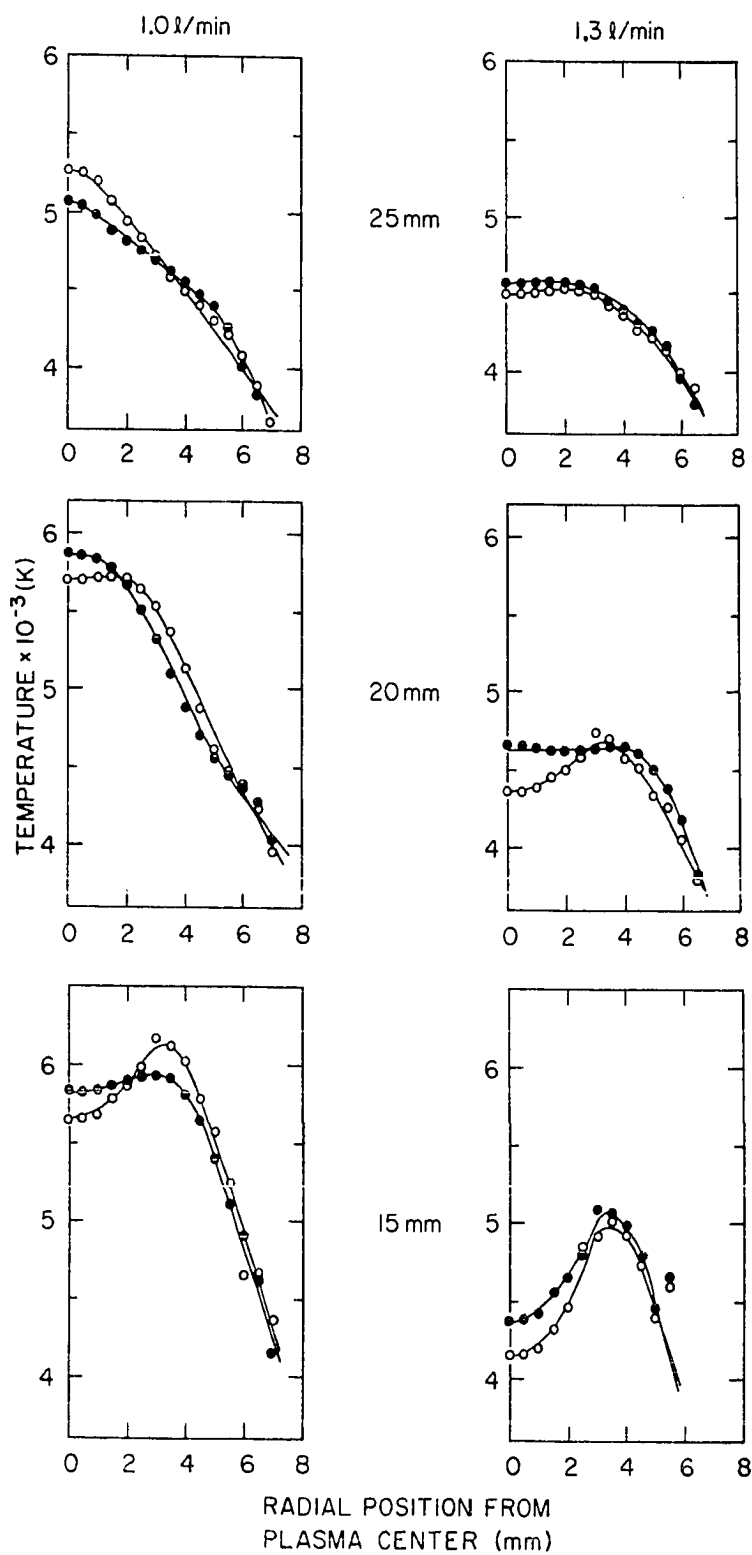


Figure 9. Radial Fe I excitation temperatures at 1000W for three observation heights and two aerosol carrier gas flows; 150 μg Fe/ml (—○—), 150 μg Fe/ml + 6900 μg Na/ml (—●—)



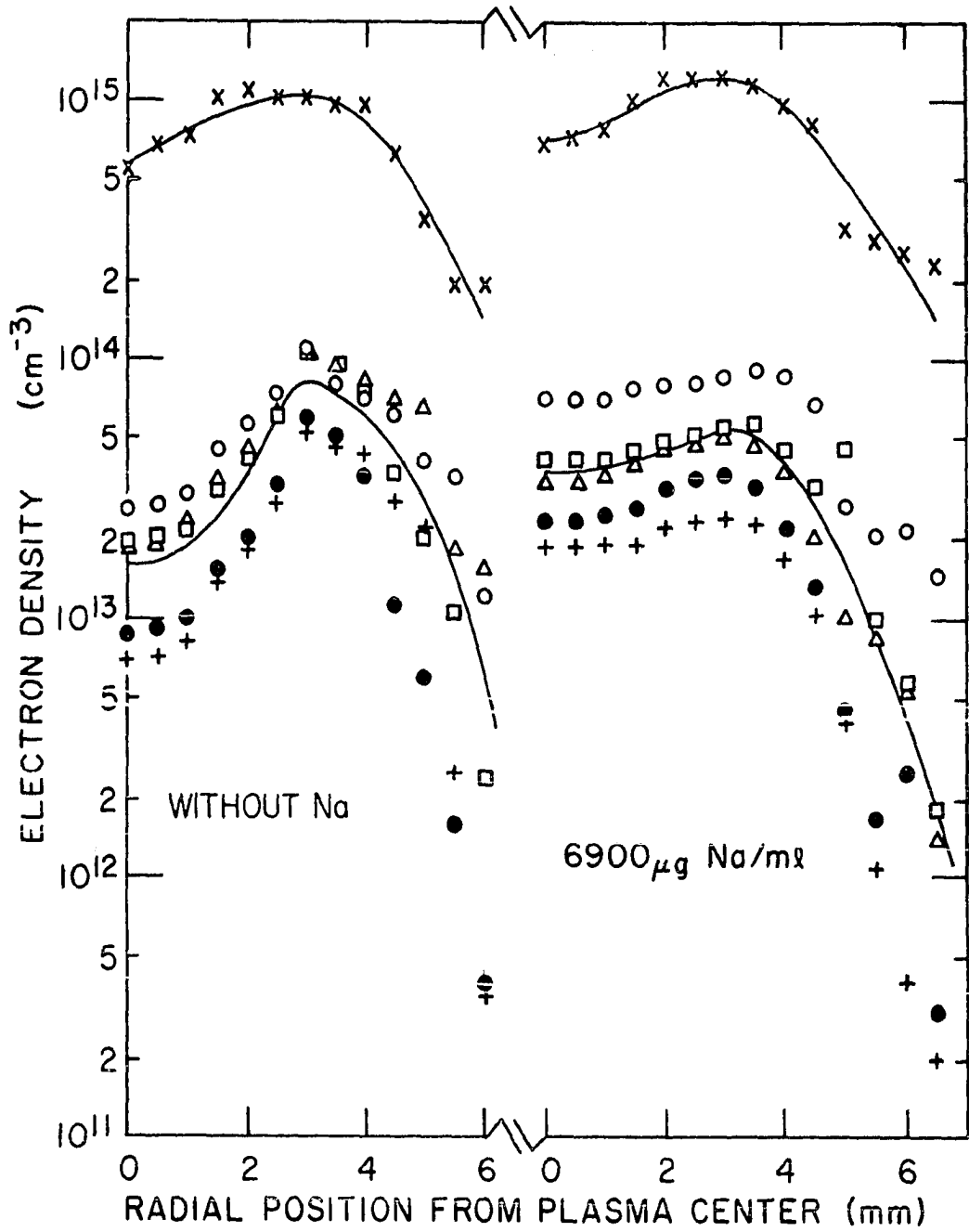
Examination of this figure reveals several important features. First, the excitation temperature distributions obtained at the respective aerosol carrier gas flows and observation heights are not significantly changed upon addition of Na as an EIE. Second, the temperatures for the higher flow are significantly lower (400 to 1400 K) than the corresponding temperatures for the lower flow. Third, for the higher carrier-gas flow, the central zone temperatures at 15 mm are relatively low and the off-axis peak is much more pronounced than for the lower flow. Finally, central zone temperatures at the lower flow are essentially unchanged from 15 to 20 mm but decrease by about 10% at 25 mm. These results correlate well with the empirical observations of others at this laboratory (103,107) namely, that the "compromise" experimental conditions which yield excellent powers of detection and also yield a high degree of freedom from interelement effects are ~ 1.0 l/min aerosol carrier gas flow and ~ 15 -20 mm observation height. Figure 9 clearly shows that there is essentially no decrease in temperature from 15 to 20 mm yet additional residence time is gained for desolvation, atomization, and excitation of the analyte. These profiles also reveal the drastic temperature drop at the higher flow which is undesirable from excited state population and residence time considerations. The substantial temperature drop between 20 and 25 mm for the lower flow is also undesirable from the excited state population standpoint for most species.

Boumans and de Boer (1c) have reported different "compromise" operating conditions which were based on their observations of interelement effects and detection limits obtained for their plasma system. These authors suggested experimental conditions of 1.3 to 1.5 l/min carrier gas flow and 15 mm observation height at 700 W power input and, 1.5 to 1.7 l/min carrier gas flow at 20 mm height for a power input of 850 W. It is worth noting that the relative intensity data in Figure 5 and the temperature data in Figure 9 combined with the observations of Larson et al. (103) suggest that an aerosol carrier gas flow of 1.3 l/min is undesirable for plasma operating conditions at this laboratory because greater interelement effects are observed at this flow.

Electron Number Density Profiles

Because the temperature profiles shown in Figure 9 exhibited definite off-axis or toroidal peaks, it was of particular interest to determine whether the n_e profiles at this observation height reflected these temperature distributions. The profiles shown in Figure 10 indeed show similar off-axis peaks, but they reveal several other features worthy of comment. First, the H_β Stark broadening n_e profiles are a factor of 30- to 50-fold greater than the Saha-Eggert's ionization profiles. Second, the n_e profiles were not significantly changed upon addition of Na as an EIE. Finally,

Figure 10. Radial electron density distributions at 1000W, 15 mm and 1.0 l/min aerosol carrier gas flow for H_β Stark broadening (—X—) and Saha calculations; 10 μg Ca/ml (—○—), 150 μg Fe/ml (—□—), 10 μg Mg/ml (—△—), 10 μg Cd/ml (—+—), 10 μg Zn/ml (—●—)



for the central axial region the Saha n_e profiles agree to within a factor of three for the five different analyte species. Considering first the disagreement among the Saha n_e values, the range of values obtained is not particularly surprising in view of the magnitude of potential errors involved. This range may reflect inherent errors in the published transition probability data for the lines employed or varying degrees of n_e contribution by the analytes because of their different degrees of ionization in the plasma. These uncertainties plus those accumulated in the lateral intensity measurements and Abel inversion calculations may account for up to a factor of two error in the Saha-Eggert's n_e values. A 10% uncertainty is generally associated with theoretical Stark data for the H_β line (36,93-96,98,99). Accumulated uncertainties from convolution calculations, instrument profile measurements, and Abel inversions account for $\sim 30\%$ error in the radial H_β half-width determinations. These considerations suggest that $\sim 40\%$ error may be associated with the n_e values determined by H_β Stark broadening calculations. Although the errors in both sets of measurements are substantial, they are clearly inadequate in accounting for the factor of 30- to 50-fold difference between the n_e values determined by the Saha and Stark methods. These large differences suggest that LTE may not prevail for the plasma operating conditions employed in this work, a subject that is discussed later in this chapter.

It is worth noting that the Stark broadening n_e values shown in Figure 10 are about a factor of five-fold smaller than the similar measurements reported by Mermet (17a) and are about two-fold smaller than the continuum calculations reported by Kornblum and de Galan (16). However, Kornblum and de Galan reported Saha n_e values obtained with Mg atom/ion lines that were two to three orders of magnitude greater than those obtained here and those reported by Mermet (17a). The effective Saha n_e values reported by Mermet were essentially identical to the similar values obtained here and reported later in this chapter.

Because the Saha n_e values obtained from the Mg atom/ion line pairs (Table IV) represented a value near the average obtained for all the species plotted in Figure 10, Mg was selected for additional n_e measurements at different observation heights. These line combinations possessed several other desirable advantages; namely, (a) four sets of transition probability data which were in good agreement, were available for both Mg atom/ion line combinations, (b) the lines were free from spectral interference, (c) the excitation energies of the atomic and ionic lines were well matched, and (d) the lines were in close wavelength proximity so that the instrument response with wavelength could be assumed constant. The results of n_e measurements on the Mg atom/ion line combinations are shown in Figure 11. Surprisingly, the n_e

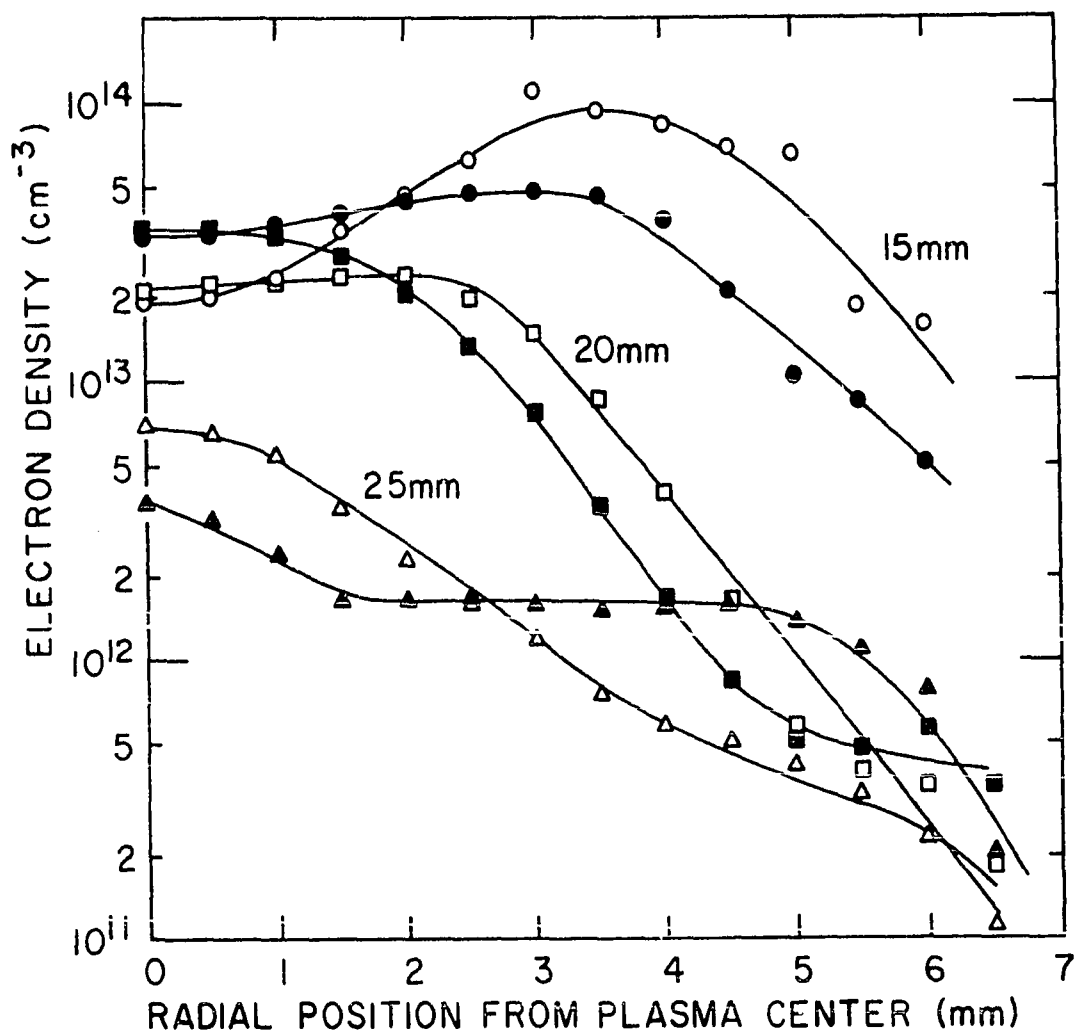
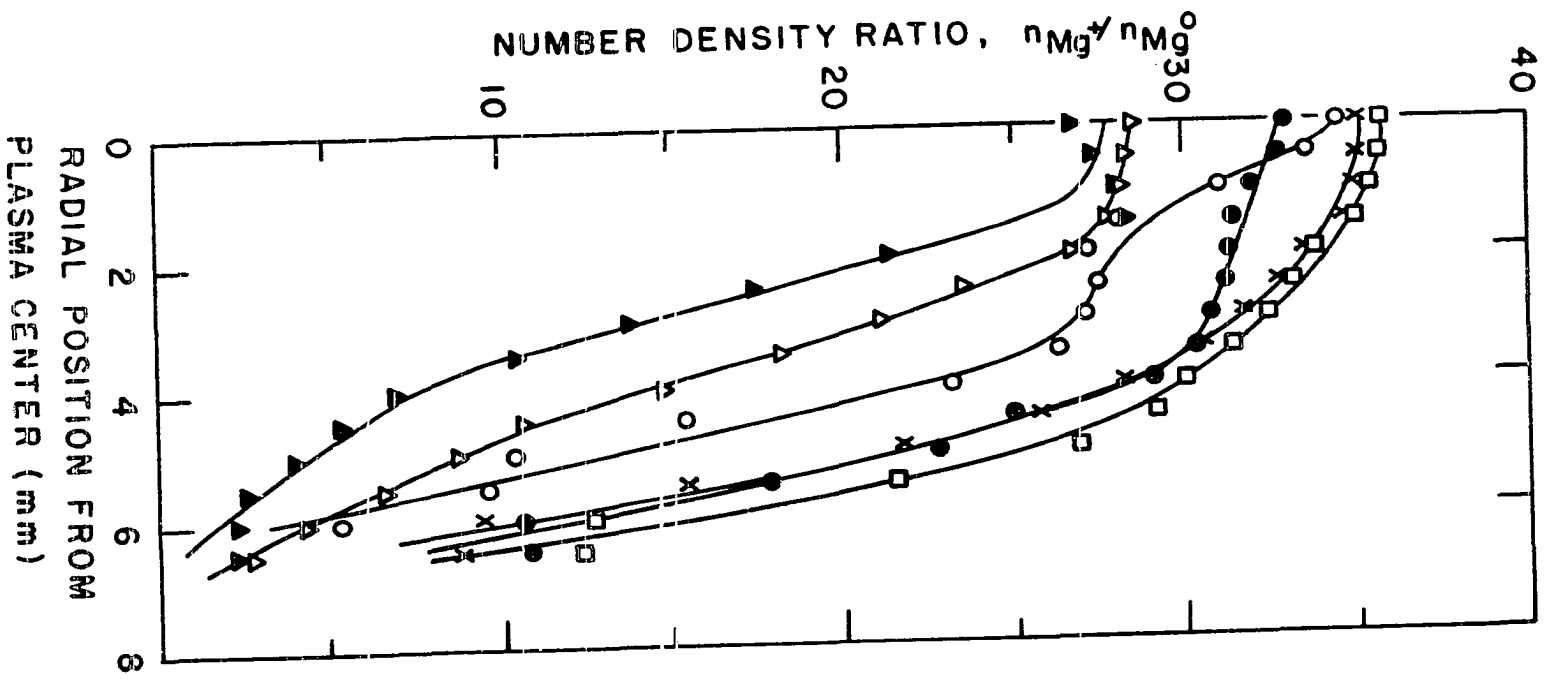


Figure 11. Radial Saha-Eggert's electron density distributions at 15, 20, and 25 mm for Mg atom/ion line combinations; 10 µg Mg/ml (—○—, —□—, —△—), 10 µg Mg/ml + 6900 µg Na/ml (—●—, —■—, —▲—)

profiles at 15 and 20 mm observation heights show little change upon the addition of an EIE to the plasma. The primary change in the 25 mm height profile is in the wing region, where there is an enhancement significantly greater than the experimental error. It is also evident that the toroidal n_e distribution at 15 mm disappears at 20 and 25 mm, being replaced at the latter heights by bell-type profiles which are relatively uniform for the central 4 mm of the plasma. The change in n_e in this central axial zone upon the addition of Na is insignificant. The surprisingly small changes in n_e and temperature profiles at 15 and 20 mm upon the addition of Na as an EIE suggest that changes in the total composition of the sample do not affect the radial excitation temperature nor degree of ionization of analyte species in a dominant manner. The significant increase in n_e in the wings of the 25 mm profile upon addition of Na as an EIE suggests that ionization suppression may play a role, if a significant fraction of the analyte diffuses into this region. These results are in harmony with empirical observations reported by Larson et al. (103) and by Boumans and de Boer (1c) which indicated low levels of interelement effects at low observation heights (15 to 20 mm) and increased effects higher in the plasma.

The radial n_{Mg^+}/n_{MgO} profiles obtained from Equation 6 for the Mg atomic and ionic lines listed in Table IV are given in Figure 12. With consideration of potential errors, the

Figure 12. Radial number density ratios, n_{Mg^+}/n_{MgO} ,
at 1000W and 1.0 l/min aerosol carrier gas
flow for Mg lines employed in electron
density calculations; 10 $\mu\text{g Mg/ml}$ at 15 mm
(—○—), 20 mm (—□—), and 25 mm (—△—);
10 $\mu\text{g Mg/ml}$ + 6900 $\mu\text{g Na/ml}$ at 15 mm
(—●—), 20 mm (—X—), and 25 mm (—▲—)



ratios are essentially unchanged upon addition of Na as an EIE. These profiles also clearly show that Mg is more than 90% ionized in the central axial zone of the plasma at all observation heights. The radial n_{X^+}/n_{X^0} ratios which were obtained for the other species given in Table IV are listed in Table VIII. The decrease in these ratios upon addition of Na to the plasma indicates the existence of some analyte ionization suppression but the degree of this suppression is much smaller than that commonly observed in flames (104). The data in this table also clearly show the high degree of ionization of analyte species in the central axial region of the plasma. In particular, Ca is more than 99% ionized and Zn more than 50% ionized even when a high concentration of an EIE is present in the plasma. These results correlate well with recent empirical observations at this laboratory which have been made on a direct-reading polychromator plasma system that has been in daily use for three years. The experience with this instrument (107) has indicated that superior powers of detection may be obtained with the ionic lines of many analytes particularly those elements with low ionization energy. Indeed, the fact that many of the most sensitive lines of these elements originated from singly ionized species was recorded by Dickinson and Fassel (108) in 1969 and later by Souilliant and Robin (109). In view of these observations it is curious that Boumans and de Boer (1c)

Table VIII. Radial ion to atom number density ratios, $n_{X^+}(R)/n_{X^0}(R)$, for Zn, Cd, Fe and Ca with and without added Na at 1000W, 1.0 l/min, and 15 mm height

Radius (mm)	Without Na				With 6900 $\mu\text{g Na/ml}$			
	Zn	Cd	Fe	Ca	Zn	Cd	Fe	Ca
0.0	2.1	6.2	18	610	1.5	4.4	15	300
0.5	2.1	6.2	18	590	1.5	4.4	15	300
1.0	2.1	5.9	17	540	1.5	4.5	15	310
1.5	2.0	5.2	16	440	1.5	4.6	15	280
2.0	1.9	5.0	16	430	1.5	4.6	16	320
2.5	1.9	4.8	16	410	1.5	4.6	15	340
3.0	1.8	4.6	15	310	1.5	4.6	15	320
3.5	1.8	4.2	15	380	1.4	4.6	13	310
4.0	1.8	3.5	14	390	1.5	4.6	12	260
4.5	1.9	3.0	14	190	1.4	4.9	11	230
5.0	1.9	2.7	13	190	1.4	4.9	8.6	240
5.5	1.9	3.8	10	170	1.0	4.3	7.1	170
6.0	2.0	2.9	8.8	160	0.3	4.2	4.9	100
6.5	---	---	---	---	0.8	4.3	4.5	100

were surprised to rediscover this fact; namely, that the ion lines of the alkaline earth elements yielded far better detection limits than the neutral atom lines for their "compromise" plasma operating conditions.

Additional documentation that n_e do not change upon addition of an EIE is found in the effective (noninverted) half-widths of the H_{β} and Ar I line profiles shown in Table IX. This observation was confirmed by the effective n_e values obtained from these Stark broadening measurements and those obtained from Saha-Eggert's calculations for Mg lines which are plotted in Figure 13. The Stark broadening n_e values for the H_{β} and the two Ar I lines are essentially identical at the various observation heights and, in harmony with the Saha n_e values, did not change significantly when the EIE was added to the plasma. In agreement with the radial measurements plotted in Figure 10, the effective Saha values are 30- to 50-fold smaller than the Stark broadening n_e values.

Analyte Excitation

The large differences between n_e values calculated from Stark broadening methods and those obtained from Saha-Eggert's ionization considerations (Figures 10 and 13) may be interpreted to support the earlier stated conclusion that LTE does not exist for the plasma operating conditions employed in this investigation. From observations quite similar to

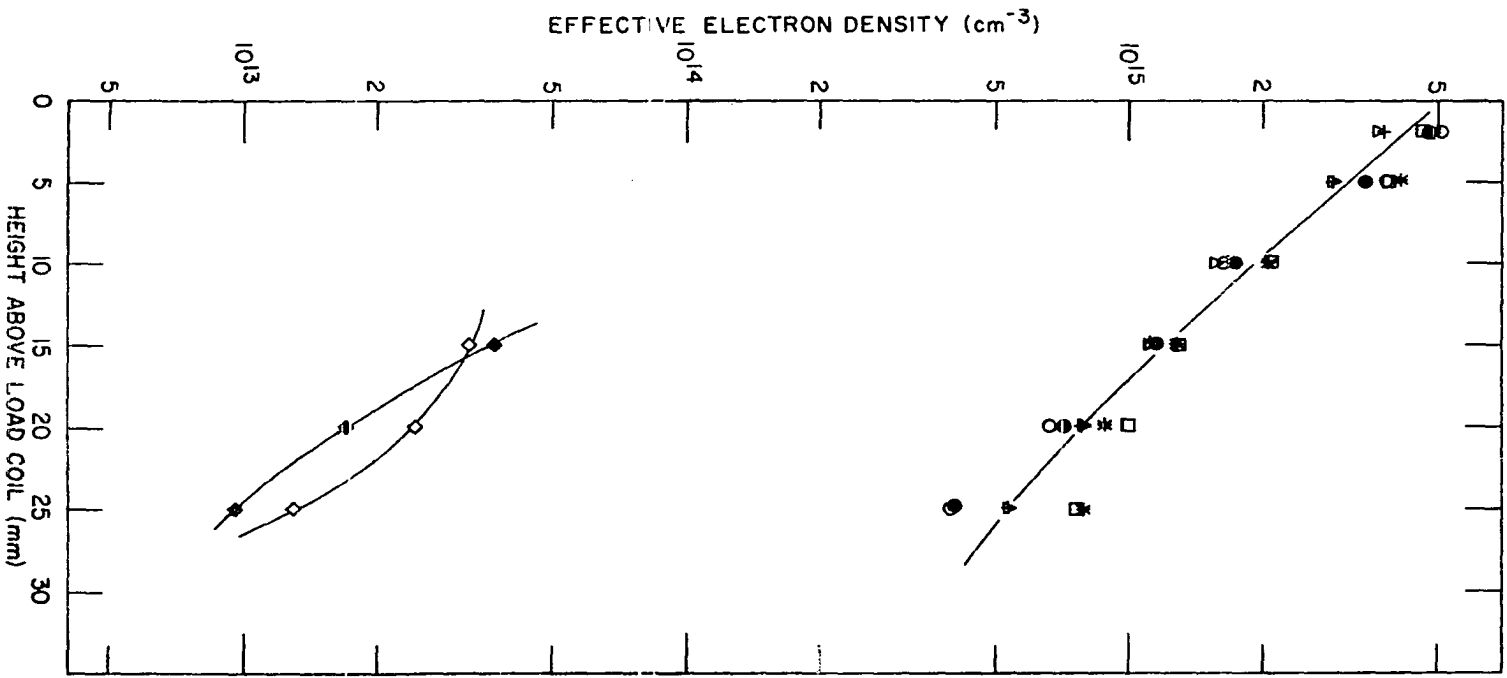
Table IX. Effective half-widths^a of H_β and Ar I lines measured at the plasma axis for 1000W forward power and 1.0 l/min aerosol carrier gas flow

Observation Height (mm)	Ar I 542.135 nm		Ar I 549.588 nm		H _β 486.13 nm	
	Without Na	With Na ^b	Without Na	With Na	Without Na	With Na
2	2.36	2.49	1.79	1.88	5.47	5.25
5	1.88	2.01	1.40	1.40	4.49	4.16
10	1.05	1.04	0.808	0.851	2.63	2.74
15	0.674	0.656	0.565	0.568	2.08	2.08
20	0.522	0.487	0.434	0.435	1.53	1.59
25	0.432	0.443	0.346	0.348	1.15	1.15

^aHalf-widths expressed in units of Angstroms (Å), 10 Å = 1 nm.

^b6900 µg Na/ml added to the plasma.

Figure 13. Effective electron density at 1000W and 1.0 l/min aerosol carrier gas flow for several observation heights. Stark broadening with deionized water nebulized; H_{β} 486.13 nm (—○—), Ar I 542.14 nm (—□—), Ar I 549.59 nm (—△—). Stark broadening with 6900 $\mu\text{g Na/ml}$ nebulized; H_{β} 486.13 nm (—●—), Ar I 542.14 nm (—*—), Ar I 549.59 nm (—+—). Saha-Eggert's ionization; 10 $\mu\text{g Mg/ml}$ (—◇—), 10 $\mu\text{g Mg/ml}$ + 6900 $\mu\text{g Na/ml}$ (—◆—)



those reported in this dissertation, Jaroz et al. (2b) and Mermet (17) have in fact concluded that LTE does not exist for their plasma operating conditions. Mermet (17b) has suggested that Ar I metastables are involved in analyte excitation through Penning ionization reactions, and that Ar II levels may also be involved through a similar process. Robin and Trassy (110) observed stimulated emission for resonance lines of Al and Ti below a critical concentration while above this concentration atomic absorption prevailed. These authors suggested that the observation of this phenomenon indicated the absence of LTE in their 40 MHz discharge. The calculations of Hey (111) and Cillars et al. (112) on the n_e criteria necessary to ensure LTE suggest that low lying metastable levels play a role in population of excited states for the species considered. Indeed, energy transfer mechanisms involving rare gas metastables are well known and are observed in many classes of low pressure discharges (113-115). However, experimental observations at atmospheric pressure are not readily obtained because the metastable level lifetimes are much shorter due to collisional deactivation. It should be noted that Hey's calculations are for homogeneous nonhydrogenic plasmas and hence, may not apply to plasmas used for spectrochemical purposes which generally possess relatively large spatial gradients in temperature and analyte number densities.

The n_e differences may alternately be interpreted to indicate the presence of significant electric and/or magnetic fields induced in the plasma region by the load coil that are not accounted for by particle field considerations in the Stark broadening theory. An approximate calculation of Stark splitting of the H_β line in a static electric field (96,116, 117) reveals that $\sim 20,000$ volts/cm would account for the increased broadening. Magnetic fields of $\sim 10,000$ gauss would be required to produce splitting equivalent to that produced by the particle field (96). Calculations for typical atmospheric pressure argon induction discharges assumed to be in LTE (6,118) indicate that axial magnetic fields and azimuthal electric fields should be on the order of a few hundred gauss and a few hundred volt/cm, respectively. For a pure induction discharge in LTE the axial electric field is zero (118). Field strength calculations for nonequilibrium plasmas are generally not available because the theory is not well understood. Although the nonparticle field strengths calculated by the models mentioned above are very much smaller than necessary to produce significant line splittings, the unknown nature of possible nonequilibrium fields precludes a definitive interpretation of their effects on line broadening in the present context.

The present inability to interpret n_e differences in a more definitive manner should not detract from the fact that the results of this dissertation research correlate very well

with empirical observations (1c,103) which indicate low levels of interelement effects at low observation heights and increased effects higher in the plasma. The surprisingly low sensitivity of n_e and temperature distributions at 15 and 20 mm to the addition of an EIE (see Figures 9 and 11) suggests that changes in the total composition of the sample should not affect radial excitation temperatures nor degree of ionization of analytes in a dominant manner. The significant increase in n_e in the wings of the 25 mm profile when Na is added as an EIE suggests that ionization suppression may play a role if a significant fraction of the analyte diffuses into these regions. Indeed, some evidence of this type of diffusion is provided by the Ca I 422.7 nm line profile data reported by Larson et al. (103), which showed a peculiar off-axis "hump" when Na was added to the plasma for an observation height of 20 mm. These results provide additional evidence that careful consideration of the region sampled by the viewing field of the spectrometer is an important factor when plasma performance is analyzed (18). This is especially true when the enlarged acceptance cone of the wide aperture optical systems commonly employed for the analytical applications of these plasmas samples a significant portion of the off-axis regions.

CHAPTER VI: SUGGESTIONS FOR FUTURE WORK

Although this investigation has aided in the understanding of several important aspects of analyte excitation in ICP's employed for spectrochemical analysis, a number of avenues of research remain open.

Certainly, the validity of the LTE assumption for different ICP operating conditions should be ascertained because the absolute interpretations of the results of many diagnostic methods (e.g., excitation temperature and Saha n_e measurements) are critically dependent upon LTE conditions prevailing in the plasma. The role of support gas and sample metastable levels should be elucidated because this may provide useful information about analyte excitation mechanisms and may help resolve the LTE question.

Studies concerning the effects on lateral intensity profiles and, subsequently Abel inversion calculations from asymmetries in the plasma torch, in the induced magnetic and electric fields, and in the gas flow patterns should be pursued. Improvements in the Abel inversion procedure should help to avert some of the problems encountered when toroidal lateral intensity distributions are inverted.

Investigations on the applications of other diagnostic techniques such as laser techniques (119-121) and interferometric (122,123) methods should be initiated because these techniques could provide powerful alternative approaches for

probing spatial particle density and temperature distributions in the plasma. The work proceeding in this laboratory on coupling a mass analyzer to an ICP (124) may also provide a valuable diagnostic tool.

Work on the spectroscopic probing of the spatially resolved radial excitation temperatures and n_e distributions experienced by analytes should continue because even though the results of these studies may lack absolute interpretation from lack of LTE in the plasma, valuable information will still be obtained on relative excitation trends (e.g., increased interelement effects may be partially or completely explained by a drastic change in the n_e distribution at 1.3 l/min aerosol carrier gas flow when an EIE is added to the plasma). Studies of the effects on excitation temperature and n_e distributions when ultrasonic nebulization of the sample solution is employed, with and without desolvation, may provide some insight into the reasons why better than order of magnitude improvements in ICP detection limits have been noted when this method was compared to pneumatic nebulization (1c,125).

Near the end of this dissertation research, work was begun on adaptation of a modular computer-controlled plasma facility (126) to perform automated lateral intensity profiling experiments. Progress in this area and suggestions for further modifications were summarized in several recent

research reports (127). An assembly language program to perform these experiments was written for the DEC PDP 8/e minicomputer on this system (127). This program was designed for the existing facilities but may easily be modified as the equipment is updated. The work on this system should be continued to facilitate profiling experiments by the efficient utilization of the minicomputer capability for on-line control of these experiments.

BIBLIOGRAPHY

1. For recent reviews on inductively-coupled plasma, analytical emission spectroscopy the reader is referred to:
 - (a) V. A. Fassel, "XVI Colloquium Spectroscopicum Internationale," Plenary Lectures, Heidelberg, 1971, pp. 63-93.
 - (b) V. A. Fassel and R. N. Kniseley, Anal. Chem., 46(13), 1110A, 1155A (1974).
 - (c) P. W. J. M. Boumans and F. J. de Boer, Spectrochim. Acta, 30B, 309 (1975).
 - (d) S. Greenfield, I. LL. Jones, H. McD. McGeachin, and P. B. Smith, Analytica Chim. Acta, 74, 225 (1975).
 - (e) S. Greenfield, H. McD. McGeachin, and P. B. Smith, Talanta, 23, 1 (1976).
2. (a) J. M. Mermet and J. P. Robin, Rev. int. Htes Temp. et Réfract., 10, 133 (1973).
- (b) J. Jaroz, J. M. Mermet, and J. Robin, C. R. Acad. Sc. Paris, 278B, 885 (1974).
3. (a) H. U. Eckert and D. C. Pridmore-Brown, J. Appl. Phys., 42(12), 5051 (1971).
- (b) H. U. Eckert, High Temp. Sci., 6, 99 (1974).
4. P. D. Scholz and T. P. Anderson, J. Quant. Spectrosc. Radiat. Transfer, 8, 1411 (1968).
5. A. D. Stokes, J. Phys. D: Appl. Phys., 4, 916 (1971).
6. R. C. Miller and R. J. Ayen, J. Appl. Phys., 40(13), 5260 (1969).
7. F. Molinet, C. R. Acad. Sc. Paris, 262B, 1377 (1966).
8. D. W. Hughes and E. B. Wooding, Phys. Lett., 24A, 70 (1967).
9. P. D. Johnston, Phys. Lett., 20(5), 499 (1966).

10. (a) V. M. Gol'dfarb and S. V. Dresvin, High Temp., 3(3), 303 (1965).
(b) S. V. Dresvin, A. V. Donskoi, and V. M. Gol'dfarb, Sov. Phys.-Tech. Phys., 10, 1270 (1966).
11. "High Frequency Induction Plasmatrons," in Physics and Technology of Low Temperature Plasmas, S. V. Dresvin, Ed., Moscow-Atomizdat, 1972, translated by T. Cheron and H. U. Eckert.
12. K. Visser, F. P. Hamm, and P. B. Zeeman, Appl. Spectrosc., 30(1), 34 (1976).
13. A. R. Apsit, Sov. Phys.-Tech. Phys., 15, 1180 (1971).
14. V. M. Gol'dfarb and V. Kh. Goikman, J. Appl. Spectrosc., 8(2), 119 (1968).
15. J. F. Alder and J. M. Mermet, Spectrochim. Acta, 28B, 421 (1973).
16. G. R. Kornblum and L. de Galan, Spectrochim. Acta, 29B, 249 (1974).
17. (a) J. M. Mermet, Spectrochim. Acta, 30B, 383 (1975).
(b) J. M. Mermet, C. R. Acad. Sc. Paris, 381B, 273 (1975).
18. D. J. Kalnicky, R. N. Kniseley, and V. A. Fassel, Spectrochim. Acta, 30B, 511 (1975).
19. P. W. J. M. Boumans and F. J. de Boer, Spectrochim. Acta, 31B (1976).
20. H. G. C. Human and R. H. Scott, preprint of paper submitted to Spectrochim. Acta.
21. R. M. Barnes and R. G. Schleicher, Spectrochim. Acta, 30B, 109 (1975).
22. R. M. Barnes and S. Nikdel, Appl. Spectrosc., 30(3), 310 (1976).
23. H. U. Eckert, Aerospace Report No. ATR-76(9472)-1, El Segundo, CA, 1976.
24. J. T. Jeffries, Spectral Line Formation, Blaisdell Pub. Co., Waltham, MA, 1968.

25. S. S. Penner, Quantitative Molecular Spectroscopy and Gas Emissivities, Addison-Wesley Pub. Co., Inc., Reading, MA, 1959.
26. M. W. Zemansky, Heat and Thermodynamics, 4th ed., McGraw-Hill, Inc., New York, NY, 1957.
27. W. Snellman and J. A. Smit, J. Internat. Metrologie Sc., 4, 123 (1968).
28. T. J. Hollander, Amer. Inst. Aeronaut. Astronaut. J., 6(3), 385 (1968).
29. H. W. Drawin, High Pres.-High Temp., 2, 359 (1970).
30. I. Reif, "Spectroscopic Temperature Measurements of Flames and their Physical Significance," Ph.D. Thesis, Iowa State University, Ames, IA, 1971.
31. H. W. Drawin and P. Felenbok, Data for Plasmas in Local Thermodynamic Equilibrium, Gauthier-Villars, Paris, 1965.
32. H. Conrads, Appl. Spectrosc. Rev., 6(2), 135 (1972).
33. I. Reif, V. A. Fassel, and R. N. Kniseley, Spectrochim. Acta, 28B, 105 (1973).
34. J. J. deGroot and A. J. Jack, J. Quant. Spectrosc. Radiat. Transfer, 13, 615 (1973).
35. R. Hefferlin, Chapter 2 in Progress in High Temperature Physics and Chemistry, C. A. Rouse, Ed., Pergamon Press, New York, NY, 1969.
36. H. R. Griem, Plasma Spectroscopy, McGraw-Hill, Inc., New York, NY, 1964.
37. J. R. Sanmartin, Phys. Fluids, 15(3), 391 (1972).
38. J. Rubinstein and J. G. Laframboise, Phys. Fluids, 15(7), 1259 (1972).
39. M. Numono, O. Furukawa, and I. Michiyoshi, Plasma Phys., 13, 992 (1971).
40. P. W. J. M. Boumans, Theory of Spectrochemical Excitation, Hilger & Watts, LTD, London, 1966; "Excitation of Spectra," in Analytical Emission Spectroscopy, E. L. Grove, Ed., Vol. 1, Part 2, Marcel Dekker, New York, NY, 1972.

41. "Electrical Probes," in Plasma Diagnostics, W. Lochte-Holtgreven, Ed., North-Holland Pub. Co., Amsterdam, 1968.
42. "Magnetic Probes" and "Electric Probes," in Plasma Diagnostic Techniques, R. H. Huddlestone and S. L. Leonard, Eds., Academic Press, New York, NY, 1965.
43. G. R. Jordon, Rev. Phys. Tech., 2, 128 (1971).
44. H. U. Eckert, J. Appl. Phys., 43(1), 46 (1972).
45. S. L. Leonard, J. Quant. Spectrosc. Radiat. Transfer, 12, 619 (1972).
46. S. V. Desai and W. H. Corcoran, J. Quant. Spectrosc. Radiat. Transfer, 8, 1721 (1968); 9, 1371 (1969).
47. A. E. Kadyshevich, Sov. Phys. Uspekhi, 5(2), 347 (1962).
48. B. Krakow, Appl. Optics, 5(2), 201 (1966).
49. O. H. Nestor and H. N. Olsen, SIAM Rev., 2(3), 200 (1960).
50. C. J. Cremers and R. C. Birkebak, Appl. Optics, 5(6), 1057 (1966).
51. M. P. Freeman and S. Katz, J. Opt. Soc. Am., 50(8), 826 (1960).
52. J. Friederish, Ann. Phys., 3, 327 (1959).
53. C. D. Maldonado, A. P. Caron, and H. N. Olsen, J. Opt. Soc. Am., 55(10), 1247 (1965).
54. C. D. Maldonado and H. N. Olsen, J. Opt. Soc. Am., 56(10), 1305 (1966).
55. H. N. Olsen, C. D. Maldonado, and G. D. Duckworth, J. Quant. Spectrosc. Radiat. Transfer, 8, 1419 (1968).
56. M. P. Freeman and S. Katz, J. Opt. Soc. Am., 53(10), 1172 (1963).
57. W. L. Barr, J. Opt. Soc. Am., 52(8), 885 (1962).
58. I. D. Kulagin, L. M. Sorokin, and E. A. Dubrouskaya, Opt. Spectrosc. (USSR), 32, 459 (1972).

59. "Radiation of Hot Gases (Thermal and Non-thermal)," in Plasma Diagnostics, W. Lochte-Holtgreven, Ed., North-Holland Pub. Co., Amsterdam, 1968.
60. R. Wilson, J. Quant. Spectrosc. Radiat. Transfer, 2, 477 (1962).
61. "Evaluation of Plasma Parameters," in Plasma Diagnostics, W. Lochte-Holtgreven, Ed., North-Holland Pub. Co., Amsterdam, 1968.
62. M. A. Gusinow, J. B. Gerado, and R. A. Hill, J. Quant. Spectrosc. Radiat. Transfer, 9, 383 (1969).
63. D. W. Swallom and P. D. Scholz, J. Quant. Spectrosc. Radiat. Transfer, 12, 107 (1972).
64. K. S. Seshadri and R. N. Jones, Spectrochim. Acta, 19, 1013 (1963).
65. L. deGalan and J. D. Winefordner, Spectrochim. Acta, 23B, 277 (1968).
66. F. P. Banfield and Martin C. E. Huber, Astrophys. J., 186, 335 (1973).
67. Martin C. E. Huber and W. H. Parkinson, Astrophys. J., 172, 229 (1972).
68. Martin C. E. Huber and E. F. Tubbs, Astrophys. J., 177, 847 (1972).
69. M. Martinez-Garcia, W. Whaling, and D. L. Mickey, Astrophys. J., 165, 213 (1971).
70. T. Garz and M. Kock, Astr. Astrophys., 2, 274 (1969).
71. T. Andersen and G. Sorensen, Astrophys. Lett., 8, 39 (1971).
72. J. M. Bridges and W. L. Weise, Astrophys. J., 161, 271 (1970).
73. (a) S. J. Wolnik, R. O. Berthal, and G. Wares, Astrophys. J., 162, 1037 (1970).
(b) J. M. Bridges and R. L. Kornblith, Astrophys. J., 192, 793 (1974).

74. A. R. Striganov and N. S. Sventitskii, Tables of Spectral Lines of Neutral and Ionized Atoms, IFI/Plenum, New York, NY, 1968.
75. B. D. Adcock and W. E. G. Plumtree, J. Quant. Spectrosc. Radiat. Transfer, 4, 29 (1964).
76. B. S. Malone and W. H. Corcoran, J. Quant. Spectrosc. Radiat. Transfer, 6, 443 (1966).
77. C. S. Corliss and J. B. Shumaker, Jr., J. Res. N. B. S., 71A, 575 (1967).
78. B. T. Wujec, Acta Phys. Polonica, 36, 269 (1969).
79. W. E. Gericke, Z. Astrophysik, 53, 68 (1961).
80. B. Wende, Z. Physik, 213, 341 (1968).
81. P. R. Bevington, Data Reduction and Error Analysis for the Physical Sciences, McGraw-Hill, Inc., New York, NY, 1969.
82. R. D. Sacks, Ph.D. Thesis, Department of Chemistry, University of Wisconsin, Madison, WI, 1969.
83. "Spectral Intensities," in Plasma Diagnostic Techniques, R. H. Huddleston and S. L. Leonard, Eds., Academic Press, New York, NY, 1965.
84. W. F. Meggers, C. H. Corliss, and B. F. Scribner, Tables of Spectral-Line Intensities Arranged by Elements, National Bureau of Standards, Washington, D.C., Monograph 32-Part I, December, 1961.
85. T. Andersen, J. Desesquelles, K. A. Jensen, and G. Sorensen, J. Opt. Soc. Am., 1199 (1970); J. Quant. Spectrosc. Radiat. Transfer, 10, 1143 (1970).
86. G. E. Assousa and W. H. Smith, Astrophys. J., 176, 259 (1972).
87. T. Andersen and G. Sorensen, J. Quant. Spectrosc. Radiat. Transfer, 13, 369 (1973).
88. Martin C. E. Huber, Astrophys. J., 190, 237 (1974).
89. S. R. Bauman and W. H. Smith, J. Opt. Soc. Am., 60, 345 (1970).

90. W. L. Weise, M. V. Smith, and B. M. Miles, Atomic Transition Probabilities, Vol. II. Sodium Through Calcium, National Bureau of Standards, Washington, D.C., NSRDS-NBS22, October, 1969.
91. W. W. Smith and A. Gallagher, Phys. Rev., 145, 26 (1966).
92. W. H. Smith and H. S. Liszt, J. Opt. Soc. Am., 61, 938 (1971).
93. "Line Broadening," in Plasma Diagnostic Techniques, R. H. Huddleston and S. L. Leonard, Eds., Academic Press, New York, NY, 1965.
94. M. Weston, "Determination of the Electron Density and Temperature of a Plasma by the Application of Line-Broadening Theory to Observed Line Profiles," National Physical Laboratory, NTIS Report No. N72-15680, 1971.
95. P. Kepple and H. R. Griem, Phys. Rev., 173, 317 (1968).
96. H. R. Griem, Spectral Line Broadening by Plasmas, Academic Press, New York, NY, 1974.
97. "Interpretation of Line Broadening and Line Shift," in Plasma Diagnostics, W. Lochte-Holtgreven, Ed., North-Holland Pub. Co., Amsterdam, 1968.
98. C. R. Vidal, J. Cooper, and E. W. Smith, Astrophys. J. Supp. Series No. 214, 25, 37-136 (1973).
99. W. L. Weise, D. E. Kelleher, and D. R. Paquette, Phys. Rev. A, 6(3), 1132 (1972).
100. R. H. Scott, V. A. Fassel, R. N. Kniseley, and D. E. Nixon, Anal. Chem., 46, 75 (1974).
101. R. N. Kniseley, V. A. Fassel, and C. C. Butler, Clin. Chem., 19(8), 807 (1973).
102. R. N. Kniseley, H. Amenson, C. C. Butler, and V. A. Fassel, Appl. Spectrosc., 28(3), 285 (1974).
103. G. F. Larson, V. A. Fassel, R. H. Scott, and R. N. Kniseley, Anal. Chem., 47, 238 (1975).
104. Analytical Flame Spectroscopy, R. Mavrodineanu, Ed., Macmillan and Co., LTD, London, 1970.

105. (a) J. M. Mermet and J. Robin, Analytica Chim. Acta, 70, 271 (1975).
(b) M. H. Abdallah, J. M. Mermet, and C. Trassy, preprint of paper submitted to Analytica Chim. Acta.
106. H. Chuang, Appl. Optics, 4(12), 1589 (1965).
107. R. K. Winge, unpublished data, Ames Laboratory, USERDA, Iowa State University, Ames, IA.
108. G. W. Dickinson and V. A. Fassel, Anal. Chem., 41, 1021 (1969).
109. J. C. Souilliant and R. P. Robin, Analisis, 1, 427 (1972).
110. J. Robin and C. Trassy, C. R. Acad. Sc. Paris, 281B, 345 (1975).
111. J. D. Hey, J. Quant. Spectrosc. Radiat. Transfer, 16, 69 (1976).
112. W. A. Cillars, J. D. Hey, and J. P. S. Rash, J. Quant. Spectrosc. Radiat. Transfer, 15, 963 (1975).
113. D. W. Setser and D. H. Stedman, J. Chem. Phys., 49, 467 (1968); 52, 3957 (1970); 53, 1004 (1970).
114. J. Jolly and M. Touzeau, J. Quant. Spectrosc. Radiat. Transfer, 15, 863 (1975).
115. K. W. Busch and T. J. Vickers, Spectrochim. Acta, 28B, 85 (1973).
116. H. E. White, Introduction to Atomic Spectra, McGraw-Hill, Inc., New York, NY, 1934.
117. H. G. Kuhn, Atomic Spectra, Academic Press, New York, NY, 1962.
118. P. W. Schreiber, A. M. Hunter, II, and P. Taylor, IEEE Trans. Plasma Sci., PS-1(4), 60 (1973).
119. T. K. Cheng and Lee W. Casperson, J. Appl. Phys., 46(5), 1961 (1975).
120. C. DeMichelis and R. Papoular, Plasma Phys., 17, 1155 (1975).

121. "The Laser as a Tool for Plasma Diagnostics," in Plasma Diagnostics, W. Lochte-Holtgreven, Ed., North-Holland Pub. Co., Amsterdam, 1968.
122. I. M. Podgorny, Topics in Plasma Diagnostics, IFI Plenum, New York, NY, 1971.
123. "Optical Interferometry," in Plasma Diagnostic Techniques, R. H. Huddleston and S. L. Leonard, Eds., Academic Press, Inc., New York, NY, 1965.
124. R. S. Houk, unpublished dissertation research, Department of Chemistry, Iowa State University, Ames, IA.
125. K. W. Olson, W. J. Haas, Jr., and V. A. Fassel, submitted to Anal. Chem.
126. A. Montaser and V. A. Fassel, submitted to Anal. Chem.
127. D. J. Kalnicky, Quarterly Research Reports, Ames Laboratory, USERDA, Iowa State University, Ames, IA.
128. D. G. Scranton and E. G. Manchester, The Use of Simplotter, A High Level Plotting System, Ames Laboratory, USERDA, Iowa State University, Ames, Ia, Report No. IS-2305 (Rev. 1), November, 1972.
129. F. B. Hildebrand, Methods of Applied Mathematics, 2nd ed., Prentice-Hall Inc., Englewood Cliffs, NJ, 1965.
130. "Plasma-Jet Temperature Measurements," in Optical Spectrometric Measurements of High Temperatures, P. J. Dickerman, Ed., The University of Chicago Press, Chicago, IL, 1961.
131. P. B. Gooderum and G. P. Wood, NACA Technical Note No. 2173, August, 1950.
132. (a) H. Hormann, Z. Physik, 97, 539 (1935).
(b) W. J. Pearce in Optical Spectrometric Measurements of High Temperatures, P. J. Dickerman, Ed., The University of Chicago Press, Chicago, IL, 1961.
133. D. W. Blair, J. Quant. Spectrosc. Radiat. Transfer, 14, 325 (1974).

134. I. D. Kulagin, I. M. Sorokin, and E. A. Dubrovskaya, Opt. Spectrosc. (USSR), 32, 459 (1972).
135. Handbook of Chemistry and Physics, 48th ed., The Chemical Rubber Co., Cleveland, OH, 1967.
136. C. E. Moore, Atomic Energy Levels, National Bureau of Standards Circular 467, Vols. 1-3, 1949, 1952, 1958.
137. W. B. Barnett, Ph.D. Thesis, Iowa State University, Ames, IA, 1968.
138. IMSL LIBRARY 1, Edition 4, International Mathematical & Statistical Libraries, Inc., Houston, TX, November, 1974.

ACKNOWLEDGEMENTS

More individuals have contributed to the events over the past twenty-seven and one-half years preceding this point in time than I can properly acknowledge; to them my deepest appreciation.

Without the expertise and many long hours contributed by George Holland of the Ames Laboratory Instrument Service Group, the stabilization of the RF generator necessary for the successful completion of this project could not have been accomplished. The unsurpassed skills and superb craftsmanship of the master machinists and glass blowers must also be acknowledged. Gary Wells, Harry Amenson, Tom Johnson, Eldon Ness, and Harold Hall were major contributors to the success of my experiments.

The guidance and critical review of this work by Dr. Velmer A. Fassel and Dr. Richard N. Kniseley is greatly appreciated. The financial support granted me by the National Science Foundation and the Shell Companies Foundation is gratefully acknowledged.

Above all, I am thankful for the loving guidance and encouragement of my parents, Frank and Bess Kalnicky, for had they made another decision some twenty-eight and one-quarter years ago, I would not have been able to begin this project.

APPENDIX A:

ABEL INVERSION AND TEMPERATURE PROGRAM

The Abel inversion and radial temperature calculations were performed in a single FORTRAN IV computer program. A complete listing of the source statements of the most recent version of this program is included as C337TEM2. [A Cal-Comp Digital Incremental Plotter could be (optionally) employed off-line to plot the radial intensity and temperature data obtained from this program.] In conjunction with the plotting subroutines (RADPL, TEMP, and SLOPET) in this program, two ISU library programs, GRAPH and GRAPHS, were utilized. These routines were part of the SIMPLOTTER (128) library, which was available for graph production. For an installation without SIMPLOTTER, the RADPL subroutine and the CALL RADPL statement in the main program should be removed. The CALL GRAPH and CALL GRAPHS statements in subroutines TEMP and SLOPET should also be removed. In this manner the program size will be reduced and the plotting capability will be lost. The data card input variable requirements are outlined in Table A-1 and these variables are defined in the beginning of the program listing.

An earlier version of this program (C337TEM1) was also employed for some inversions of the lateral relative intensity profiles obtained for Fe I lines. This earlier program incorporated a different polynomial fitting method in the Abel

inversion subroutine (CBABEL) than the one used in the C337TEM2 subroutine, DKABEL (see Appendix B). An F-test for goodness to fit (81) was incorporated into the latter program; this test sometimes yielded fits of artificially high degree to the bell-type Fe I relative intensity data. Subsequently, erroneous radial temperature profiles were calculated from the resulting intensities, particularly for the observation height of 15 mm. These profiles were recognized by: (1) very large calculation uncertainties for the radial intensities and temperatures obtained (cf., Equation B36, Appendix B), and (2) the peculiar shaped radial intensity and temperature profiles that resulted from these inversions especially at 15 mm. For the latter, unrealistically steep off-axis peaks were sometimes obtained in the toroidal temperature profiles typical for this observation height. These situations were corrected by: (1) employing DKABEL in C337TEM2 but, restricting the fits to be a maximum of 2-nd degree, or (2) employing CBABEL in C337TEM1, which incorporated fixed 2-nd degree fits to all profile zones (cf., Figure B-3, Appendix B) but was more restrictive with respect to data input. For the latter, the lateral relative intensity profiles were required to consist of equally spaced data points in multiples of $5n+1$ where, $n \geq 2$. It was sometimes difficult to obtain lateral relative intensity data that complied with these criteria. However, in most cases employing the

restricted 2-nd degree (maximum) fits with C337TEM2 remedied the problem, precluding the necessity of resorting to the C337TEM1 method.

Table A-1. Data card requirements for C337TEM2

Type #	# Cards	Columns	Variable Name	Format	Remarks
1	1	1- 5	NSETS	I5	Number of profile data sets
2	1/set	1-60 61-80	TITLE DLAB	15A4 5A4	Experiment description label Plot description label
3	1/set	1- 5 6-10 11-30	LKODE IARTP ELNAME	I5 I5 5A4	Indicates Fe/Ar or other lines used Selects Ar transition probability data set Name of element other than Fe or Ar (punch LKODE = 99, this is redefined to be LKODE = 3 in subroutine PNTORG)
4	1/set	1- 5 6-10	NLZ IWT	I5 I5	Number of lines (4 max) End point weighting selection (used with subroutine SPLINE)
5	1/set	1-28 31-70	WAVE DELA	4F7.2 4F10.0	Line wavelength array (Angstrom units) Transition probability uncertainty array
6	1/set	1- 5 6-10 11-15 21-25 26-30 31-35 36-40 41-45 46-50	L1 L2 L3 L5 NL NH KPLOT1 KPLOT2 KPLOT3	I5 I5 I5 I5 I5 I5 I5 I5 I5	Intensity plot option switch Spline fit option switch Two-line temperature calculation option (Fe lines only) Slope temperature calculation option Pointer to starting F-test value Pointed to ending F-test value Option to plot Fe two-line T's Option to plot average Fe two-line T's Option to plot slope T's

Table A-1. (Continued)

Type #	# Cards	Columns	Variable Name	Format	Remarks	
		51-55	KLINE1	I5	Option to select Fe two-line T's to plot	
		56-60	KLINE2	I5		
		61-65	KPNED1	I5		Option to punch lateral T's on cards
		66-70	KPNED2	I5		Option to punch radial T's on cards
7	1/set	1- 2	N	I2	Number of lateral intensities (15 max)	
8a	N/set	1-10 11-20	RBP(i,1) ARI(i,1)	F10.0 F10.0	Lateral displacement array for line #1 Corresponding lateral intensity array	
8b	N/set		RBP(i,2) ARI(i,2)		Same as 8a except for line #2 Same as 8a except for line #2	
8c	N/set		RBP(i,3) ARI(i,3)		Same as 8a except for line #3 Same as 8a except for line #3	
8d	N/set		RBP(i,4) ARI(i,4)		Same as 8a except for line #4 Same as 8a except for line #4	
9a-1	1/line	1- 5	NPTS	I5	Number of points for segmented spline fit	
		6-10	NS1	I5	Defines number of zones for Abel inversion poly fit	
		16-35	ELEMNT	5A4	Element identifier in subroutine SPLINE	
		36-45	ZPNT	F10.0	Distance between successive radial intensity calculations	
		46-50	LSHIFT	I5	Option to zero correct lateral displacements	
		51-60	XZERO	F10.0	Zero position for lateral displacement array (used when LSHIFT = 1 specified)	

Table A-1. (Continued)

Type #	# Cards	Columns	Variable Name	Format	Remarks
		61-65	NFACTR	I5	Weight factor selection for endpoints of spline fits
		66-70	KWT	I5	Option to select reading uncertainty array for lateral intensities from cards
9a-2	NPTS/ line	1-10 11-20 21-30	XDIST YINT SIGMAY	F10.0 F10.0 F10.0	Smoothed lateral displacement array Corresponding lateral intensity array Corresponding uncertainty array
9b-1	1/line	1-5 6-10 11-20 21-30	IMA NS1 XPNT XBIG	I5 I5 F10.0 F10.4	Number of points in lateral intensity array Defines number of zones for Abel inversion poly fit (same as 9a-1 NS1) Distance between successive radial intensity calculations (same as 9a-1 ZNPT) Lateral position of profile maximum
9b-2	IMA/ line		XDIST YINT SIGMAY		Same as 9a-2 XDIST Same as 9a-2 YINT Same as 9a-2 SIGMAY

NOTE: Types 9a-1 and 9b-1 are mutually exclusive; 9a-1 is used only with subroutine SPLINE (L2 = 0) and 9b-1 only with subroutine XYCALC (L2 = 1)

Table A-1. (Continued)

Type #	# Cards	Columns	Variable Name	Format	Remarks
10a	1/set	1-40	GA	4F10.0	OPTIONAL: $g_{q,qp}^A$ array for Ar I lines listed in comment card section, used when LKODE = 2 and IARTP > 6
10b-1	1/set	1-40	EQ	4F10.0	OPTIONAL: Excitation energy of ELNAME lines employed, used when LKODE = 3
10b-2	1/set	1-40	GA	4F10.0	OPTIONAL: $g_{q,qp}^A$ array for ELNAME lines, used when LKODE = 3


```

        = 4, 4TH " " " " " " " " 51
        = 5, 5TH " " " " " " " " 52
        = 6, 6TH " " " " " " " " 53
    V 6, ALL 2-LINE T'S PLOTTED 54
KPNED1 = 1, LATERAL SLOPE T'S PUNCHED ON CARDS FOR USE IN 55
      THE ELECTRON DENSITY PROGRAM (C337EDEN) 56
KPNED2 = 1, RADIAL SLOPE T'S PUNCHED ON CARDS FOR USE IN 57
      THE ELECTRON DENSITY PROGRAM (C337EDEN) 58
IARTP  = 1, MALONE AND CORCORAN GA VALUES; ARGON LINES 59
      = 2, BUJEC GA 60
      = 3, ADDOCK AND PLUMTREE GA 61
      = 4, CORLISS AND SHUMAKER GA 62
      = 5, WENDE GA 63
      = 6, GERICKE GA 64
    > 6, READ IN GA DATA CARD AT END OF DATA DECK, 65
      4F10.0 FORMAT 66
      ARGON LINES USED: 4251.2,4259.4,4266.3,4272.2 ANG 67
LKODE=1, IARTP=9, BANFIELD AND HUBER (1973) GA VALUES 68
      USED FOR FE I LINES 69
LKODE=99, INPUT SPECIES IDENTIFIER AS ELNAME AND READ IN 70
      GA, EQ VALUES FOR SLOPE TEMP CALCULATION 71
      (TEMP CALCN OPTIONAL, SEE L5 SPECIFICATION) 72
73
74
75
76
** ARRAYS ** 77
78
RBP = EXPERIMENTALLY MEASURED LATERAL DISTANCE ARRAY 79
ARI = " " " " PEAK INTENSITY ARRAY 80
      CORRESPONDING TO 'RBP' ARRAY 81
N = NUMBER OF ELEMENTS IN 'RBP' OR 'ARI' ARRAY (NOT MORE 82
XDIST = MEASURED AND SMOOTHED LATERAL DISTANCE ARRAY, 83
      ORIGIN ZERO SHIFT CORRECTED WITH RESPECT TO 84
      EXPT MEASURED RBP ARRAY SO THAT XDIST=0 85
      CORRESPONDS TO GEOMETRIC CENTER 86
YINT = CORRESPONDING MEASURED AND SMOOTHED LATERAL INTENS 87
SIGMAY=CORRESPONDING ARRAY OF SIGMA VALUES FOR YINT 88
      ARRAY 89
RAD = INTERMEDIATE RADIAL INTENSITY ARRAY 90
RDI = " " " " DISTANCE " " CORRESPONDING T 91
      'RAD' ARRAY 92
RADINT = FINAL RADIAL DISTANCE ARRAY CONTAINING ELEMENTS 93
      CORRESPONDING TO 'RADINT' ARRAY 94
95
96
** INDEXES ** 97
98
KT = NUMBER OF ELEMENTS IN 'RAD' OR 'ARI' ARRAY 99
100

```


	DATA FNUM/0.5,1.0,2.5,5.0,10.0,25.0,50.0/	151
	READ (5,1003) NSETS	152
1003	FORMAT (I5)	153
	DO 10 NUM=1,NSETS	154
	READ (5,100) TITLE,DLAB	155
100	FORMAT (15A4,5A4)	156
	WRITE (6,101) TITLE,DLAB	157
101	FORMAT (1H1,10X,15A4,5A4,///)	158
	READ(5,1001) LKODE,IARTP,ELNAME	159
	READ(5,1000) NLZ,IWT	160
1000	FORMAT(2I5)	161
1001	FORMAT(2I5,5A4)	162
	READ (5,102) (WAVE(I),I=1,NLZ),(DELA(J),J=1,NLZ)	163
102	FORMAT (4F7.2,2X,4F10.0)	164
	CALL LINDEX (L1,L2,L3,L4,LS,NL,NH,KPLOT1,KPLOT2,KPLOT3,KLINE1,	165
	1KLINE2,KPNED1,KPNED2)	166
	READ (5,106) N	167
106	FORMAT (I2)	168
	DO 1 J=1,NLZ	169
	DO 1 I=1,N	170
107	FORMAT (2F10.0)	171
1	READ (5,107) RBP(I,J),ARI(I,J)	172
	DO 8 LZ=1,NLZ	173
	LAM=1	174
	CALL PNTORG(LZ,KM,WAVE,RBP,ARI,N,LKODE,ELNAME)	175
	GO TO (2,3),L2	176
2	CALL SPLINE (IMA,NS1,XDIV,XDIST,YINT,LAM,XPNT,LZ,XDTR,XD,XBIG,SIGM	177
	1AY,WAVE,IWT)	178
	GO TO 4	179
3	CALL XYCALC (IMA,NS1,XDIV,XDIST,YINT,LAM,XPNT,LZ,XDTR,XD,XBIG,SIGM	180
	1AY)	181
4	DO 8 NZ=NL,NH	182
	CALL DKABEL (XDTR,YINT,IMA,NS1,NZ,XPNT,RAD,RDI,KT,XD,XBIG,LZ,DELIR	183
	1,SIGMAY,L1,IWT)	184
	IF(KPNED2.NE.1) GO TO 5	185
	DO 199 IPUNCH=1,KT	186
2001	FORMAT(3F10.4,2X,'LINE',I3,2X,'FTEST PROB',F5.2,1X,5A4)	187
199	WRITE(7,2001) RAD(IPUNCH),RDI(IPUNCH),DELIR(IPUNCH),LZ,FNUM(NZ),DL	188
	1AB	189
	5 GO TO (7,6),L1	190
6	CALL RADPL (IMA,XDIST,YINT,N,RBP,ARI, LZ,RAD,RDI,LAM, DLA	191
	1B,KT,NZ)	192
7	CALL PNTMAP (LZ,KT,RAD,RDI,KM,ILZ,RADINT,RADIST,DELIR,DELINT)	193
8	CONTINUE	194
11	GO TO (9,10),LS	195
9	CALL TEMP (N,KT,RBP,ARI,RADIST,RADINT,NLZ,DLAB,L3,KM,NL,NH,LKODE,	196
	1KPLOT1,KPLOT2,KLINE1,KLINE2,DELA,DELINT,IARTP)	197
13	CALL SLOPET (N,KT,RBP,ARI,RADIST,RADINT,NLZ,DLAB,WAVE,KM,NL,NH,LKO	198
	1DE,KPLOT3,KPNED1,KPNED2,DELA,DELINT,IARTP)	199
10	CONTINUE	200

STOP	201
END	202
SUBROUTINE LINDEX (L1,L2,L3,L4,L5,NL,NH,KPLOT1,KPLOT2,KPLOT3,	203
IKLINE1,KLINE2,KPNED1,KPNED2)	204
READ (5,101) L1,L2,L3,L4,L5,NL,NH,KPLOT1,KPLOT2,KPLOT3,KLINE1,	205
IKLINE2,KPNED1,KPNED2	206
101 FORMAT(14I5)	207
L4=1	208
IF (NL) 4,3,1	209
1 IF (NH-NL) 4,2,2	210
3 IF (NH) 4,5,4	211
5 NL=1	212
NH=1	213
2 IF (L4) 6,6,7	214
7 IF (L1) 8,10,10	215
10 IF (L3) 8,11,11	216
11 L1=L1+1	217
L2=L2+1	218
L3=L3+1	219
L5=L5+1	220
RETURN	221
4 WRITE (6,102)	222
GO TO 12	223
6 WRITE (6,103)	224
GO TO 12	225
8 WRITE (6,104)	226
12 STOP	227
102 FORMAT (//10X'INPUT ERROR IN SWITCH NL OR NH')	228
103 FORMAT (//10X'INPUT ERROR IN SWITCH L4')	229
104 FORMAT (//10X'INPUT ERROR IN SWITCH L1 OR L3')	230
END	231
SUBROUTINE PNTORG(LZ,KM,WAVE,RBP,ARI,N,LKODE,ELNAME)	232
DIMENSION ELNAME(5)	233
DIMENSION WAVE(1),RBP(15,4),ARI(15,4)	234
KM=0	235
IF(LKODE.EQ.99) LKODE=3	236
GO TO (2,1,1,1),LZ	237
1 WRITE (6,100)	238
2 GO TO (4,5,7),LKODE	239
4 WRITE (6,101) LZ,WAVE(LZ)	240
GO TO 6	241
5 WRITE (6,103) LZ,WAVE(LZ)	242
GO TO 6	243
7 WRITE(6,104) LZ,ELNAME,WAVE(LZ)	244
104 FORMAT(5X,'LINE',I3,5X,'SA4,F7.2//,14X,'EXPERIMENTALLY MEASURED LAT	245
ERAL INTENSITY DATA'/21X,'CORRECTED FOR SPECTRAL RESPONSE'//26X,'X	246
2',11X,'I(X)')//)	247
100 FORMAT (1H1)	248
101 FORMAT (5X,'LINE',I3,5X,'- FE 1 - ',F7.2,//14X,'EXPERIMENTALLY	249
MEASURED LATERAL INTENSITY DATA'/21X,'CORRECTED FOR SPECTRAL RESPO	250

2NSE'//26X,'X',11X,'I(X)'	251
103 FORMAT (5X,'LINE',13,5X,'- AR I - ',F7.2, '//14X,'EXPERIMENTALLY	252
1MEASURED LATERAL INTENSITY DATA'//21X,'CORRECTED FOR SPECTRAL RESPO	253
2NSE'//26X,'X',11X,'I(X)'	254
6 DO 3 I=1,N	255
3 WRITE (6,102) RBP(I,LZ),ARI(I,LZ)	256
102 FORMAT (22X,F8.4,6X,F8.4)	257
RETURN	258
END	259
SUBROUTINE XYCALC (IMA,NS1, XDIV,XDIST,YINT,LAM,XPNT,LZ,	260
1XDTR,XD,XBIG,SIGMAY)	261
DIMENSION SIGMAY(1)	262
DIMENSION XDIST(1),YINT(1),XBIG(4),XDTR(1)	263
READ (5,100) IMA,NS1,XPNT,XBIG(LZ)	264
100 FORMAT (2I5,2(F10.4))	265
IF(XBIG(LZ).LT.0.0) GO TO 8	266
IF (LAM-1) 2,2,1	267
1 WRITE (6,101)	268
101 FORMAT (1H1)	269
2 WRITE (6,102) IMA	270
102 FORMAT(//14X,'LATERAL INTENSITY DISTRIBUTION HAS BEEN EXPERIMENTAL	271
1LY MEASURED WITHOUT SPLINE INTERPOLATION'//14X,'INPUT LATERAL DATA	272
2HAS BEEN ZERO CORRECTED FOR',13,2X,'POINTS',//T25,'X',T38,'U(X)',T	273
360,'SIGMA(U(X))',//)	274
DO 3 I=1,IMA	275
103 FORMAT (3F10.0)	276
104 FORMAT (T20,F10.4,T33,F10.4,T60,E11.4)	277
READ (5,103) XDIST(I),YINT(I),SIGMAY(I)	278
3 WRITE(6,104) XDIST(I),YINT(I),SIGMAY(I)	279
XD=ABS(XDIST(IMA))	280
DO 7 I=1,IMA	281
7 XDTR(I)=XDIST(I)/XD	282
XDIV=ABS(XDTR(2)-XDTR(1))	283
XPNT=XPNT/XD	284
RETURN	285
8 WRITE (6,105)	286
105 FORMAT (10X'ERROR IN XBIG INPUT')	287
STOP	288
END	289
SUBROUTINE PNTMAP (LZ,KT,RAD,RDI,KM,ILZ,RADINT,RADIST,DELIR,DELINT	290
1)	291
DIMENSION RAD(1),RDI(1),RADINT(51,4,7),RADIST(51,4,7),ILZ(4,7)	292
1,XHOLD(51),YHOLD(51),DELIR(51),DELINT(51,4,7)	293
KTHOLD=KT	294
KM=KM+1	295
WRITE (6,100) LZ,KT	296
DO 4 I=1,5	297
IF (KT - 30*I) 1,1,4	298
1 J=KT/I	299
IF (KT - I*J) 3,3,2	300

2	J=J+1	301
3	GO TO (5,6,7,8,9), I	302
4	CONTINUE	303
	WRITE (6,101)	304
	STOP	305
5	WRITE (6,102)	306
	GO TO 10	307
6	WRITE (6,103)	308
	GO TO 10	309
7	WRITE (6,104)	310
	GO TO 10	311
8	WRITE (6,105)	312
	GO TO 10	313
9	WRITE (6,106)	314
10	DO 16 L=1,J	315
	L1=L+J	316
	L2=L+2*J	317
	L3=L+3*J	318
	L4=L+4*J	319
	GO TO (11,12,13,14,15), I	320
11	WRITE (6,107) RDI(L),RAD(L)	321
	GO TO 16	322
12	WRITE (6,108) RDI(L),RAD(L),RDI(L1),RAD(L1)	323
	GO TO 16	324
13	WRITE (6,109) RDI(L),RAD(L),RDI(L1),RAD(L1),RDI(L2),RAD(L2)	325
	GO TO 16	326
14	WRITE (6,110) RDI(L),RAD(L),RDI(L1),RAD(L1),RDI(L2),RAD(L2),	327
	1RDI(L3),RAD(L3)	328
	GO TO 16	329
15	WRITE (6,111) RDI(L),RAD(L),RDI(L1),RAD(L1),RDI(L2),RAD(L2),	330
	1RDI(L3),RAD(L3),RDI(L4),RAD(L4)	331
16	CONTINUE	332
	WRITE (6,1000)	333
1000	FORMAT (1H1)	334
	WRITE (6,1001)	335
1001	FORMAT (20X,'J',8X,'LZ',8X,'KM',8X,'RADIST(J,LZ,KM)',6X,'RADINT(J,	336
	1LZ,KM)',6X,'DELINT(J,LZ,KM)')	337
	IF (RDI(1).GE.0.) GO TO 22	338
	INZERO=0	339
	DO 20 IN=1,KT	340
	IF (RDI(IN).LT.0.) GO TO 20	341
	INZERO=INZERO+1	342
	XHOLD(INZERO)=RDI(IN)	343
	YHOLD(INZERO)=RAD(IN)	344
20	CONTINUE	345
	DO 21 IOUT=1,INZERO	346
	RAD(IOUT)=YHOLD(IOUT)	347
21	RDI(IOUT)=XHOLD(IOUT)	348
	KT=INZERO	349
22	ILZ(LZ,KM)=KT	350


```

DO 17 I=1,KT
J=KT-I+1
RADIST(J,LZ,KM)=RDI(I)
RADINT(J,LZ,KM)=RAD(I)
DELINT(J,LZ,KM)=DELIR(I)
WRITE (6,1002) J,LZ,KM,RADIST(J,LZ,KM),RADINT(J,LZ,KM),DELINT(J,LZ
1,KM)
1002 FORMAT (20X,3(I3,8X),3(E11.4,10X))
RAD(I)=0.0
17 RDI(I)=0.0
KT=KTHOLD
RETURN
100 FORMAT (//19X,'LINE ',I1,' - RADIAL INTENSITIES FOR ',I3,
1' RADIAL POSITIONS IN SOURCE'//)
101 FORMAT (19X,'PRINT ERROR')
102 FORMAT (42X,'R',12X,'I(R)'//)
103 FORMAT (31X,'R',8X,'I(R)',20X,'R',8X,'I(R)'//)
104 FORMAT (31X,'R',8X,'I(R)',10X,'R',8X,'I(R)',10X,'R',8X,'I(R)'//)
105 FORMAT (31X,'R',8X,'I(R)',3(10X,'R',8X,'I(R)'//)
106 FORMAT (8X,'R',8X,'I(R)',4(10X,'R',8X,'I(R)'//)
107 FORMAT (39X,F7.4,6X,F9.5)
108 FORMAT (28X,F7.4,2X,F9.5,15X,F7.4,2X,F9.5)
109 FORMAT (28X,F7.4,2X,F9.5,2(5X,F7.4,2X,F9.5))
110 FORMAT (28X,F7.4,2X,F9.5,3(5X,F7.4,2X,F9.5))
111 FORMAT (5X,F7.4,2X,F9.5,4(5X,F7.4,2X,F9.5))
END
SUBROUTINE SPLINE (IMA,NS1,ZDIV,ZDIST,ZINT,LAM,ZPNT,LZ,ZDTR,ZD,ZBI
1G,ZSIG,ZWAVE,IWT)
IMPLICIT REAL*8(B-H,O-Y)
DIMENSION ZDIST(1),ZINT(1),ELEMNT(5),ZSIG(1),ZWAVE(1),FACTOR(6),YO
1UT(101,3),YINT(51),XDIST(51),SIGMAY(51),YMID(50,3),SIGMAS(50),ZDTR
2(1),WAVE(4),ZBIG(4)
DATA FACTOR/0.825D0,0.85D0,0.875D0,0.90D0,0.925D0,0.95D0/
EXECUTE SPLINE FIT AND VARIANCE ESTIMATE FO MIDPTS FOR EACH LINE:
TOT SIGMA = SQRT(FIT SIGMA**2+DATA SIGMA**2) DATA SIGMA IS TAKEN
AS AVERAGE OF SIGMA OF FOUR NEIGHBORING INPUT DATA POINTS EXCEPT
FOR THE ENDPOINTS WHERE IT IS TAKEN AS THE AVERAGE OF THE ENDPOINT
SIGMA AND THE TWO ADJACENT INTERIOR POINT SIGMA VALUES
WAVE(LZ)=ZWAVE(LZ)
I=LZ
CALL READS(NPTS,YINT,XDIST,ELEMNT,WAVE,XZERO,I,SIGMAY,LSHIFT,SCHK,
1NFACTR,NS1,ZPNT,KWT)
IWT=KWT
CALL INTERP (NPTS,YINT,XDIST,I,SCHK,YMID,NFACTR,FACTOR)
SIGMAS(1)=YMID(1,3)
SIG=(SIGMAY(1)+SIGMAY(2)+SIGMAY(3))/3.D0
YMID(1,3)=DSQRT(SIG**2+SIGMAS(1)**2)
NPTSS=NPTS-1

```

351
352
353
354
355
356
357
358
359
360
361
362
363
364
365
366
367
368
369
370
371
372
373
374
375
376
377
378
379
380
381
382
383
384
385
386
387
388
389
390
391
392
393
394
395
396
397
398
399
400

C
C
C
C
C
C

	DO 10 N=3,NPTSS	401
	J=N-1	402
	JJ=N-2	403
	NN=N+1	404
	SIGMAS(J)=YMID(J,3)	405
	SIG=(SIGMAY(JJ)+SIGMAY(J)+SIGMAY(N)+SIGMAY(NN))/4.DO	406
10	YMID(J,3)=DSQRT(SIGMAS(J)**2+SIG**2)	407
	N=NPTSS-1	408
	SIGMAS(NPTSS)=YMID(NPTSS,3)	409
	SIG=(SIGMAY(N)+SIGMAY(NPTSS)+SIGMAY(NPTS))/3.DO	410
	YMID(NPTSS,3)=DSQRT(SIG**2+SIGMAS(NPTSS)**2)	411
	NUP=NPTS+NPTS-1	412
	DO 30 N=1,NUP	413
	NN=(N/2)*2	414
	IF(NN.NE.N) GO TO 25	415
	LL=N/2	416
	DO 24 L=1,3	417
24	YOUT(N,L)=YMID(LL,L)	418
	GO TO 30	419
25	LLL=(N+1)/2	420
	YOUT(N,1)=XDIST(LLL)	421
	YOUT(N,2)=YINT(LLL)	422
	YOUT(N,3)=SIGMAY(LLL)	423
30	CONTINUE	424
C		425
C	CORRECT YOUT FOR ZERO SHIFT	426
C		427
	ITAG=0	428
	IF(LSHIFT.NE.1) GO TO 41	429
	JSTART=1	430
	DO 40 J=1,NUP	431
	YOUT(J,1)=YOUT(J,1)-XZERO	432
	IF(YOUT(J,1).GE.0.0) GO TO 40	433
	JSTART=J+1	434
40	CONTINUE	435
41	IF(LSHIFT.NE.1) JSTART=1	436
	DO 45 J=JSTART,NUP	437
	ITAG=ITAG+1	438
	ZDIST(ITAG)=YOUT(J,1)	439
	ZINT(ITAG)=YOUT(J,2)	440
45	ZSIG(ITAG)=YOUT(J,3)	441
	IMA=ITAG	442
C		443
C	DETERMINE POSITION OF MAX IN LATERAL INTENSITY ARRAY	444
C		445
	ZBIG(LZ)=ZDIST(3)	446
	DO 60 J=4,IMA	447
	JJJ=J-1	448
	IF(ZINT(J).GE.ZINT(JJJ)) ZBIG(LZ)=ZDIST(J)	449
60	CONTINUE	450

```

        IF(LAM-1) 65,65,64
64 WRITE(6,1000)
1000 FORMAT(1H1)
65 WRITE(6,1001) IMA
1001 FORMAT(//14X,'LATERAL INTENSITY DISTRN HAS BEEN FIT BY SEGMENTED
1 SPLINE, MIDPOINTS INTERPOLATED, AND SIGMAS DETERMINED',/,14X,'RESU
2 LTING LATERAL DATA HAS BEEN ZERO CORRECTED FOR',I3.2X,'POINTS',//T
325,'X',T38,'U(X)',T60,'SIGMA(U(X))',//)
        DO 66 J=1,IMA
1002 FORMAT (T20,F10.4,T33,F10.4,T60,E11.4)
66 WRITE(6,1002) ZDIST(J),ZINT(J),ZSIG(J)
        ZD=ABS(ZDIST( IMA))
        DO 67 J=1, IMA
67 ZDTR(J)=ZDIST(J)/ZD
        ZDIV=ABS(ZDTR(2)-ZDTR(1))
        ZPNT=ZPNT/ZD
        RETURN
        END
        SUBROUTINE READS (NPTS,YINT,XDIST,ELEMNT,WAVE,XZERO,I,SIGMAY,LSHIF
IT,SCHK,NFACTR,NS1,ZPNT,KWT)
        IMPLICIT REAL*8(A-H,O-Y)
        DIMENSION YINT(1),XDIST(1),ELEMNT(5),WAVE(1),SIGMAY(1)
C
C
C
        READ INPUT X,Y PAIRS FOR LINE I
C
C
        READ(5,100) NPTS,NS1,ELEMNT,ZPNT,LSHIFT,XZERO,NFACTR,KWT
100 FORMAT(2I5,5X,5A4,F10.0,IS,F10.0,2I5)
        DO 10 J=1,NPTS
101 FORMAT (3F10.0)
10 READ (5,101) XDIST(J),YINT(J),SIGMAY(J)
        SCHK=XDIST(NPTS)
        RETURN
        END
        SUBROUTINE INTERP (NPTS,YINT,XDIST,I,SCHK,YMID,NFACTR,FACTOR)
        IMPLICIT REAL*8(A-H,O-Z)
        DIMENSION YHOLD(50,5),XNORM(5),YNORM(6),XMID(5),YSTOR(50,5),YAVE(5
10),COEF(6,4),FACTOR(1),YINT(1),XDIST(1),YMID(50,3),SIGMA(50)
C
C
C
        CALCULATE SPLINE FIT FOR 6 PT INTERVALS BEGINNING AT XDIST(1) AND
        CONTINUE TO STOP: TABULATE MIDPOINT DIST, AVE VALUE,AND SIGMA
C
C
C
        DO 5 J=1,35
        YAVE(J)=0.DO
5 SIGMA(J)=0.DO
        KOUNT=0
        DO 999 J=1,NPTS
        JJ=J+5
        IF(JJ.GT.NPTS) GO TO 9999
        IF(XDIST(JJ).LE.SCHK) GO TO 6
        WRITE (6,888)

```

451
452
453
454
455
456
457
458
459
460
461
462
463
464
465
466
467
468
469
470
471
472
473
474
475
476
477
478
479
480
481
482
483
484
485
486
487
488
489
490
491
492
493
494
495
496
497
498
499
500

888	FORMAT (//,T25,'***** TRANSFER ERROR IN XDIST(NPTS) TO INTERP	501
1	END RUN *****')	502
	STOP	503
6	KOUNT=KOUNT+1	504
	H SIZE=1.00/3.00	505
	K=J+1	506
	YMID(KOUNT,1)=(XDIST(J)+XDIST(K))/2.00	507
	XNORM(1)=-H SIZE	508
	DO 10 L=2,6	509
	XL=L-2	510
10	XNORM(L)=XL*H SIZE	511
	YNORM(1)=FACTOR(NFACTR)*YINT(KOUNT)	512
11	L=KOUNT	513
	DO 20 LL=2,6	514
	L=L+1	515
20	YNORM(LL)=YINT(L)	516
	YNORM(6)=FACTOR(NFACTR)*YNORM(6)	517
C		518
C		519
C	CALL MATRIX INVERSION ROUTINE TO SOLVE FOR SPLINE COEFFICIENTS AND	520
C	CALCULATE MIDPOINT X VALUES AND SPLINE FIT INTENSITY VALUES	521
C		522
29	CALL XMATRIX(6,YNORM,COEF,I,H SIZE,KOUNT)	523
	DO 30 LL=2,6	524
	L=LL-1	525
30	XMID(L)=(XNORM(LL)+XNORM(L))/2.00	526
	CALL CALCY (I,6,COEF, XMID,H SIZE,YHOLD,KOUNT)	527
	XINC=XDIST(2)-XDIST(1)	528
	DO 40 JJ=1,4	529
	JJJ=KOUNT+JJ	530
	XJJ=JJ	531
40	YMID(JJJ,1)=YMID(KOUNT,1)+(XJJ*XINC)	532
	DO 50 L=1,5	533
	LL=KOUNT+L-1	534
50	YAVE(LL)=YAVE(LL)+YHOLD(KOUNT,L)	535
C		536
C		537
C	DEFINE STORAGE ARRAY 'YSTOR' FOR SIGMA CALCULATION	538
85	IF(KOUNT.LT.5) GO TO 100	539
	DO 90 N1=1,5	540
	N2=N1-1	541
	N3=KOUNT-N2	542
	YSTOR(KOUNT,N1)=YHOLD(N3,N1)	543
90	CONTINUE	544
	KN=NPTS-5	545
	IF(KOUNT.LT.KN) GO TO 999	546
	DO 91 N1=1,4	547
	N2=KOUNT+N1	548
	NN=N1+1	549
		550

	DO 91 NNN=NN,5	551
	N3=NNN-N1	552
	N4=KOUNT+1-N3	553
91	YSTOR(N2,N3)=YHOLD(N4,NNN)	554
	GO TO 999	555
100	IF(KOUNT.GT.1) GO TO 101	556
	YSTOR(1,1)=YHOLD(1,1)	557
	GO TO 999	558
101	DO 102 N1=1,KOUNT	559
	N2=N1-1	560
	N3=KOUNT-N2	561
102	YSTOR(KOUNT,N1)=YHOLD(N3,N1)	562
999	CONTINUE	563
C		564
C	CALCULATE SIGMA AND STORE 'YAVE' AND 'SIGMA' IN 'YMID' AS	565
C	YMID(J,2) AND YMID(J,3), RESPECTIVELY	566
C		567
9999	J=NPTS-1	568
	DO 70 JJ=1,J	569
	IF(JJ.LT.5) GO TO 57	570
	KK=NPTS-5	571
	IF(JJ.GT.KK) GO TO 65	572
	YMID(JJ,2)=YAVE(JJ)/5.00	573
	DO 56 II=1,5	574
56	SIGMA(JJ)=(YSTOR(JJ,II)-YMID(JJ,2))*2	575
	SIGMA(JJ)=DSQRT(SIGMA(JJ)/4.00)	576
	YMID(JJ,3)=SIGMA(JJ)	577
	GO TO 70	578
57	XJJ=JJ	579
	YMID(JJ,2)=YAVE(JJ)/XJJ	580
	IF(JJ.GT.1) GO TO 58	581
	YMID(JJ,3)=0.00	582
	GO TO 70	583
58	DO 59 II=1,JJ	584
59	SIGMA(JJ)=(YSTOR(JJ,II)-YMID(JJ,2))*2	585
	XII=XJJ-1.00	586
	SIGMA(JJ)=DSQRT(SIGMA(JJ)/XII)	587
	YMID(JJ,3)=SIGMA(JJ)	588
	GO TO 70	589
65	XKK=NPTS-JJ	590
	YMID(JJ,2)=YAVE(JJ)/XKK	591
	IF(JJ.LT.J) GO TO 66	592
	YMID(JJ,3)=0.00	593
	GO TO 70	594
66	III=NPTS-JJ	595
	DO 67 II=1,III	596
67	SIGMA(JJ)=(YSTOR(JJ,II)-YMID(JJ,2))*2	597
	XII=III-1	598
	SIGMA(JJ)=DSQRT(SIGMA(JJ)/XII)	599
	YMID(JJ,3)=SIGMA(JJ)	600

	70	CONTINUE	601
		RETURN	602
		END	603
		SUBROUTINE XMATRX(NPTS,YINT,COEF,I,HSIZE,KOUNT)	604
		IMPLICIT REAL*8(A-H,O-Z)	605
		DIMENSION YINT(6),S(6,6),COEF(6,4),SCALC(6,6),SOUT(36),YCAL(6)	606
C			607
C		DETERMINE COEFS OF SPLINE FIT WITH FORTRAN SSP ROUTINE 'DGELG' AND	608
C		RETURN TO INTERP AS 'COEF'	609
C			610
		DO 10 M=1,NPTS	611
		DO 10 L=1,NPTS	612
		K=M-L	613
		J=L-M	614
		IF(K.EQ.1) GO TO 8	615
		IF(J.EQ.1) GO TO 8	616
		IF(L.EQ.M) GO TO 9	617
		S(M,L)=0.D0	618
		GO TO 10	619
	8	S(M,L)=0.25D0	620
		GO TO 10	621
	9	S(M,L)=1.D0	622
	10	CONTINUE	623
		DO 15 J=1,NPTS	624
		DO 15 K=1,NPTS	625
	15	SCALC(J,K)=S(J,K)	626
		DO 16 J=1,NPTS	627
	16	YCAL(J)=YINT(J)	628
		IF(NPTS.EQ.6) GO TO 25	629
		IX=0	630
		DO 17 L=1,NPTS	631
		DO 17 K=1,NPTS	632
		IX=IX+1	633
	17	SOUT(IX)=SCALC(K,L)	634
		GO TO 26	635
	25	CALL DGELG (YCAL,SCALC,6,1,1,0E-16,IER)	636
		GO TO 27	637
	26	CALL DGELG (YCAL,SOUT,NPTS,1,1,0E-16,IER)	638
	27	CONTINUE	639
		DO 30 K=1,NPTS	640
	30	COEF(K,I)=YCAL(K)	641
		IF(IER.NE.0) GO TO 99999	642
		RETURN	643
99999		WRITE(6,2000) IER,KOUNT	644
2000		FORMAT(//////,T15,'***** IER =',I3,2X,'KOUNT =',I4)	645
		RETURN	646
		END	647
		SUBROUTINE CALCY (I,NPTS,COEF,XMID,HSIZE,YHOLD,KOUNT)	648
		IMPLICIT REAL*8(A-H,O-Z)	649
		DIMENSION X(5),F(5),COEF(6,4),XMID(5),YHOLD(50,5)	650

C
C
C
C

```

CALCULATE MIDPOINT INTERPOLATED VALUES AND RETURN TO 'INTERP' AS
ARRAY 'YHOLD'
DO 10 J=1,5
10 X(J)=XMID(J)
DO 20 J=1,5
F(J)=0.D0
DO 15 K=1,NPTS
XK=K
X1=X(J)-((XK-2.D0)*HSIZE)
HL=-2.D0*HSIZE
HU=2.D0*HSIZE
IF(X1.GE.HL) GO TO 11
F(J)=F(J)+0.D0
GO TO 15
11 H=-HSIZE
IF(X1.GT.H) GO TO 12
F(J)=F(J)+(((X1+(2.D0*HSIZE))**3.D0)/(4.D0*(HSIZE**3.D0))*COEF(K,I
1))
GO TO 15
12 IF(X1.GT.0.D0) GO TO 13
TERM=(HSIZE**3.D0)+((3.D0*(HSIZE**2.D0))*(X1+HSIZE))+((3.D0*HSIZE
1)*((X1+HSIZE)**2.D0))-((3.D0*(X1+HSIZE)**3.D0))
TERM=(TERM/(4.D0*(HSIZE**3.D0)))*COEF(K,I)
F(J)=F(J)+TERM
GO TO 15
13 IF(X1.GT.HSIZE) GO TO 14
TERM=(HSIZE**3.D0)+((3.D0*(HSIZE**2.D0))*(HSIZE-X1))+((3.D0*HSIZE
1)*((HSIZE-X1)**2.D0))-((3.D0*(HSIZE-X1)**3.D0))
TERM=(TERM/(4.D0*(HSIZE**3.D0)))*COEF(K,I)
F(J)=F(J)+TERM
GO TO 15
14 IF(X1.GT.HU) GO TO 16
TERM=((2.D0*HSIZE)-X1)**3.D0
TERM=(TERM/(4.D0*(HSIZE**3.D0)))*COEF(K,I)
F(J)=F(J)+TERM
GO TO 15
16 F(J)=F(J)+0.D0
15 CONTINUE
20 CONTINUE
DO 40 N=1,5
40 YHOLD(KOUNT,N)=F(N)
RETURN
END
SUBROUTINE DKABEL (XDTR,YINT,IMA,NS1,NZ,XPNT,RAD,RDI,KT,XD,XBIG,LZ
1,DELIR,SIGMAY,L1,IWT)
DIMENSION XDTR(1),YINT(1),RAD(1),RDI(1),XBIG(1),DELIR(1),SEGEND(5)
1,SIGMAY(1),COEF(5,5),DELCOF(5,5),RA(2),XA(51),YA(51),YCHECK(51,5),
2DIFY(51),PERCNT(51),AVEPCT(12),STDDEV(5),DEVAVE(5),YC(51,5),NTAG(5
651
652
653
654
655
656
657
658
659
660
661
662
663
664
665
666
667
668
669
670
671
672
673
674
675
676
677
678
679
680
681
682
683
684
685
686
687
688
689
690
691
692
693
694
695
696
697
698
699
700

```

	3),RDST(5)	701
	DATA NTAG/0.0,0.0,0/	702
	DATA RDST/1.0,1.0,1.0,1.0,1.0/	703
	WRITE (6,1000)	704
1000	FORMAT (////,T2,'INPUT DATA TRANSFERRED TO DKABEL')	705
	WRITE (6,1001)	706
1001	FORMAT (/T4,' IDEX',T25,'XDTR',T50,'YINT')	707
	DO 100 IDEX=1,IMA	708
1002	FORMAT (/T6,I2,T20,E11.4,T45,E11.4)	709
100	WRITE (6,1002) IDEX,XDTR(IDEX),YINT(IDEX)	710
	DO 5 J=1,5	711
	SEGEND(J)=0.0	712
	DO 5 I=1,5	713
	COEF(I,J)=0.0	714
5	DELCOF(I,J)=0.0	715
C		716
C	SET UP ZONE SEGMENTS FOR POLY FIT (3 TO 5 ZONES)	717
C		718
	NSEGS=NS1	719
	XBIG(LZ)=XBIG(LZ)/XD	720
	IF(NSEGS-4) 10,25,29	721
10	CHECK=XBIG(LZ)-0.3333333	722
	CHECK=ABS(CHECK)	723
	IF(CHECK.GT.0.100) GO TO 12	724
	IF(XBIG(LZ)-0.3333333) 11,11,12	725
11	SEGEND(1)=0.450	726
	SEGEND(2)=0.750	727
	SEGEND(3)=1.000	728
	NSEGS=3	729
	GO TO 30	730
12	CHECK=XBIG(LZ)-0.6666667	731
	CHECK=ABS(CHECK)	732
	IF(CHECK.GT.0.100) GO TO 14	733
	IF(XBIG(LZ)-0.6666667) 13,13,14	734
13	SEGEND(1)=0.350	735
	SEGEND(2)=0.750	736
	SEGEND(3)=1.000	737
	NSEGS=3	738
	GO TO 30	739
14	IF(XBIG(LZ)-0.2333333) 15,15,16	740
15	SEGEND(1)=0.3333333	741
	SEGEND(2)=0.6666667	742
	SEGEND(3)=1.0000000	743
	NSEGS=3	744
	GO TO 30	745
16	IF(XBIG(LZ)-0.6666667) 17,19,19	746
17	IF(XBIG(LZ)-0.4333333) 18,18,19	747
18	SEGEND(1)=0.250	748
	SEGEND(2)=0.650	749
	SEGEND(3)=1.000	750

	NSEGS=3	751
	GO TO 30	752
19	IF(XBIG(LZ)-0.7666667) 20,20,21	753
20	SEGEND(1)=0.300	754
	SEGEND(2)=0.550	755
	SEGEND(3)=1.000	756
	NSEGS=3	757
	GO TO 30	758
21	SEGEND(1)=0.3333333	759
	SEGEND(2)=0.6666667	760
	SEGEND(3)=1.0000000	761
	NSEGS=3	762
	GO TO 30	763
25	SEGEND(1)=0.250	764
	SEGEND(2)=0.500	765
	SEGEND(3)=0.750	766
	SEGEND(4)=1.000	767
	NSEGS=4	768
	GO TO 30	769
29	NSEGS=5	770
	SEGEND(1)=0.2	771
	SEGEND(2)=0.4	772
	SEGEND(3)=0.6	773
	SEGEND(4)=0.8	774
	SEGEND(5)=1.0	775
30	CONTINUE	776
C		777
C	CALL ROUTINE SEGMENT FOR ZONE COEFS AND SIGMA VALUES	778
C		779
	CALL SEGMENT (XDTR,YINT,IMA,NS1,NSEGS,NZ,COEF,DELCOF,SEGEND,SIGMA, INTAG,IWT)	780
	DO 35 I=1,IMA	781
	XA(I)=XDTR(I)	782
35	YA(I)=YINT(I)	783
C		784
C		785
C	COMPARE CALCULATED TO INPUT Y VALUES FOR EACH ZONE	786
		787
	WRITE (6,2000)	788
2000	FORMAT (/////,T10,'REGION',T22,'DIST',T33,'CALCY',T45,'REALY',T56, 1'DIFF',T73,'PERCENT',T88,'AVE PERCENT',T102,'WEIGHTED STD DEV')	789
	IMS1=NTAG(1)	790
	NSEG=NSEGS	791
	IZONE=1	792
	SUMPCT=0.0	793
	SUMERR=0.0	794
	AVEDEV=0.0	795
	YSUM=0.0	796
	DO 75 I=1,IMS1	797
	XCHEC2=XA(I)*XA(I)	798
	XCHEC4=XCHEC2*XCHEC2	799
		800

	XCHEC6=XCHEC4*XCHEC2	801
	XCHEC8=XCHEC6*XCHEC2	802
	YCHECK(I,1)=CDEF(1,1)+(COEF(2,1)*XCHEC2)+(COEF(3,1)*XCHEC4)+(COEF(803
	14,1)*XCHEC6)+(COEF(5,1)*XCHEC8)	804
	DIFY(I)=YA(I)-YCHECK(I,1)	805
	PERCNT(I)=(DIFY(I)*100.)/YA(I)	806
	PERCNT(I)=ABS(PERCNT(I))	807
	SUMPCT=SUMPCT+PERCNT(I)	808
	SUMERR=SUMERR+(DIFY(I)*DIFY(I)/YA(I))	809
	AVEDEV=AVEDEV+(DIFY(I)*DIFY(I))	810
	YSUM=YSUM+YA(I)	811
	IF(I.NE.IMS1) GO TO 74	812
	XI=I	813
	AVEPCT(1)=SUMPCT/XI	814
	STDDEV(1)=SQRT(SUMERR/(XI-1.0))	815
	DEVAVE(1)=SQRT(AVEDEV/(XI-1.0))/(YSUM/XI)	816
	WRITE(6,3000) IZONE,XA(I),YCHECK(I,1),YA(I),DIFY(I),PERCNT(I),AVE	817
	1PCT(1),STDDEV(1),DEVAVE(1)	818
3000	FORMAT (T12,I2,T20,F8.4,T32,F8.4,T44,F8.4,T54,E11.4,T72,E11.4,T87,	819
	1E11.4,T105,E11.4,T117,E11.4)	820
	GO TO 75	821
74	WRITE(6,2001) IZONE ,XA(I),YCHECK(I,1),YA(I),DIFY(I),PERCNT(I)	822
2001	FORMAT (T12,I2,T20,F8.4,T32,F8.4,T44,F8.4,T54,E11.4,T72,E11.4)	823
75	CONTINUE	824
	DO 80 J=2,NSEG	825
	NHOLD=0	826
	JJ=J-1	827
	N1=NTAG(JJ)+1	828
	N2=NTAG(J)	829
	SUMPCT=0.0	830
	SUMERR=0.0	831
	AVEDEV=0.0	832
	YSUM=0.0	833
	IF (J.NE.NSEG) GO TO 78	834
	N2=IMA	835
78	DO 79 K=N1,N2	836
76	XCHEC1=XA(K)	837
	XCHEC2=XA(K)*XA(K)	838
	XCHEC3=XCHEC2*XA(K)	839
	XCHEC4=XCHEC3*XA(K)	840
77	YCHECK(K,J)=CDEF(1,J)+(COEF(2,J)*XCHEC1)+(COEF(3,J)*XCHEC2)+(COEF(841
	14,J)*XCHEC3)+(COEF(5,J)*XCHEC4)	842
	DIFY(K)=YA(K)-YCHECK(K,J)	843
	DIFYI=DIFY(K)*DIFY(K)	844
	IF (YA(K).EQ.0.0) GO TO 200	845
	PERCNT(K)=ABS((DIFY(K)*100.)/YA(K))	846
	DIF2=DIFY(K)*DIFY(K)/YA(K)	847
	GO TO 201	848
200	PERCNT(K)=0.0	849
	DIF2=DIFY(K)*DIFY(K)	850

	NHOLD=NHOLD+1	851
201	SUMPCT=SUMPCT+PERCNT(K)	852
	AVEDEV=AVEDEV+DIFYI	853
	YSUM=YSUM+YA(K)	854
	SUMERR=SUMERR+DIF2	855
	IF(K,NE,N2) GO TO 202	856
	XK=N2-N1+1-NHOLD	857
	AVEPCT(J)=SUMPCT/XK	858
	XFREE=N2-N1	859
	IF(XFREE.LE.0,0) XFREE=1.0	860
	STDDEV(J)=SQRT(SUMERR/XFREE)	861
	DEVAVE(J)=SQRT(AVEDEV/XFREE)/(YSUM/(XFREE+1.0))	862
	WRITE (6,3001) J,XA(K),YCHECK(K,J),YA(K),DIFY(K),PERCNT(K),AVEPCT(863
	1J),STDDEV(J),DEVAVE(J)	864
3001	FORMAT (T12,I2,T20,F8.4,T32,F8.4,T44,F8.4,T54,E11.4,T72,E11.4,T87,	865
	1E11.4,T105,E11.4,T117,E11.4)	866
	GO TO 79	867
202	WRITE (6,2002) J,XA(K),YCHECK(K,J),YA(K),DIFY(K),PERCNT(K)	868
2002	FORMAT (T12,I2,T20,F8.4,T32,F8.4,T44,F8.4,T54,E11.4,T72,E11.4)	869
	79 CONTINUE	870
	80 CONTINUE	871
	WRITE (6,3999)	872
3999	FORMAT (/////,T10,'WEIGHTED STD DEV DEFINED AS:',/,T15,'SQUARE ROO	873
	IT OF: (SUM(DIFF**2/REALY))/[NUM PTS IN ZONE - 1)]',/,T10,'LAST C	874
	2OLUMN: (SQRT(SUM(DIFF**2/(NPTS-1)))/(MEAN VALUE REALY FOR ZONE)')	875
	WRITE (6,4000)	876
4000	FORMAT (/////,T10,'REGION',T22,'DIST',T33,'CALCY')	877
	IZ=1	878
	DO 49 I=2,IMS1	879
	J=I-1	880
	XAVE=(XA(I)+XA(J))/2.	881
	XC2=XAVE*XAVE	882
	XC4=XC2*XC2	883
	XC6=XC4*XC2	884
	XC8=XC6*XC2	885
	YC(J,1)=COEF(1,1)+(COEF(2,1)*XC2)+(COEF(3,1)*XC4)+(COEF(4,1)*XC6)+	886
	1(COEF(5,1)*XC8)	887
	WRITE (6,4001) IZ,XAVE,YC(J,1)	888
4001	FORMAT (T12,I2,T20,F8.4,T32,F8.4)	889
	49 CONTINUE	890
	DO 48 J=2,NSEG	891
	JJ=J-1	892
	N1=NTAG(JJ)+2	893
	N2=NTAG(J)	894
	IF(J.NE.NSEG) GO TO 46	895
	N2=IMA	896
46	DO 47 K=N1,N2	897
	K2=K-1	898
	XAVE=(XA(K)+XA(K2))/2.	899
	XC1=XAVE	900

	XC2=XAVE*XAVE	901
	XC3=XC2*XAVE	902
	XC4=XC3*XAVE	903
	YC(K2,J)=COEF(1,J)+(COEF(2,J)*XC1)+(COEF(3,J)*XC2)+(COEF(4,J)*XC3)	904
	1+(COEF(5,J)*XC4)	905
	WRITE(6,4002) J,XAVE,YC(K2,J)	906
4002	FORMAT(T12,I2,T20,F8.4,T32,F8.4)	907
47	CONTINUE	908
48	CONTINUE	909
C		910
C	CALCULATE RADIAL INTENSITY VALUES BASED ON POLY FIT	911
		912
500	RM=0.0	913
	X=SEGEND(1)	914
	X3=X**3	915
	X5=X**5	916
	X7=X**7	917
	RA1=COEF(2,1)*X+2.*COEF(3,1)*X3/3.+3.*COEF(4,1)*X5/5.+4.*COEF(5,1)	918
	1*X7/7.	919
	RA2=-2.*RA1/3.141593	920
	DO 521 J=2,NSEGS	921
	I=1	922
	XLC=SEGEND(J)	923
518	RA(I)=COEF(2,J)*ALOG(XLC)+2.*COEF(3,J)*XLC+3.*COEF(4,J)*XLC*XLC/2.	924
	1+4.*COEF(5,J)*XLC*XLC*XLC/3.	925
	GO TO(519,520),I	926
519	I=2	927
	XLC=SEGEND(J-1)	928
	GO TO 518	929
520	RM1=-(RA(1)-RA(2))/3.141593	930
	RM=RM1+RM	931
521	CONTINUE	932
	RAD(1)=RA2+RM	933
	RDI(1)=0.0	934
	KT=1	935
	R=0.0	936
	LC=1	937
550	R=R+XPNT	938
	IF(R.GT.SEGEND(NSEGS)) GO TO 600	939
	IF(R.GT.SEGEND(LC)) LC=LC+1	940
	KT=KT+1	941
	RDI(KT)=R	942
	RM=0.0	943
	R2=R*R	944
	GO TO(575,555,555,555,555),LC	945
555	X=SEGEND(LC)	946
	X2=X*X	947
	B=SQRT(X2-R2)	948
	B3=B*B*B	949
556	RA1=COEF(2,LC)*ALOG((X+B)/R)+2.*COEF(3,LC)*B+3./2.*COEF(4,LC)*(X*B	950

	1+R2*ALOG((X+B)/R))+4.*COEF(5,LC)*(B3/3.+R2*B)	951
	RA2=-RA1/3.141593	952
	IF(LC.LT.NSEGS) GO TO 557	953
	RAD(KT)=RA2+RM	954
	GO TO 550	955
557	LCUP=LC+1	956
	RM=0.0	957
	DO 565 J=LCUP,NSEGS	958
	I=1	959
	XLC=SEGEND(J)	960
558	X2LC=XLC*XLC	961
	A=SQRT(X2LC-R2)	962
	A3=A*A*A	963
	RA(I)=COEF(2,J)*ALOG(XLC+A)+2.*COEF(3,J)*A+3./2.*COEF(4,J)*(XLC*A+	964
	1R2*ALOG(XLC+A))+4.*COEF(5,J)*(A3/3.+R2*A)	965
	GO TO (559,560),I	966
559	I=2	967
	XLC=SEGEND(J-1)	968
	GO TO 558	969
560	RM1=- (RA(1)-RA(2))/3.141593	970
	RM=RM1+RM	971
565	CONTINUE	972
	RAD(KT)=RA2+RM	973
	GO TO 550	974
575	X=SEGEND(1)	975
	X2=X*X	976
	B=SQRT(X2-R2)	977
	R4=R2*R2	978
	R6=R2*R4	979
	B2=B*B	980
	B3=B2*B	981
	B5=B2*B3	982
	B7=B2*B5	983
	RA1=2.*COEF(2,1)*B+4.*COEF(3,1)*(B3/3.+R2*B)+6.*COEF(4,1)*(R4*B+2.	984
	1R2*B3/3.+B5/5.)+8.*COEF(5,1)*(R6*B+R4*B3+3.*R2*B5/5.+B7/7.)	985
	RA2=-RA1/3.141593	986
	GO TO 557	987
600	DO 610 I=1,KT	988
610	RDI(I)=RDI(I)*XD	989
	WRITE (6,5002) NSEGS,NSEGS,(SEGEND(I),I=1,NSEGS)	990
5002	FORMAT (///,T5,'ZONE DIVISIONS FOR',I3,2X,'SEGMENTS',//,T5,'REGION	991
	1(1)-----REGION(' ,I1,')= ',5(E11.4,5X))	992
C		993
C		994
C	CALCULATE SIGMA VALUES FOR RADIAL INTENSITIES	995
	DO 66 I=1,NSEGS	996
66	RDST(I)=SEGEND(I)	997
	DO 67 I1=1,KT	998
67	RDI(I1)=RDI(I1)/XD	999
	DO 90 I=1,KT	1000

```

IF(RDI(I).GT.RDST(1)) GO TO 82
G=SQRT(RDST(1)**2.-RDI(I)**2.)
DEL1=(2.*ABS(G)*DELCOF(2,1))+(4.*ABS(((G**3.)/3.)+(RDI(I)**2.)*G
1)*DELCOF(3,1))+(6.*ABS(((RDI(I)**4.)*G)+((2./3.)*(RDI(I)**2.)*(G**
23.)))+(1./5.)*(G**5.)))*DELCOF(4,1))+(8.*ABS(((RDI(I)**6.)*G)+((RD
3I(I)**4.)*(G**3.)))+(3./5.)*(RDI(I)**2.)*(G**5.)))+(1./7.)*(G**7.
4)*DELCOF(5,1))
DEL2=0.0
DO 89 J=2,NSEGS
K=J-1
GJ=SQRT(RDST(J)**2.-RDI(I)**2.)
GK=SQRT(RDST(K)**2.-RDI(I)**2.)
ADD=(ABS(ALOG((RDST(J)+GJ)/(RDST(K)+GK)))*DELCOF(2,J))+(2.*ABS(GJ-
1GK)*DELCOF(3,J))+(1.5*ABS((RDST(J)*GJ)-(RDST(K)*GK)+((RDI(I)**2.)*
2ALOG((RDST(J)+GJ)/(RDST(K)+GK)))*DELCOF(4,J)))+(4.*ABS(((GJ**3.)/3
3.)-(GK**3.)/3.)+(RDI(I)**2.)*(GJ-GK))*DELCOF(5,J))
89 DEL2=DEL2+ADD
DELIR(I)=((DEL1+DEL2)/3.141593)*100.0
DELIR(I)=DELIR(I)/RAD(I)
GO TO 90
82 IF(RDI(I).LE.RDST(2)) L=2
IF(RDI(I).LE.RDST(3)) L=3
IF(RDI(I).LE.RDST(4)) L=4
IF(RDI(I).LE.RDST(5)) L=5
IF(RDI(I).GT.RDST(5)) GO TO 92
G=SQRT(RDST(L)**2.-RDI(I)**2.)
RDI2=RDI(I)*RDI(I)
XTMLOG=ALOG((RDST(L)+G)/RDI(I))
DEL1=(ABS(XTMLOG)*DELCOF(2,L))+(2.*ABS(G)*DELCOF(3,L))+(1.5*ABS((R
1DST(L)*G)+(RDI2*XTMLOG))*DELCOF(4,L))+(4.*ABS(((G**3.)/3.)+(RDI2*G
2))*DELCOF(5,L))
IF(L.LT.NSEGS) GO TO 87
DELIR(I)=(DEL1/3.141593)*100.0
DIFRNC=RAD(I)-0.0
ABDIF=ABS(DIFRNC)
IF(ABDIF.LT.0.0000001) GO TO 90
DELIR(I)=DELIR(I)/RAD(I)
GO TO 90
87 N1=L+1
DEL2=0.0
DO 88 M=N1,NSEGS
N=M-1
GM=SQRT(RDST(M)**2.-RDI(I)**2.)
GN=SQRT(RDST(N)**2.-RDI(I)**2.)
ADD=(ABS(ALOG((RDST(M)+GM)/(RDST(N)+GN)))*DELCOF(2,M))+(2.*ABS(GM-
1GN)*DELCOF(3,M))+(1.5*ABS((RDST(M)*GM)-(RDST(N)*GN)+((RDI(I)**2.)*
2ALOG((RDST(M)+GM)/(RDST(N)+GN)))*DELCOF(4,M)))+(4.*ABS(((GM**3.)/3
3.)-(GN**3.)/3.)+(RDI(I)**2.)*(GM-GN))*DELCOF(5,M))
88 DELI=DEL2+ADD
DELIR(I)=((DEL1+DEL2)/3.141593)*100.0

```

1001
1002
1003
1004
1005
1006
1007
1008
1009
1010
1011
1012
1013
1014
1015
1016
1017
1018
1019
1020
1021
1022
1023
1024
1025
1026
1027
1028
1029
1030
1031
1032
1033
1034
1035
1036
1037
1038
1039
1040
1041
1042
1043
1044
1045
1046
1047
1048
1049
1050

	DEL IR(I)=DEL IR(I)/RAD(I)	1051
90	CONTINUE	1052
	IF(I.EQ.KT) GO TO 93	1053
92	KT=I-1	1054
93	DO 91 I2=1,KT	1055
91	RDI(I2)=RDI(I2)*XD	1056
	SUMR=0.	1057
	WRITE (6,6000)	1058
6000	FORMAT (//////,T29,'I',T45,'RDI(I)',T67,'RAD(I)',T83,'DELTA RAD IN	1059
	1PERCENT')	1060
	DO 23 K=1,KT	1061
101	FORMAT (27X,I3,2(12X,E11.4),T90,E11.4)	1062
	SUMR=SUMR+RAD(K)	1063
23	WRITE (6,101) K,RDI(K),RAD(K),DEL IR(K)	1064
	WRITE (6,102) SUMR	1065
102	FORMAT (///,T80,'SUM I(R) = ',2X,E11.4)	1066
	WRITE (6,5000)	1067
5000	FORMAT (//////,T10,'J',T15,'I',T30,'DELCOF(I,J)')	1068
	DO 28 J=1,NSEG	1069
	DO 28 I=2,5	1070
5001	FORMAT (T9,I2,T14,I2,T30,E11.4)	1071
28	WRITE (6,5001) J,I,DELCOF(I,J)	1072
	IF (L1.EQ.2) GO TO 300	1073
	DO 299 NABS=1,KT	1074
299	RAD(NABS)=ABS(RAD(NABS))	1075
300	RETURN	1076
	END	1077
	SUBROUTINE SEGMNT (XA,YA,IMA,NS1,NSEGS,NZ,COEF,DELCOF,SEG,SIGA,NTA	1078
	1G,IWT)	1079
	DIMENSION RELCOF(5,5),SRELC(5,5),FTEST5(5),FTEST6(5),FTEST7(5)	1080
	DIMENSION XA(1),YA(1),COEF(5,5),DELCOF(5,5),SEG(1),SIGA(1),PERCT(7	1081
	1),FTEST1(5),FTEST2(5),FTEST3(5),FTEST4(5),NTAG(5),XSTOR(11,5),YSTO	1082
	2R(11,5),SSTOR(11,5),XFIT(35),YFIT(35),SFIT(35),FTEST(5),YCALC(35),	1083
	3REALC(5),SIGMAC(5),RELC(5),SIGMAR(5),CHISQR(5)	1084
	DATA FTEST1/16200.0,198.0,55.6,31.3,22.8/,FTEST2/4050.0,98.5,34.1,	1085
	121.2,16.3/,FTEST3/648.0,38.5,17.4,12.2,10.0/,FTEST4/161.0,18.5,10.	1086
	21,7.71,6.61/,PERCT/0.5,1.0,2.5,5.0,10.0,25.0,50.0/	1087
	DATA FTEST5/39.9,8.53,5.54,4.54,4.06/,FTEST6/5.83,2.57,2.02,1.81,1	1088
	1.69/,FTEST7/1.00,0.667,0.585,0.549,0.528/	1089
	GO TO (1,3,5,7,11,21,31),NZ	1090
1	DO 2 I=1,5	1091
2	FTEST(I)=FTEST1(I)	1092
	GO TO 9	1093
3	DO 4 I=1,5	1094
4	FTEST(I)=FTEST2(I)	1095
	GO TO 9	1096
5	DO 6 I=1,5	1097
6	FTEST(I)=FTEST3(I)	1098
	GO TO 9	1099
7	DO 8 I=1,5	1100

8	FTEST(I)=FTEST4(I)	1101
	GO TO 9	1102
11	DO 12 I=1,5	1103
12	FTEST(I)=FTEST5(I)	1104
	GO TO 9	1105
21	DO 22 I=1,5	1106
22	FTEST(I)=FTEST6(I)	1107
	GO TO 9	1108
31	DO 32 I=1,5	1109
32	FTEST(I)=FTEST7(I)	1110
9	WRITE (6,1000) PERCT(NZ),NSEGS	1111
1000	FORMAT (1H1,T15,'RADIAL INTENSITY DISTRIBUTION CALCULATION',//,T15	1112
	1,'ABEL INVERSION UTILIZING WEIGHTED LEAST-SQUARES POLYNOMIAL FITTI	1113
	2NG OF THE LATERAL INTENSITY DISTRIBUTION',/,T20,'F-TEST FOR SIGNIF	1114
	3ICANCE OF ADDED COEFFICIENT FOR',F6.2,2X,'PERCENT PROBABILITY OF E	1115
	4XCEEDING THE F-VALUE',//,T25,'THE LATERAL I(X) PROFILE HAS BEEN DI	1116
	5VIDED INTO',I3,2X,'ZONES')	1117
	WRITE (6,1001)	1118
1001	FORMAT (////,T15,'ZONE DIVISIONS ON REDUCED RADIUS SCALE',/,T15,'	1119
	1ZONE NUMBER',T35,'DISTANCE')	1120
	DO 10 I=1,NSEGS	1121
1002	FORMAT (T20,I2,T32,E14.7)	1122
10	WRITE (6,1002) I,SEG(I)	1123
	WRITE (6,2000) (FTEST(I),I=1,5)	1124
2000	FORMAT (//,T15,'FTEST(1)---FTEST(5)=' ,5(2X,E13.6))	1125
	WRITE (6,1003)	1126
1003	FORMAT (////,T20,'THE FOLLOWING COEFFICIENTS WERE OBTAINED',//,T27,	1127
	1'POLY',5X,'Y',5X,'=' ,6X,'A',6X,'+' ,5X,'B*X',5X,'+' ,6X,'C*X**2',4X,	1128
	2'+' ,4X,'D*X**3',4X,'+' ,4X,'E*X**4',//,T20,'REGION',2X,'DEG',19X,'A	1129
	3',14X,'B',14X,'C',14X,'D',14X,'E',//)	1130
	DO 15 J=1,NSEGS	1131
	DO 15 I=1,IMA	1132
	IF(XA(I).GT.SEG(J)) GO TO 15	1133
	NTAG(J)=I	1134
15	CONTINUE	1135
	N1=NTAG(1)	1136
	DO 20 I=1,N1	1137
	XSTOR(I,1)=XA(I)	1138
	YSTOR(I,1)=YA(I)	1139
20	SSTOR(I,1)=SIGA(I)	1140
	DO 25 LC=2,NSEGS	1141
	N1=LC-1	1142
	N2=NTAG(N1)+1	1143
	N3=NTAG(LC)	1144
	I=0	1145
	DO 25 J=N2,N3	1146
	I=I+1	1147
	XSTOR(I,LC)=XA(J)	1148
	YSTOR(I,LC)=YA(J)	1149
25	SSTOR(I,LC)=SIGA(J)	1150

	DO 999 LC=1,NSEGS	1151
	IF(NSEGS-4) 100,200,300	1152
100	GO TO (110,120,130),LC	1153
110	N=NTAG(1)	1154
	DO 115 I=1,N	1155
	XFIT(I)=XSTOR(I,1)**2	1156
	YFIT(I)=YSTOR(I,1)	1157
115	SFIT(I)=SSTOR(I,1)	1158
	I=N	1159
	DO 116 J=1,3	1160
	I=I+1	1161
	XFIT(I)=XSTOR(J,2)**2	1162
	YFIT(I)=YSTOR(J,2)	1163
116	SFIT(I)=SSTOR(J,2)	1164
	NFIT=N+3	1165
	GO TO 500	1166
120	N1=NTAG(1)-2	1167
	N2=NTAG(1)	1168
	N3=NTAG(2)	1169
	I=0	1170
	DO 125 J=N1,N2	1171
	I=I+1	1172
	XFIT(I)=XSTOR(J,1)	1173
	YFIT(I)=YSTOR(J,1)	1174
125	SFIT(I)=SSTOR(J,1)	1175
	NN=N3-N2	1176
	DO 126 J=1,NN	1177
	I=I+1	1178
	XFIT(I)=XSTOR(J,2)	1179
	YFIT(I)=YSTOR(J,2)	1180
126	SFIT(I)=SSTOR(J,2)	1181
	DO 127 J=1,3	1182
	I=I+1	1183
	XFIT(I)=XSTOR(J,3)	1184
	YFIT(I)=YSTOR(J,3)	1185
127	SFIT(I)=SSTOR(J,3)	1186
	NFIT=I	1187
	GO TO 500	1188
130	N1=(NTAG(2)-NTAG(1))-2	1189
	N2=NTAG(2)-NTAG(1)	1190
	N3=NTAG(3)-NTAG(2)	1191
	I=0	1192
	DO 135 J=N1,N2	1193
	I=I+1	1194
	XFIT(I)=XSTOR(J,2)	1195
	YFIT(I)=YSTOR(J,2)	1196
135	SFIT(I)=SSTOR(J,2)	1197
	DO 136 J=1,N3	1198
	I=I+1	1199
	XFIT(I)=XSTOR(J,3)	1200

	YFIT(I)=YSTOR(J,3)	1201
136	SFIT(I)=SSTOR(J,3)	1202
	NFIT=I	1203
	GO TO 500	1204
200	GO TO (210,220,230,240),LC	1205
210	N1=NTAG(1)	1206
	N2=NTAG(2)-NTAG(1)	1207
	I=0	1208
	DO 215 J=1,N1	1209
	I=I+1	1210
	XFIT(I)=XSTOR(J,1)**2	1211
	YFIT(I)=YSTOR(J,1)	1212
215	SFIT(I)=SSTOR(J,1)	1213
	DO 216 J=1,N2	1214
	I=I+1	1215
	XFIT(I)=XSTOR(J,2)**2	1216
	YFIT(I)=YSTOR(J,2)	1217
216	SFIT(I)=SSTOR(J,2)	1218
	NFIT=I	1219
	GO TO 500	1220
220	N1=NTAG(1)*3/4	1221
	N2=NTAG(1)-N1+1	1222
	N3=NTAG(1)	1223
	N4=NTAG(2)-NTAG(1)	1224
	N5=(NTAG(3)-NTAG(2))*3/4	1225
	I=0	1226
	DO 225 J=N2,N3	1227
	I=I+1	1228
	XFIT(I)=XSTOR(J,1)	1229
	YFIT(I)=YSTOR(J,1)	1230
225	SFIT(I)=SSTOR(J,1)	1231
	DO 226 J=1,N4	1232
	I=I+1	1233
	XFIT(I)=XSTOR(J,2)	1234
	YFIT(I)=YSTOR(J,2)	1235
226	SFIT(I)=SSTOR(J,2)	1236
	DO 227 J=1,N5	1237
	I=I+1	1238
	XFIT(I)=XSTOR(J,3)	1239
	YFIT(I)=YSTOR(J,3)	1240
227	SFIT(I)=SSTOR(J,3)	1241
	NFIT=I	1242
	GO TO 500	1243
230	N1=(NTAG(2)-NTAG(1))*3/4	1244
	N2=(NTAG(2)-NTAG(1))-N1+1	1245
	N3=NTAG(2)-NTAG(1)	1246
	N4=NTAG(3)-NTAG(2)	1247
	N5=(NTAG(4)-NTAG(3))*3/4	1248
	I=0	1249
	DO 235 J=N2,N3	1250

	I=I+1	1251
	XFIT(I)=XSTOR(J,2)	1252
	YFIT(I)=YSTOR(J,2)	1253
235	SFIT(I)=SSTOR(J,2)	1254
	DO 236 J=1,N4	1255
	I=I+1	1256
	XFIT(I)=XSTOR(J,3)	1257
	YFIT(I)=YSTOR(J,3)	1258
236	SFIT(I)=SSTOR(J,3)	1259
	DO 237 J=1,N5	1260
	I=I+1	1261
	XFIT(I)=XSTOR(J,4)	1262
	YFIT(I)=YSTOR(J,4)	1263
237	SFIT(I)=SSTOR(J,4)	1264
	NFIT=I	1265
	GO TO 500	1266
240	N1=NTAG(3)-NTAG(2)	1267
	N2=NTAG(4)-NTAG(3)	1268
	I=0	1269
	DO 245 J=1,N1	1270
	I=I+1	1271
	XFIT(I)=XSTOR(J,3)	1272
	YFIT(I)=YSTOR(J,3)	1273
245	SFIT(I)=SSTOR(J,3)	1274
	DO 246 J=1,N2	1275
	I=I+1	1276
	XFIT(I)=XSTOR(J,4)	1277
	YFIT(I)=YSTOR(J,4)	1278
246	SFIT(I)=SSTOR(J,4)	1279
	NFIT=I	1280
	GO TO 500	1281
300	GO TO (310,320,320,320,330),LC	1282
310	N1=NTAG(1)	1283
	N2=NTAG(2)-NTAG(1)	1284
	I=0	1285
	DO 315 J=1,N1	1286
	I=I+1	1287
	XFIT(I)=XSTOR(J,1)**2	1288
	YFIT(I)=YSTOR(J,1)	1289
315	SFIT(I)=SSTOR(J,1)	1290
	DO 316 J=1,N2	1291
	I=I+1	1292
	XFIT(I)=XSTOR(J,2)**2	1293
	YFIT(I)=YSTOR(J,2)	1294
316	SFIT(I)=SSTOR(J,2)	1295
	NFIT=I	1296
	GO TO 500	1297
320	IF(LC.NE.2) GO TO 321	1298
	N1=NTAG(1)	1299
	N2=NTAG(2)-NTAG(1)	1300

	N3=NTAG(3)-NTAG(2)	1301
	GO TO 324	1302
321	LCL1=LC-1	1303
	LCL2=LC-2	1304
	LCU=LC+1	1305
	N1=NTAG(LCL1)-NTAG(LCL2)	1306
	N2=NTAG(LC)-NTAG(LCL1)	1307
	N3=NTAG(LCU)-NTAG(LC)	1308
324	I=0	1309
	DO 325 J=1,N1	1310
	I=I+1	1311
	XFIT(I)=XSTOR(J,LC-1)	1312
	YFIT(I)=YSTOR(J,LC-1)	1313
325	SFIT(I)=SSTOR(J,LC-1)	1314
	DO 326 J=1,N2	1315
	I=I+1	1316
	XFIT(I)=XSTOR(J,LC)	1317
	YFIT(I)=YSTOR(J,LC)	1318
326	SFIT(I)=YSTOR(J,LC)	1319
	DO 327 J=1,N3	1320
	I=I+1	1321
	XFIT(I)=XSTOR(J,LC+1)	1322
	YFIT(I)=YSTOR(J,LC+1)	1323
327	SFIT(I)=SSTOR(J,LC+1)	1324
	NFIT=I	1325
	GO TO 500	1326
330	N1=NTAG(4)-NTAG(3)	1327
	N2=NTAG(5)-NTAG(4)	1328
	I=0	1329
	DO 335 J=1,N1	1330
	I=I+1	1331
	XFIT(I)=XSTOR(J,4)	1332
	YFIT(I)=YSTOR(J,4)	1333
335	SFIT(I)=SSTOR(J,4)	1334
	DO 336 J=1,N2	1335
	I=I+1	1336
	XFIT(I)=XSTOR(J,5)	1337
	YFIT(I)=YSTOR(J,5)	1338
336	SFIT(I)=SSTOR(J,5)	1339
	NFIT=I	1340
500	SUMS=0.0	1341
	DO 510 I=1,IMA	1342
510	SUMS=SUMS+SIGA(I)	1343
	IF(SUMS.GT.0.0) GO TO 520	1344
	IWT=0	1345
520	NEVEN=0	1346
	NORDER=4	1347
	MODE=IWT	1348
	NUMCDF=0	1349
	MFIT=NFIT-1	1350

	IF((MFIT-NORDER).GT.0) GO TO 524	1351
	NORDER=3	1352
	IF((MFIT-NORDER).GT.0) GO TO 524	1353
	NORDER=2	1354
	IF((MFIT-NORDER).GT.0) GO TO 524	1355
	NORDER=1	1356
524	CALL FITPOL(XFIT,YFIT,SFIT,NFIT,NORDER,NEVEN,MODE,FTEST,YCALC,REAL	1357
	LC,SIGMAC,RELC,SIGMAR,CHI,NUMCOF)	1358
	CHISQR(LC)=CHI	1359
	DO 525 I=1,NUMCOF	1360
	COEF(I,LC)=REALC(I)	1361
	DELCOF(I,LC)=SIGMAC(I)	1362
	RELCOF(I,LC)=RELC(I)	1363
525	SRELC(I,LC)=SIGMAR(I)	1364
	NPLUS=NUMCOF+1	1365
	IF(NPLUS.GT.5) GO TO 527	1366
	DO 526 I=NPLUS,5	1367
	REALC(I)=0.0	1368
	RELCOF(I,LC)=0.0	1369
526	SRELC(I,LC)=0.0	1370
527	DO 530 I=1,5	1371
	TEST=ABS(COEF(I,LC))	1372
	IF(TEST.GT.0.0) GO TO 530	1373
	NPOLY=I-2	1374
	GO TO 532	1375
530	IF(I.EQ.5) NPOLY=4	1376
532	WRITE(6,1004) LC,NPOLY,(REALC(I),I=1,5)	1377
1004	FORMAT(T22,I1,6X,I1,14X,E13.6,4(2X,E13.6))	1378
	WRITE(6,1008) (RELCOF(I,LC),I=1,5)	1379
1008	FORMAT(T22,'RELATIVE COEFS = ',3X,5(2X,E13.6))	1380
	WRITE(6,1005) LC,CHISQR(LC),IWT,NUMCOF	1381
1005	FORMAT(T40,'REDUCED CHI-SQUARE FOR REGION',I2,' = ',E13.6,2X,'WEIG	1382
	IHT CODE=',I2,2X,'NO. COEFS=',I2, '//)	1383
999	CONTINUE	1384
	RETURN	1385
	END	1386
	SUBROUTINE FITPOL(X,Y,SIGMAY,NPTS,NORDER,NEVEN,MODE,FTEST,YFIT,A,S	1387
	IGMAA,B,SIGMAB,CHISQR,NTERMS)	1388
	DOUBLE PRECISION P,BETA,ALPHA,CHISQ,DSQRT	1389
	DIMENSION X(1),Y(1),SIGMAY(1),FTEST(1),YFIT(1),A(1),SIGMAA(1),B(1)	1390
	,SIGMAB(1)	1391
	DIMENSION WEIGHT(51),P(51,5),BETA(5),ALPHA(5,5)	1392
C		1393
C	ACCUMULATE WEIGHTS AND POWER SERIES TERMS	1394
C		1395
	11 NTERMS=1	1396
	NCOEFF=1	1397
	JMAX=NORDER+1	1398
	20 DO 40 I=1,NPTS	1399
	21 IF(MODE) 22,27,29	1400

	22	IF(Y(I))	25.27,23	1401
	23	WEIGHT(I)	=1.0/Y(I)	1402
		GO TO	31	1403
	25	WEIGHT(I)	=1.0/(-Y(I))	1404
		GO TO	31	1405
	27	WEIGHT(I)	=1.0	1406
		GO TO	31	1407
	29	WEIGHT(I)	=1.0/(SIGMAY(I)**2)	1408
	31	P(I,1)	=1.0	1409
		DO 36	L=1,NORDER	1410
	36	P(I,L+1)	=X(I)**L	1411
	40	CONTINUE		1412
C				1413
C		ACCUMULATE	MATRICES ALPHA AND BETA	1414
C				1415
	51	DO 54	J=1,NTERMS	1416
		BETA(J)	=0.0	1417
		DO 54	K=1,NTERMS	1418
	54	ALPHA(J,K)	=0.0	1419
	61	DO 66	I=1,NPTS	1420
		DO 66	J=1,NTERMS	1421
		BETA(J)	=BETA(J)+P(I,J)*Y(I)*WEIGHT(I)	1422
		DO 66	K=J,NTERMS	1423
		ALPHA(J,K)	=ALPHA(J,K)+P(I,J)*P(I,K)*WEIGHT(I)	1424
	66	ALPHA(K,J)	=ALPHA(J,K)	1425
C				1426
C		DELETE	FIXED COEFFICIENTS	1427
C				1428
	70	IF(NEVEN)	71,91,81	1429
	71	DO 76	J=3,NTERMS,2	1430
		BETA(J)	=0.0	1431
		DO 75	K=1,NTERMS	1432
		ALPHA(J,K)	=0.0	1433
	75	ALPHA(K,J)	=0.0	1434
	76	ALPHA(J,J)	=1.0	1435
		GO TO	91	1436
	81	DO 86	J=2,NTERMS,2	1437
		BETA(J)	=0.0	1438
		DO 85	K=1,NTERMS	1439
		ALPHA(J,K)	=0.0	1440
	85	ALPHA(K,J)	=0.0	1441
	86	ALPHA(J,J)	=1.0	1442
C				1443
C		INVERT	CURVATURE MATRIX ALPHA	1444
C				1445
	91	DO 95	J=1,JMAX	1446
		A(J)	=0.0	1447
		SIGMAA(J)	=0.0	1448
		B(J)	=0.0	1449
	95	SIGMAB(J)	=0.0	1450

	DO 97 I=1,NPTS	1451
	97 YFIT(I)=0.0	1452
	101 CALL MATINV(ALPHA,NTERMS,DET)	1453
	IF(DET) 111,103,111	1454
	103 CHISQR=0.0	1455
	GO TO 170	1456
C		1457
C	CALCULATE COEFFICIENTS, FIT, AND CHI SQUARE	1458
C		1459
	111 DO 115 J=1,NTERMS	1460
	DO 113 K=1,NTERMS	1461
	113 A(J)=A(J)+BETA(K)*ALPHA(J,K)	1462
	DO 115 I=1,NPTS	1463
	115 YFIT(I)=YFIT(I)+A(J)*P(I,J)	1464
	121 CHISQ=0.0	1465
	DO 123 I=1,NPTS	1466
	123 CHISQ=CHISQ+(Y(I)-YFIT(I))**2*WEIGHT(I)	1467
	FREE=NPTS-NCOEFF	1468
	CHISQR=CHISQ/FREE	1469
C		1470
C	TEST FOR END OF FIT	1471
C		1472
	131 IF(NTERMS-JMAX) 132,151,151	1473
	132 IF(NCOEFF-2) 133,134,141	1474
	133 IF(NEVEN) 137,137,135	1475
	134 IF(NEVEN) 135,137,135	1476
	135 NTERMS=NTERMS+2	1477
	GO TO 138	1478
	137 NTERMS=NTERMS+1	1479
	138 NCOEFF=NCOEFF+1	1480
	CHISQ1=CHISQ	1481
	GO TO 51	1482
	141 FVALUE=(CHISQ1-CHISQ)/CHISQR	1483
	IF(FTEST(NTERMS)-FVALUE) 134,143,143	1484
	143 IF(NEVEN) 144,146,144	1485
	144 NTERMS=NTERMS-2	1486
	GO TO 147	1487
	146 NTERMS=NTERMS-1	1488
	147 NCOEFF=NCOEFF-1	1489
	JMAX=NTERMS	1490
	149 GO TO 51	1491
C		1492
C	CALCULATE REMAINDER OF OUTPUT	1493
C		1494
	151 IF(MODE) 152,154,152	1495
	152 VARNCE=1.0	1496
	GO TO 155	1497
	154 VARNCE=CHISQR	1498
	155 DO 156 J=1,NTERMS	1499
	156 SIGMAA(J)=DSQRT(VARNCE*ALPHA(J,J))	1500

	161	IF(A(1))	162,170,162	1501
	162	DO 166 J=2,NTERMS		1502
		IF(A(J))	164,166,164	1503
	164	B(J)=A(J)/A(1)		1504
	165	SIGMAB(J)=B(J)*DSORT((SIGMAA(J)/A(J))**2+(SIGMAA(1)/A(1))**2-2.0*V		1505
		IARNCE*ALPHA(J,1)/(A(J)*A(1)))		1506
	166	CONTINUE		1507
		B(1)=1.0		1508
	170	RETURN		1509
		END		1510
		SUBROUTINE MATINV(ARRAY,NORDER,DET)		1511
		DOUBLE PRECISION ARRAY,AMAX,SAVE,DABS		1512
		DIMENSION ARRAY(5,5),IK(5),JK(5)		1513
	10	DET=1.0		1514
	11	DO 100 K=1,NORDER		1515
C				1516
C		FIND LARGEST ELEMENT ARRAY(I,J) IN REST OF MATRIX		1517
C				1518
		AMAX=0.00		1519
	21	DO 30 I=K,NORDER		1520
		DO 30 J=K,NORDER		1521
	23	IF(DABS(AMAX)-DABS(ARRAY(I,J)))	24,24,30	1522
	24	AMAX=ARRAY(I,J)		1523
		IK(K)=I		1524
		JK(K)=J		1525
	30	CONTINUE		1526
C				1527
C		INTERCHANGE ROWS AND COLUMNS TO PUT AMAX IN ARRAY(K,K)		1528
C				1529
	31	IF(AMAX)	41,32,41	1530
	32	DET=0.0		1531
		GO TO 140		1532
	41	I=IK(K)		1533
		IF(I-K)	21,51,43	1534
	43	DO 50 J=1,NORDER		1535
		SAVE=ARRAY(K,J)		1536
		ARRAY(K,J)=ARRAY(I,J)		1537
	50	ARRAY(I,J)=-SAVE		1538
	51	J=JK(K)		1539
		IF(J-K)	21,61,53	1540
	53	DO 60 I=1,NORDER		1541
		SAVE=ARRAY(I,K)		1542
		ARRAY(I,K)=ARRAY(I,J)		1543
	60	ARRAY(I,J)=-SAVE		1544
C				1545
C		ACCUMULATE ELEMENTS OF INVERSE MATRIX		1546
C				1547
	61	DO 70 I=1,NORDER		1548
		IF(I-K)	63,70,63	1549
	63	ARRAY(I,K)=-ARRAY(I,K)/AMAX		1550

DATA DL9/'10.0', 'PERC', 'ENT', 'PROB', 'FOR'//	1601
DATA DL10/'25.0', 'PERC', 'ENT', 'PROB', 'FOR'//	1602
DATA DL11/'50.0', 'PERC', 'ENT', 'PROB', 'FOR'//	1603
IZERO=0	1604
DO 1 I=1, IMA	1605
IF (XDIST(I).LT.0.) GO TO 1	1606
IZERO=IZERO+1	1607
X(IZERO)=XDIST(I)	1608
Y(IZERO)=YINT(I)	1609
1 CONTINUE	1610
IZE=IMA	1611
IMA=IZERO	1612
NZERO=0	1613
DO 4 IJ=1, N	1614
IF (RBP(IJ, LZ).LT.0.) GO TO 4	1615
NZERO=NZERO+1	1616
XA(NZERO)=RBP(IJ, LZ)	1617
YA(NZERO)=ARI(IJ, LZ)	1618
4 CONTINUE	1619
NHOLD=N	1620
N=NZERO	1621
IGL(5)=IGL(5)+LZ	1622
CALL GRAPH (IMA, X, Y, 0, 2, 7.00, 9.00, 0, 0, 0, 0, XL1, YL1, IGL, DLAB)	1623
CALL GRAPHS (IMA, X, Y, 4, 107, DL1)	1624
CALL GRAPHS (N, XA, YA, 1, 107, DL2)	1625
IGL(5)=IGL(5)-LZ	1626
LZERO=0	1627
DO 6 LDEX=1, KT	1628
IF (RDI(LDEX).LT.0.) GO TO 6	1629
LZERO=LZERO+1	1630
XX(LZERO)=RDI(LDEX)	1631
YY(LZERO)=RAD(LDEX)	1632
6 CONTINUE	1633
KTHOLD=KT	1634
KT=LZERO	1635
8 GO TO (9, 10, 11, 15, 16, 16, 16), NZ	1636
9 CALL GRAPHS(KT, XX, YY, 2, 111, DL3)	1537
CALL GRAPHS(KT, XX, YY, 0, 107, DL4)	1638
CALL GRAPHS(KT, XX, YY, 0, 107, DL8)	1639
GO TO 12	1640
10 CALL GRAPHS(KT, XX, YY, 2, 111, DL3)	1641
CALL GRAPHS(KT, XX, YY, 0, 107, DL5)	1642
CALL GRAPHS(KT, XX, YY, 0, 107, DL8)	1643
GO TO 12	1644
11 CALL GRAPHS(KT, XX, YY, 2, 111, DL3)	1645
CALL GRAPHS(KT, XX, YY, 0, 107, DL6)	1646
CALL GRAPHS(KT, XX, YY, 0, 107, DL8)	1647
GO TO 12	1648
15 CALL GRAPHS(KT, XX, YY, 2, 111, DL3)	1649
CALL GRAPHS(KT, XX, YY, 0, 107, DL7)	1650

CALL GRAPHS(KT,XX,YY,0,107,DL8)	1651
GO TO 12	1652
16 CALL GRAPHS (KT,XX,YY,2,111,DL3)	1653
NN=NZ-4	1654
GO TO (17,18,19),NN	1655
17 CALL GRAPHS (KT,XX,YY,0,107,DL9)	1656
GO TO 20	1657
18 CALL GRAPHS (KT,XX,YY,0,107,DL10)	1658
GO TO 20	1659
19 CALL GRAPHS (KT,XX,YY,0,107,DL11)	1660
20 CALL GRAPHS (KT,XX,YY,0,107,DL8)	1661
12 KT=KTHOLD	1662
IMA=IZE	1663
N=NHOLD	1664
DO 13 IPOS=1,KT	1665
13 RAD(IPOS)=ABS(RAD(IPOS))	1666
RETURN	1667
END	1668
SUBROUTINE TEMP (NT,IMAT,RBP,ARI,RADIST,RADINT,NLZT,DLAB,L3,KM,NL,	1669
INH,LKODE,KPLOT1,KPLOT2,KLINE1,KLINE2,DELA,DELINT,IARTP)	1670
DIMENSION FNUM(7)	1671
DIMENSION RBP(15,4),ARI(15,4),RADIST(51,4,7),RADINT(51,4,7),TLAT1(1672
AS1),X(15),RDIST(51),RA(6,51),LA(6,51),Y1(15),Y2(51),	1673
1TLAT2(51),TLAT3(51),TLAT4(51),TLAT5(51),TRAD1(51),TRAD2(51),TRAD3(1674
251),TRAD4(51),TRAD5(51),DLAB(5),IXL(5),IXR(5)	1675
3,SUMLAT(51),AVELAT(51),SUMRAD(51),AVERAD(51),DELINT(51,4,7)	1676
4,XTHOLD(15,4),YTHOLD(15,4),TLAT6(51),TRAD6(51),DELA(4),DELTR(6,51)	1677
DATA FNUM/0.5,1.0,2.5,5.0,10.0,25.0,50.0/	1678
DATA IXL/' TLO',4*' '/	1679
1IXR/' TRO',4*' '/	1680
DO 6 NLINE=1,NLZT	1681
KODEN=0	1682
IF (RBP(1,NLINE).GE.0.0) GO TO 3	1683
KODEN=KODEN+1	1684
ITZERO=0	1685
DO 2 NTSHIF=1,NT	1686
IF (RBP(NTSHIF,NLINE).LT.0.0) GO TO 2	1687
ITZERO=ITZERO+1	1688
XTHOLD(ITZERO,NLINE)=RBP(NTSHIF,NLINE)	1689
YTHOLD(ITZERO,NLINE)=ARI(NTSHIF,NLINE)	1690
2 CONTINUE	1691
DO 4 NSUB1=1,ITZERO	1692
RBP(NSUB1,NLINE)=XTHOLD(NSUB1,NLINE)	1693
4 ARI(NSUB1,NLINE)=YTHOLD(NSUB1,NLINE)	1694
3 IF (NLINE.LT.NLZT) GO TO 6	1695
IF (KODEN.EQ.0) GO TO 6	1696
NT=ITZERO	1697
6 CONTINUE	1698
IMAT=IMAT-1	1699
NT=NT-1	1700

```

NL=NL-1
IF (LKODE.EQ.1) GO TO 97
RETURN
97 IF (NLZT.GE.2) GO TO 1
WRITE (6,1000)
1000 FORMAT (//,10X,'TEMPS. CANNOT BE CALCULATED; ONLY ONE LINE')
RETURN
1 DO 96 NPOLY=1,KM
NL=NL+1
WRITE (6,1001)
1001 FORMAT (1H1)
WRITE (6,3000) NT,KODEN
3000 FORMAT (T10,'TEMP CONTROL PARAMETERS'///,T15,'NT = ',I2.5X,
2'KODEN = ',I2)
IF (KM.EQ.1) GO TO 5
WRITE (6,100) FNUM(NL)
100 FORMAT (10X,'DKABEL MULTIPLE F-TEST POLYNOMIAL TEMPERATURE CALCULA
TIONS FOR'/T15,F5.2,' PERCENT PROBABILITY OF EXCEEDING THE F-VALU
2E')
5 WRITE (6,1002)
1002 FORMAT (10X,'CALCULATION OF LATERAL AND RADIAL TEMPERATURESF 2-LIN
1E METHOD'///)
WRITE (6,1003)
1003 FORMAT (10X,'SYMBOL KEY')
WRITE (6,1004)
1004 FORMAT (5X,'SYMBOL LINE1 LINE2 EQ1 EQ2 INTEN.
1USED')
WRITE (6,1005)
1005 FORMAT (//,5X,'TLAT1 3815.84 3820.43 38175 33096 LAT
1ERAL')
WRITE (6,1006)
1006 FORMAT (/,5X,'TLAT2 " 3824.44 " 26140 "'
1')
WRITE (6,1007)
1007 FORMAT (/,5X,'TLAT3 3820.43 " 33096 "'
1')
WRITE (6,1008)
1008 FORMAT (/,5X,'TLAT4 3815.84 3825.88 38175 33507 "'
1')
WRITE (6,1009)
1009 FORMAT (/,5X,'TLAT5 3824.44 " 26140 "'
1')
WRITE (6,4000)
4000 FORMAT (/,5X,'TLAT6 3820.43 " 33096 "'
1')
WRITE (6,1010)
1010 FORMAT (/,5X,'TRAD1 THRU TRAD6 SIMILAR EXCEPT RADIAL INTEN. USED',
1////)
WRITE (6,5000) (DELA(I),I=1,NLZT)
5000 FORMAT (T10,'DELA(1)= ',F5.2,10X,'DELA(2)= ',F5.2,10X,'DELA(3)= ',

```

```

1701
1702
1703
1704
1705
1706
1707
1708
1709
1710
1711
1712
1713
1714
1715
1716
1717
1718
1719
1720
1721
1722
1723
1724
1725
1726
1727
1728
1729
1730
1731
1732
1733
1734
1735
1736
1737
1738
1739
1740
1741
1742
1743
1744
1745
1746
1747
1748
1749
1750

```

```

IF5.2,10X,'DELA(4)=',F5.2)
IF(IARTP.EQ.9) WRITE(6,5001)
5001 FORMAT(//,T10,'*****BANFIELD AND HUBER (1973) GA VALUES',//)
WRITE(6,1011) NT
1011 FORMAT(40X,'LATERAL TEMPERATURES FOR',I4,2X,'EXPERIMENTAL LATERAL
1 POSITIONS IN EMISS. SOURCE',//,T20,'X TLAT1(X) TLAT2(X)
2 TLAT3(X) TLAT4(X) TLAT5(X) TLAT6(X)',//)
DO 10 I=1,NT
TLAT1(I)=3173./ALOG10(1.1605*(ARI(I,2)/ARI(I,1)))
IF(IARTP.EQ.9) TLAT1(I)=TLAT1(I)/(1.0+6.218E-5*TLAT1(I))
IF(NLZT.EQ.2) GO TO 10
TLAT2(I)=7518./ALOG10(33.937*(ARI(I,3)/ARI(I,1)))
IF(IARTP.EQ.9) TLAT2(I)=TLAT2(I)/(1.0+2.559E-5*TLAT2(I))
TLAT3(I)=4345./ALOG10(29.244*(ARI(I,3)/ARI(I,2)))
IF(IARTP.EQ.9) TLAT3(I)=TLAT3(I)/(1.0-1.031E-6*TLAT3(I))
IF(NLZT.EQ.3) GO TO 10
TLAT4(I)=2916./ALOG10(1.676*(ARI(I,4)/ARI(I,1)))
IF(IARTP.EQ.9) TLAT4(I)=TLAT4(I)/(1.0+6.144E-5*TLAT4(I))
TLAT5(I)=-4608./ALOG10(0.0494*(ARI(I,4)/ARI(I,3)))
IF(IARTP.EQ.9) TLAT5(I)=TLAT5(I)/(1.0+2.906E-6*TLAT5(I))
TLAT6(I)=-256.9/ALOG10(1.444*(ARI(I,4)/ARI(I,2)))
IF(IARTP.EQ.9) TLAT6(I)=TLAT6(I)/(1.0+6.894E-5*TLAT6(I))
1012 FORMAT(15X,F8.3,6(4X,F8.1))
10 WRITE(6,1012) RBP(I,1),TLAT1(I),TLAT2(I),TLAT3(I),TLAT4(I),TLAT5(
1I),TLAT6(I)
WRITE(6,1013) IMAT
1013 FORMAT(//////////,40X,'RADIAL TEMPERATURES FOR',I4,2X,'RADIAL POS
1ITIONS IN THE EMISSION SOURCE',//,T20,'R TRAD1(R) TRAD2(R)
2 TRAD3(R) TRAD4(R) TRAD5(R) TRAD6(R)',//)
DO 20 J=1,IMAT
K=(IMAT-J)+2
TRAD1(J)=3173./ALOG10(1.1605*(RADINT(K,2,NPOLY)/RADINT(K,1,NPOLY))
1)
IF(IARTP.EQ.9) TRAD1(J)=TRAD1(J)/(1.0+6.218E-5*TRAD1(J))
DELTR(1,J)=(TRAD1(J)/(1.439*5079.))*(DELA(1)+DELA(2)+DELINT(K,1,NP
1OLY)+DELINT(K,2,NPOLY))
IF(NLZT.EQ.2) GO TO 20
TRAD2(J)=7518./ALOG10(33.937*(RADINT(K,3,NPOLY)/RADINT(K,1,NPOLY))
1)
IF(IARTP.EQ.9) TRAD2(J)=TRAD2(J)/(1.0+2.559E-5*TRAD2(J))
DELTR(2,J)=(TRAD2(J)/(1.439*12035.))*(DELA(1)+DELA(3)+DELINT(K,1,N
1POLY)+DELINT(K,3,NPOLY))
TRAD3(J)=4345./ALOG10(29.244*(RADINT(K,3,NPOLY)/RADINT(K,2,NPOLY))
1)
IF(IARTP.EQ.9) TRAD3(J)=TRAD3(J)/(1.0-1.031E-6*TRAD3(J))
DELTR(3,J)=(TRAD3(J)/(1.439*6956.))*(DELA(2)+DELA(3)+DELINT(K,2,NP
1OLY)+DELINT(K,3,NPOLY))
IF(NLZT.EQ.3) GO TO 20
TRAD4(J)=2916./ALOG10(1.676*(RADINT(K,4,NPOLY)/RADINT(K,1,NPOLY))
1)
IF(IARTP.EQ.9) TRAD4(J)=TRAD4(J)/(1.0+6.144E-5*TRAD4(J))

```

```

      DELTR(4,J)=(TRAD4(J)/(1.439*5668.))*(DELA(1)+DELA(4)+DELINT(K,1,NP
1014 1OLY)+DELINT(K,4,NPOLY))
      TRAD5(J)=-4608./ALOG10(0.0494*(RADINT(K,4,NPOLY)/RADINT(K,3,NPOLY)
1801 1))
      IF(IARTP.EQ.9) TRAD5(J)=TRAD5(J)/(1.0+2.906E-6*TRAD5(J))
1802 1803 1804
      DELTR(5,J)=(TRAD5(J)/(1.439*7367.))*(DELA(3)+DELA(4)+DELINT(K,3,NP
1805 1OLY)+DELINT(K,4,NPOLY))
      TRAD6(J)=-256.9/ALOG10(1.444*(RADINT(K,4,NPOLY)/RADINT(K,2,NPOLY))
1806 1807 1808 1809
      IF(IARTP.EQ.9) TRAD6(J)=TRAD6(J)/(1.0+6.894E-6*TRAD6(J))
      DELTR(6,J)=(TRAD6(J)/(1.439*411.))*(DELA(2)+DELA(4)+DELINT(K,2,NP
1810 1LY)+DELINT(K,4,NPOLY))
      FORMAT(15X,F8.3,6(4X,F8.1))
1811 1812 1813
20 WRITE(6,1014) RADIST(K,1,NPOLY),TRAD1(J),TRAD2(J),TRAD3(J),TRAD4(
1814 1J),TRAD5(J),TRAD6(J)
      WRITE(6,2999)
1815 1816
2999 FORMAT(//////,T10,'RADIAL POS',T26,'DELTA TRAD1',T43,'DELTA TRAD2'
1817 1,T60,'DELTA TRAD3',T76,'DELTA TRAD4',T94,'DELTA TRAD5',T111,'DELTA
1818 1 TRAD6')
      DO 29 I=1,IMAT
1819 1820
      J=(IMAT-I)+2
1821
3001 FORMAT(T8,E11.4,T26,5(E11.4,6X),E11.4)
1822
29 WRITE(6,3001) RADIST(J,1,NPOLY),(DELTR(K,I),K=1,6)
1823
      DO 30 L=1,IMAT
1824
      KK=(IMAT-L)+2
1825
30 RDIST(L)=RADIST(KK,1,NPOLY)
1826
      DO 40 M=1,NT
1827
      X(M)=RBP(M,1)
1828
      NN=IMAT
1829
      IF(KPLOT1.EQ.1) GO TO 65
1830
      IF(NLZT.EQ.2) GO TO 15
1831
      IF(NLZT.EQ.3) GO TO 21
1832
      IF(NLZT.EQ.4) GO TO 21
1833
      RETURN
1834
15 CALL GRAPH(NT,X,TLAT1,0,2,7,0,9,0,0,0,2500.,'X AND R (MM);','T(X
1835 1) AND T(R);','TEMPERATURE PROFILE;',DLAB)
      CALL GRAPHS(NT,X,TLAT1,4,107,'LATERAL TEMPS.;;')
1836 1837
      CALL GRAPHS(NN,RDIST,TRAD1,1,111,'RADIAL TEMPS.;;')
1838
      GO TO 12
1839
21 DO 22 N=1,NT
1840
      LA(1,N)=TLAT1(N)
1841
      IF(NLZT.EQ.2) GO TO 22
1842
      LA(2,N)=TLAT2(N)
1843
      LA(3,N)=TLAT3(N)
1844
      IF(NLZT.EQ.3) GO TO 22
1845
      LA(4,N)=TLAT4(N)
1846
      LA(5,N)=TLAT5(N)
1847
      LA(6,N)=TLAT6(N)
1848
22 CONTINUE
1849
      DO 23 II=1,IMAT
1850

```

	RA(1,II)=TRAD1(II)	1851
	IF (NLZT.EQ.2) GO TO 23	1852
	RA(2,II)=TRAD2(II)	1853
	RA(3,II)=TRAD3(II)	1854
	IF (NLZT.EQ.3) GO TO 23	1855
	RA(4,II)=TRAD4(II)	1856
	RA(5,II)=TRAD5(II)	1857
	RA(6,II)=TRAD6(II)	1858
23	CONTINUE	1859
	IF (NLZT.EQ.4) GO TO 50	1860
	DO 35 JJ=1,3	1861
	IF (JJ.LT.KLINE1) GO TO 34	1862
	IF (JJ.EQ.KLINE2) GO TO 34	1863
	DO 24 KK=1,NT	1864
24	Y1(KK)=LA(JJ,KK)	1865
	DO 25 LL=1,IMAT	1866
25	Y2(LL)=RA(JJ,LL)	1867
	IXL(1)=IXL(1)+1	1868
	IXR(1)=IXR(1)+1	1869
	CALL GRAPH (NT,X,Y1,0,2,7,0,9,,0,0,0,2500.,X AND R (MM);',T(X) A	1870
	IND T(R);',TEMPERATURE PROFILE;',DLAB)	1871
	CALL GRAPHS (NT,X,Y1,4,107,IXL)	1872
	CALL GRAPHS (NN,RDIST,Y2,1,111,IXR)	1873
	GO TO 35	1874
34	IXL(1)=IXL(1)+1	1875
	IXR(1)=IXR(1)+1	1876
35	CONTINUE	1877
	IXL(1)=IXL(1)-3	1878
	IXR(1)=IXR(1)-3	1879
	GO TO 12	1880
50	DO 60 JK=1,6	1881
	IF (JK.LT.KLINE1) GO TO 59	1882
	IF (JK.EQ.KLINE2) GO TO 59	1883
	DO 51 KL=1,NT	1884
51	Y1(KL)=LA(JK,KL)	1885
	DO 52 LM=1,IMAT	1886
52	Y2(LM)=RA(JK,LM)	1887
	IXL(1)=IXL(1)+1	1888
	IXR(1)=IXR(1)+1	1889
	CALL GRAPH (NT,X,Y1,0,2,7,0,9,,0,0,0,2500.,X AND R (MM);',T(X) A	1890
	IND T(R);',TEMPERATURE PROFILE;',DLAB)	1891
	CALL GRAPHS (NT,X,Y1,4,107,IXL)	1892
	CALL GRAPHS (NN,RDIST,Y2,1,111,IXR)	1893
	GO TO 60	1894
59	IXL(1)=IXL(1)+1	1895
	IXR(1)=IXR(1)+1	1896
60	CONTINUE	1897
	IXL(1)=IXL(1)-6	1898
	IXR(1)=IXR(1)-6	1899
12	IF (L3.EQ.1) GO TO 65	1900

IF (NPOLY.LT.KM) GO TO 96	1901
RETURN	1902
65 DO 75 IJK=1,NT	1903
SUMLAT(IJK)=0.0	1904
SUMLAT(IJK)=SUMLAT(IJK)+TLAT1(IJK)	1905
IF (NLZT.EQ.2) GO TO 66	1906
SUMLAT(IJK)=SUMLAT(IJK)+TLAT2(IJK)+TLAT3(IJK)	1907
IF (NLZT.EQ.3) GO TO 67	1908
SUMLAT(IJK)=SUMLAT(IJK)+TLAT4(IJK)+TLAT5(IJK)+TLAT6(IJK)	1909
AVELAT(IJK)=SUMLAT(IJK)/6.	1910
GO TO 75	1911
66 AVELAT(IJK)=SUMLAT(IJK)	1912
GO TO 75	1913
67 AVELAT(IJK)=SUMLAT(IJK)/3.	1914
75 CONTINUE	1915
DO 85 LMN=1,IMAT	1916
SUMRAD(LMN)=0.0	1917
SUMRAD(LMN)=SUMRAD(LMN)+TRAD1(LMN)	1918
IF (NLZT.EQ.2) GO TO 76	1919
SUMRAD(LMN)=SUMRAD(LMN)+TRAD2(LMN)+TRAD3(LMN)	1920
IF (NLZT.EQ.3) GO TO 77	1921
SUMRAD(LMN)=SUMRAD(LMN)+TRAD4(LMN)+TRAD5(LMN)+TRAD6(LMN)	1922
AVERAD(LMN)=SUMRAD(LMN)/6.	1923
GO TO 85	1924
76 AVERAD(LMN)=SUMRAD(LMN)	1925
GO TO 85	1926
77 AVERAD(LMN)=SUMRAD(LMN)/3.	1927
85 CONTINUE	1928
WRITE (6,2000)	1929
2000 FORMAT(10X,'DISTANCE AVE. RADIAL T')	1930
DO 90 NNN=1,IMAT	1931
2001 FORMAT (T10,E11.4,8X,E11.4)	1932
90 WRITE (6,2001) RDIST(NNN),AVERAD(NNN)	1933
WRITE (6,2002)	1934
2002 FORMAT (//////////,10X,'DISTANCE AVE. LATERAL T')	1935
DO 95 MMM=1,NT	1936
2003 FORMAT (T10,E11.4,8X,E11.4)	1937
95 WRITE (6,2003) X(MMM),AVELAT(MMM)	1938
IF (KPLOT2.EQ.1) GO TO 96	1939
CALL GRAPH (NT,X,AVELAT,0.2,7.0,9.,0,0,0,2500.,'X AND R (MM);','AV	1940
E. LINE PAIR TEMP.','AVE. LP TEMP PROFILE',DLAB)	1941
CALL GRAPHS (NT,X,AVELAT,4,107,'AVE. LATERAL TEMPS.')	1942
CALL GRAPHS (IMAT,RDIST,AVERAD,1,111,'AVE. RADIAL TEMPS.')	1943
96 CONTINUE	1944
RETURN	1945
END	1946
SUBROUTINE SLOPET (NT,IMAT,RBP,ARI,RADIST,RADINT,NLZT,DLAB,WAVE,KM	1947
1,NL,NH,LKODE,KPLOT3,KPNED1,KPNED2,DELA,DELINT,IARTP)	1948
C LEAST SQUARES SLOPE METHOD OF TEMPERATURE CALCULATION	1949
DIMENSION FNUM(7)	1950

	DIMENSION YCALCN(51,4),YINLA(51),TS(5),TLA(51),DLAB(5),RBP(15,4),	1951
	IARI(15,4),RADINT(51,4,7),RADIST(51,4,7),SLOPEL(51),ERRORL(51),	1952
	2RAYIN(51),WAVE(4),EQ(4),GA(4),RAT(51),RSLOPE(51),RERROR(51)	1953
	3,X1(15),X2(51),D(51,4)	1954
	4,CALYLA(51,4),YLA(51,4),YLADIF(51,4),CALYRA(51,4),YRA(51,4)	1955
	5,YRADIF(51,4),DELA(4),DELINT(51,4,7),DELTRS(51),COEFT(4)	1956
	DATA FNUM/0.5,1.0,2.5,5.0,10.0,25.0,50.0/	1957
	DATA TS/0.0,12.706,4.303,3.182,2.776/	1958
	IF(LKODE.EQ.2) GO TO 30	1959
	IF(LKODE.EQ.3) GO TO 1999	1960
	NL=NL-KM	1961
	DATA EQ/38175.,33096.,26140.,33507./,GA/7.49,6.462,0.2212,4.480/	1962
	IF(IARTP.NE.9) GO TO 35	1963
	WRITE (6,9999)	1964
9999	FORMAT (///,T10,'***** BAINFIELD AND HUBER GA VALUES USED*****')	1965
	GA(1)=10.25	1966
	GA(2)=5.619	1967
	GA(3)=0.1994	1968
	GA(4)=4.059	1969
	GO TO 35	1970
30	CONTINUE	1971
	EQ(1)=116634.	1972
	EQ(2)=118893.	1973
	EQ(3)=117199.	1974
	EQ(4)=117118.	1975
	GO TO (100,101,102,103,104,105),IARTP	1976
	READ (5,2000) (GA(JJJ),JJJ=1,NLZT)	1977
2000	FORMAT (4F10.0)	1978
	GO TO 35	1979
1999	READ(5,2000) (EQ(III),III=1,NLZT)	1980
	READ(5,2000) (GA(JJJ),JJJ=1,NLZT)	1981
	GO TO 35	1982
100	CONTINUE	1983
	GA(1)=2.67	1984
	GA(2)=36.65	1985
	GA(3)=13.25	1986
	GA(4)=20.64	1987
	GO TO 35	1988
101	CONTINUE	1989
	GA(1)=2.25	1990
	GA(2)=36.43	1991
	GA(3)=14.7	1992
	GA(4)=23.07	1993
	GO TO 35	1994
102	CONTINUE	1995
	GA(1)=2.55	1996
	GA(2)=36.0	1997
	GA(3)=14.0	1998
	GA(4)=21.3	1999
	GO TO 35	2000

```

103 CONTINUE
    GA(1)=3.96
    GA(2)=45.0
    GA(3)=18.0
    GA(4)=27.0
    GO TO 35
104 CONTINUE
    GA(1)=2.28
    GA(2)=32.0
    GA(3)=11.5
    GA(4)=18.9
    GO TO 35
105 CONTINUE
    GA(1)=2.37
    GA(2)=36.0
    GA(3)=14.0
    GA(4)=21.3
35 IF (NLZT.GE.3) GO TO 1
    WRITE (6,99)
99 FORMAT (15X,'INSUFFICIENT NUMBER OF DATA POINTS TO CALCULATE SLOPE
1 TEMP.')
```

RETURN

```

1 DO 25 NPOLY=1,KM
    NL=NL+1
    WRITE (6,1005)
1005 FORMAT (//////)
    IF (KM.EQ.1) GO TO 15
    WRITE (6,1006) FNUM(NL)
1006 FORMAT (10X,'DKABEL MULTIPLE F-TEST POLYNOMIAL TEMPERATURE CALCULA
1 TIONS FOR',T15,F5.2,' PERCENT PROBABILITY OF EXCEEDING THE F-VALU
2E')
```

15 WRITE (6,1000)

```

1000 FORMAT (5X,'CALCULATION OF TEMPERATURE BY THE LEAST-SQUARES SLOPE
1 METHOD')
    DO 2 II=1,NLZT
    DO 2 IJ=1,NT
    2 YCALCN(IJ,II)=ARI(IJ,II)
    CALL LSO (NT,YCALCN,NLZT,TS,GA,EQ,YINLA,TLA,SLOPEL,ERRORL,WAVE,
1 CALYLA,YLA,YLADIF)
    WRITE (6,1001)
1001 FORMAT ('          X          T(X)          SLOPE(X)          95 CL
1 Y-INTERCEPT')
```

DO 3 I=1,NT

```

1002 FORMAT (T2,E11.4,1X,E11.4,2X,E11.4,2(4X,E11.4))
3 WRITE (6,1002) RBP(I,1),TLA(I),SLOPEL(I),ERRORL(I),YINLA(I)
    IF (KPNED1.NE.1) GO TO 28
    WRITE (7,7000) DLAB
7000 FORMAT (10X,'LATERAL SLOPE TEMP. DATA FOR',5X,5A4,5X,'RUN')
```

DO 29 I2=1,NT

```

7001 FORMAT (2F10.3)
```

2001
2002
2003
2004
2005
2006
2007
2008
2009
2010
2011
2012
2013
2014
2015
2016
2017
2018
2019
2020
2021
2022
2023
2024
2025
2026
2027
2028
2029
2030
2031
2032
2033
2034
2035
2036
2037
2038
2039
2040
2041
2042
2043
2044
2045
2046
2047
2048
2049
2050

29	WRITE (7,7001) TLA(I2),RBP(I2,1)	2051
	WRITE (6,7002) DLAB	2052
7002	FORMAT (///,T10,'LATERAL SLOPE TEMP DATA HAS BEEN PUNCHED FOR USE	2053
	1 IN THE ELECTRON',/,T10,'DENSITY PROGRAM FOR THE DATA RUN',5X,5A4)	2054
28	DO 4 KK=1,NLZT	2055
	DO 4 KL=1,IMAT	2056
	K=(IMAT-KL)+2	2057
4	YCALCN(KL,KK)=RADINT(K,KK,NPOLY)	2058
	CALL LSQ (IMAT,YCALCN,NLZT,TS,GA,EQ,RAYIN,RAT,RSLOPE,RROR,WAVE,	2059
	ICALYRA,YRA,YRADIF)	2060
	DO 40 I=1,NLZT	2061
	DO 40 J=1,IMAT	2062
	K=(IMAT-J)+2	2063
40	D(J,I)=DELINT(K,I,NPOLY)	2064
	SUMEQ=0.0	2065
	SUMEQ2=0.0	2066
	DO 39 L=1,NLZT	2067
	SUMEQ=SUMEQ+EQ(L)	2068
39	SUMEQ2=SUMEQ2+(EQ(L)*EQ(L))	2069
	DENOMT=ABS((NLZT*SUMEQ2)-(SUMEQ*SUMEQ))	2070
	DO 38 M=1,NLZT	2071
38	COEFT(M)=ABS((NLZT*EQ(M))-SUMEQ)	2072
	DO 37 N=1,IMAT	2073
	XMULT=RAT(N)/(1.439*DENOMT)	2074
	TERM=0.0	2075
	DO 36 M=1,NLZT	2076
36	TERM=TERM+(COEFT(M)*(DELA(M)+D(N,M)))	2077
37	DELTRS(N)=XMULT*TERM	2078
	WRITE (6,1003)	2079
1003	FORMAT (' R T(R) SLOPE(R) 95 CL	2080
	1 Y-INTERCEPT',6X,'DELTA T(R) IN PERCENT')	2081
	DO 5 J=1,IMAT	2082
	K1=(IMAT-J)+2	2083
1004	FORMAT (T2,E11.4,1X,E11.4,2X,E11.4,2(4X,E11.4),12X,E11.4)	2084
5	WRITE (6,1004) RADIST(K1,1,NPOLY),RAT(J),RSLOPE(J),RROR(J),RAYIN	2085
	1(J),DELTRS(J)	2086
	IF (KPNED2.NE.1) GO TO 33	2087
	WRITE (7,8000) DLAB	2088
8000	FORMAT (10X,'RADIAL SLOPE TEMP. DATA FOR',5X,5A4,5X,'RUN')	2089
	DO 34 J2=1,IMAT	2090
	K2=(IMAT-J2)+2	2091
8001	FORMAT (2F10.3,15X,'DEGREE',15,5A4)	2092
34	WRITE (7,8001) RAT(J2),RADIST(K2,1,NPOLY),NL,DLAB	2093
	WRITE (6,8002) DLAB	2094
8002	FORMAT (///,T10,'RADIAL SLOPE TEMP. DATA HAS BEEN PUNCHED FOR USE	2095
	1 IN THE ELECTRON',/,T10,'DENSITY PROGRAM FOR THE DATA RUN',5X,5A4)	2096
33	WRITE (6,3000)	2097
3000	FORMAT (////////)	2098
	WRITE (6,3001)	2099
3001	FORMAT (T25,'LATERAL INTENSITY DATA. Y=LOG(GA/WAVE*I(X))',///)	2100

```

DO 6 N1=1,NT
WRITE (6,3002) RBP(N1,1),TLA(N1)
3002 FORMAT(/T15,'LATERAL DISTANCE = ',E11.4,2X,'T(X) = ',E11.4)
WRITE (6,3003)
3003 FORMAT (/T3,'WAVELENGTH      CALC Y      EXPT Y      DEL Y
1EXC. POT.',/)
DO 6 N2=1,NLZT
3004 FORMAT (T2,5(E11.4,2X))
6 WRITE (6,3004) WAVE(N2),CALYLA(N1,N2),YLA(N1,N2),YLADIF(N1,N2),EQ(
1N2)
WRITE (6,3005)
3005 FORMAT (//////////,T25,'RADIAL INTENSITY DATA, Y=LOG(GA/WAVE*I(R))
1',//)
DO 7 N3=1,IMAT
KKK=(IMAT-N3)+2
WRITE (6,3006) RADIST(KKK,1,NPOLY),RAT(N3)
3006 FORMAT (/T15,'RADIAL DISTANCE = ',E11.4,2X,'T(R) = ',E11.4)
WRITE (6,3007)
3007 FORMAT (/T3,'WAVELENGTH      CALC Y      EXPT Y      DEL Y
1EXC. POT.',/)
DO 7 N4=1,NLZT
3008 FORMAT (T2,5(E11.4,2X))
7 WRITE (6,3008) WAVE(N4),CALYRA(N3,N4),YRA(N3,N4),YRADIF(N3,N4),EQ(
1N4)
IF (KPLOTT3.EQ.1) GO TO 25
DO 10 M=1,NT
10 X1(M)=RBP(M,1)
DO 20 N=1,IMAT
K2=(IMAT-N)+2
20 X2(N)=RADIST(K2,1,NPOLY)
CALL GRAPH (NT,X1,TLA,0.2,7.0,9.,0.0,0.2500.,'X AND R (MM);','SLOP
1E T(X) AND T(R);','SLOPE TEMP, PROFILE;',DLAB)
CALL GRAPHS (NT,X1,TLA,4,107,'LATERAL SLOPE TEMP.:',)
CALL GRAPHS (IMAT,X2,RAT,1,11,'RADIAL SLOPE TEMP.:',)
25 CONTINUE
RETURN
END
SUBROUTINE LSQ (INDEX,YCALCN,NLZT,TS,GA,EQ,YIN,TEMP,SLOPE,ERRORM,
1WAVE,CALCY,Y,YDIF)
DIMENSION YCALCN(51,4),TS(5),GA(4),EQ(4),YIN(51),TEMP(51),SLOPE(51
1),ERRORM(51),SUMX(51),SUMY(51),SUMXX(51),SUMXY(51),WAVE(4),DENOM(5
21),SSE(51),SSEX(51),XBAR(51),DIFY(4),DIFX(4)
3,CALCY(51,4),Y(51,4),YDIF(51,4)
8 DO 50 I=1,INDEX
SUMX(I)=0.0
SUMY(I)=0.0
SUMXX(I)=0.0
SUMXY(I)=0.0
DO 2 J=1,NLZT
SUMX(I)=SUMX(I)+EQ(J)

```

```

2101
2102
2103
2104
2105
2106
2107
2108
2109
2110
2111
2112
2113
2114
2115
2116
2117
2118
2119
2120
2121
2122
2123
2124
2125
2126
2127
2128
2129
2130
2131
2132
2133
2134
2135
2136
2137
2138
2139
2140
2141
2142
2143
2144
2145
2146
2147
2148
2149
2150

```

	SUMY(I)=SUMY(I)+ALOG10(GA(J)/(WAVE(J)*YCALCN(I,J)))	2151
	SUMXX(I)=SUMXX(I)+(EQ(J)*EQ(J))	2152
2	SUMXY(I)=SUMXY(I)+(EQ(J)*ALOG10(GA(J)/(WAVE(J)*YCALCN(I,J))))	2153
	D=NLZT	2154
	DENOM(I)=(D*SUMXX(I))-(SUMX(I)*SUMX(I))	2155
	SLOPE(I)=((D*SUMXY(I))-(SUMX(I)*SUMY(I)))/DENOM(I)	2156
	YIN(I)=((SUMXX(I)*SUMY(I))-(SUMXY(I)*SUMX(I)))/DENOM(I)	2157
	SSE(I)=0.0	2158
	SSEX(I)=0.0	2159
	XBAR(I)=SUMX(I)/D	2160
	DO 3 L=1,NLZT	2161
	CALCY(I,L)=SLOPE(I)*EQ(L)+YIN(I)	2162
	Y(I,L)=ALOG10(GA(L)/(WAVE(L)*YCALCN(I,L)))	2163
	YDIF(I,L)=Y(I,L)-CALCY(I,L)	2164
	DIFY(L)=YDIF(I,L)*YDIF(I,L)	2165
	SSE(I)=SSE(I)+DIFY(L)	2166
	XDIF=EQ(L)-XBAR(I)	2167
	DIFX(L)=XDIF*XDIF	2168
3	SSEX(I)=SSEX(I)+DIFX(L)	2169
	SSEX(I)=SQRT(SSEX(I))	2170
	S=SQRT(SSE(I)/(D-2.))	2171
	ERRORM(I)=(TS(NLZT)*S)/SSEX(I)	2172
	TEMP(I)=1./(1.60013*SLOPE(I))	2173
50	CONTINUE	2174
	RETURN	2175
	END	2176

APPENDIX B:
ABEL INVERSION CALCULATIONS

General Considerations and the
Abel Integral Equation

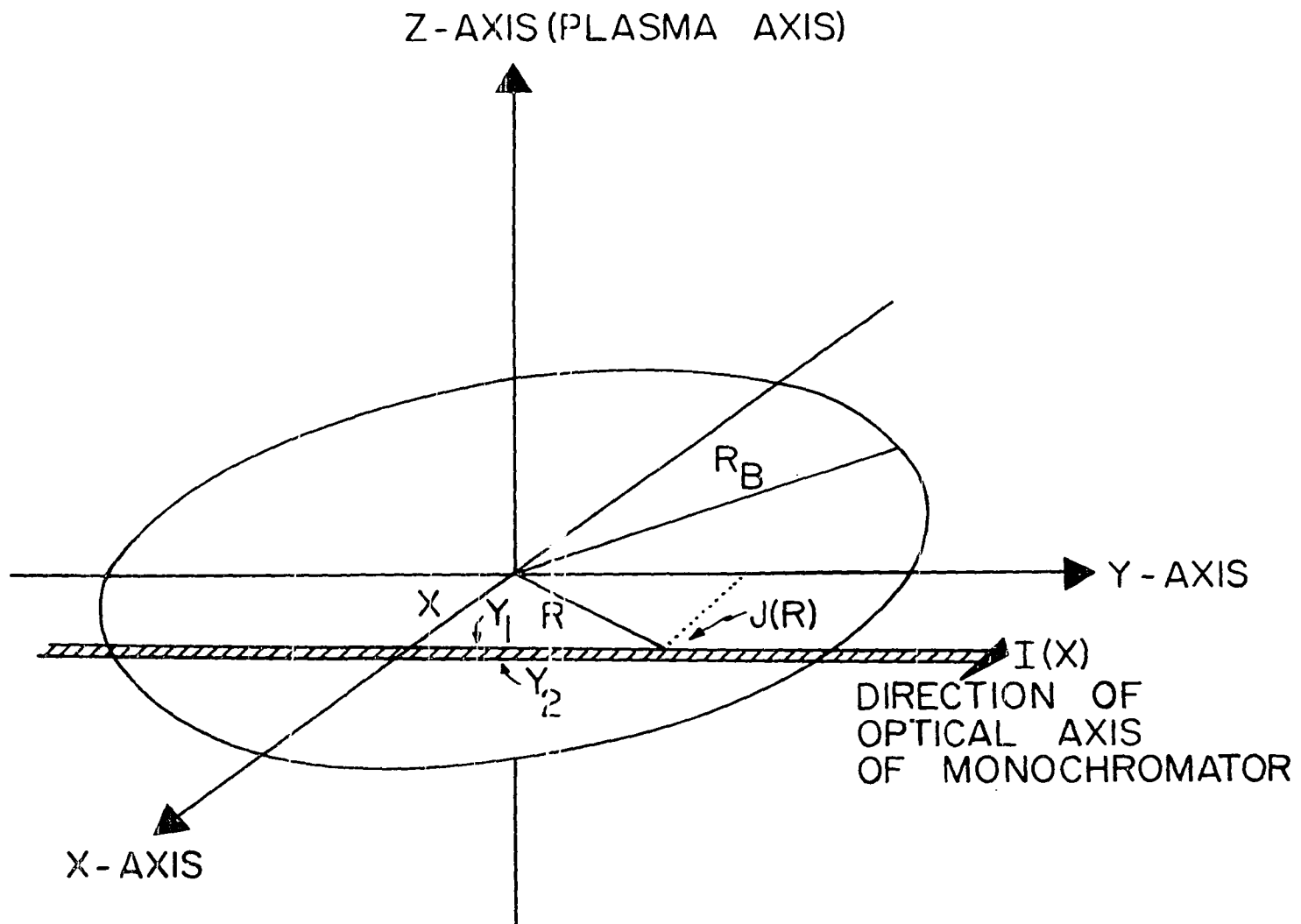
We consider a cross-section of the plasma which is circularly symmetric with respect to the Z-axis as illustrated in Figure B-1. The experimentally measured lateral intensity, $I(X)$, at displacement X , is given by the integral of the radial intensity distribution function $J(R)$, which is collected in the monochromator viewing field over the depth of the source from a horizontal section parallel to the Y-axis,¹

$$I(X) = 2 \int_0^{Y(X)} J(R) dY \quad (B1)$$

The factor of 2 in Equation B1 arises from the fact that the integral limits apply to only half of the source and the radial distribution function has been assumed to be symmetric about the X-axis. When the transformation of variables defined by

¹It is important to realize that Equation B1 expresses the geometrical relationship between the spatially resolved emission, which is projected from unit volume of a horizontal section of the source parallel to the Y-axis, i.e., $J(R)$ and, the space integrated intensity radiated over the depth of that section, i.e., $I(X)$.

Figure B-1. Spatial relationship between the measured lateral intensity, $I(X)$, at displacement X ; and, the radial intensity, $J(R)$, at radius R from the center of a circularly symmetric source employing side-on observation. R_B is the boundary radius at which no lateral intensity is detected



$$\begin{aligned}
 R^2 &= X^2 + Y^2 \\
 Y &= (R^2 - X^2)^{1/2} \\
 dY &= R(R^2 - X^2)^{-1/2} dR
 \end{aligned}
 \tag{B2}$$

is performed, Equation B1 becomes

$$I(X) = 2 \int_X^{R_B} R J(R) (R^2 - X^2)^{-1/2} dR
 \tag{B3}$$

where, R is the radial distance from the center of the source, R_B is the radius at the outer boundary, X is the lateral displacement from the center (Figure B-1) and, the change in limits is given by

$$R = X \quad \text{at} \quad Y = 0
 \tag{B4}$$

and,

$$R = R_B \quad \text{at} \quad Y = Y(X)$$

Equation B3 is the Abel integral equation and is a special case of the Volterra equation of the first kind (129). To solve for the unknown $J(R)$ function, Equation B3 may be analytically inverted to yield (36,40,129).

$$J(R) = - \frac{1}{\pi} \int_R^{R_B} \frac{I'(X)}{(X^2 - R^2)^{1/2}} dX
 \tag{B5}$$

provided $J(R)=0$ for all $R>R_B$. $I'(X)$ is the first derivative of the radiance function with respect to the lateral coordinate X , i.e.,

$$I'(X) = d(I(X))/dX$$

Various methods for solving Equation B5 have been devised; these methods can be broken into three general categories (49, 50): (1) graphical, (2) numerical, and (3) data approximation schemes. The latter two approaches utilize curve fitting or other mathematical approximations. A number of graphical or semigraphical methods for solving Equation B3 or B5 have appeared in the literature (52,130-132). Friederish (52) made the assumption that the ratio, $I(X)/X$, was constant in a given increment interval to simplify evaluation of the Abel integral over that interval; a graphical method was employed to obtain the $I(X)/X$ values. Hormann (132a) transformed the variables in Equation B5 to obtain an integral which he evaluated by graphical techniques. Despite some successful applications of these graphical methods, all are time consuming and have been outmoded by faster computer methods. We shall focus our attention on these rapid analysis methods in the following sections.

Numerical Methods

In 1935, Hormann (132a) and more recently in 1950, Gooderum and Wood (131) suggested methods for numerical integration of Equation B5. Both methods could be applied when the spectrometric measurement of lateral intensities was accomplished with a low aperture optical transfer system similar to that described in this work. Nestor and Olsen (49)

simplified these procedures to yield a significantly improved method, especially when a large number of observed functions were to be inverted. This method was also compatible with computer analysis.

For the Nestor and Olsen method, the numerical integration of Equation B5 was performed by dividing the X-axis into N zones of equal width a, as shown in Figure B-2; the n-th zone was defined by the relationships, $X_n \leq X \leq X_{n+1}$ and $X_n = na$. With the transformation

$$v = R^2 \text{ and } u = X^2 \quad (B6)$$

Equation B5 became

$$J(R(v)) = - (1/\pi) \int_v^{R_B^2} I'(u) (u - v)^{-1/2} du \quad (B7)$$

where, the following relationships were employed

$$\begin{aligned} dX &= (1/2) u^{-1/2} du \\ (X^2 - R^2)^{1/2} &= (u - v)^{1/2} \\ d(I(u))/du &= (d(I(X))/dX)(d(g(u))/du) \end{aligned} \quad (B8)$$

and,

$$\begin{aligned} g(u) &= X = u^{1/2} \\ I'(X) &= 2 u^{1/2} I'(u) \end{aligned} \quad (B9)$$

When the integral in Equation B7 was divided into sub-integrals for each zone and $I(u)$ was assumed to be a linear function of u in each zone, the following form was obtained

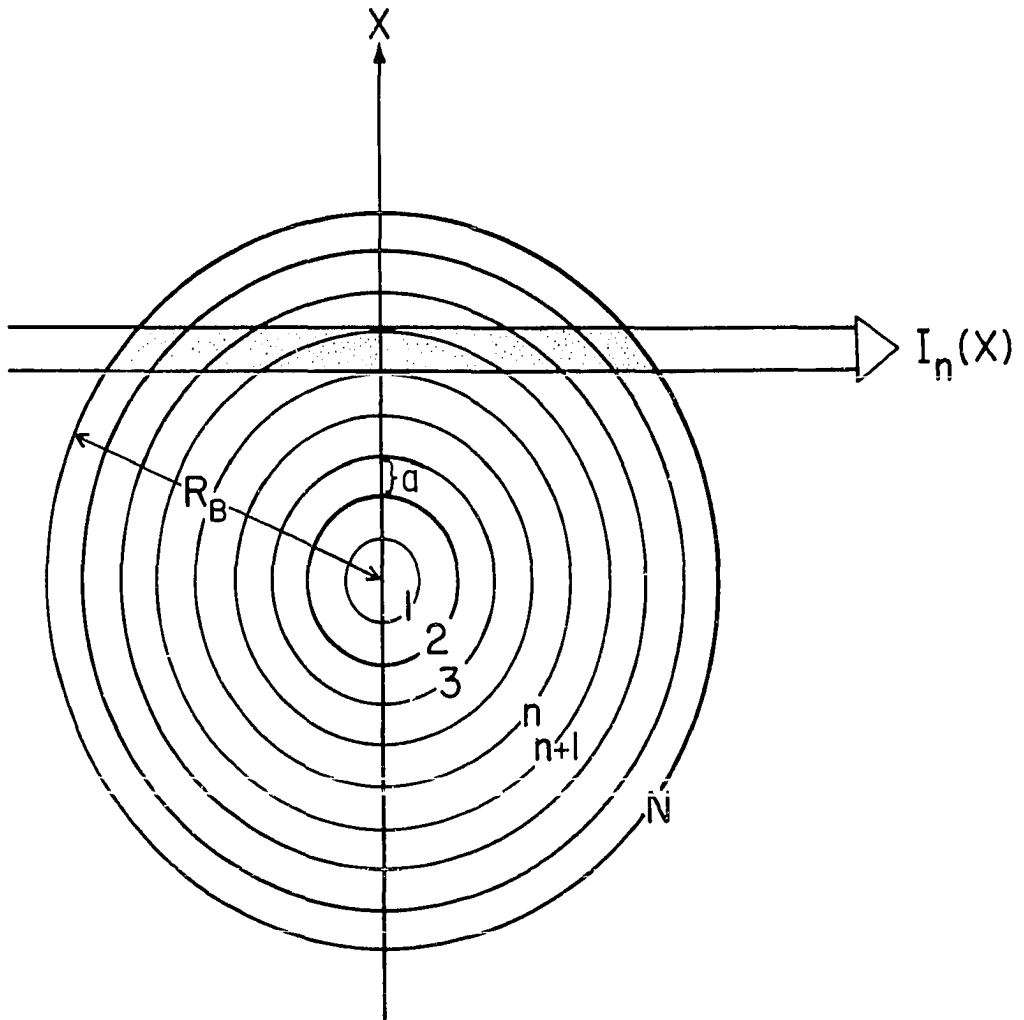


Figure B-2. Two-dimensional representation of a circularly symmetric source divided into N zones of equal width, a

for any zone, k

$$J_k = J(ak) = (-1/\pi) \sum_{n=k}^{N-1} I'_n(u) \int_{(an)^2}^{(a(n+1))^2} (u - (ak)^2)^{-1/2} du \quad (B10)$$

where, the integral limits and the v variable were replaced by the appropriate zone constants. $I'_n(u)$ was approximated within each zone by

$$I'_n(u) = \frac{(I_{n+1}(u) - I_n(u))}{a^2((n+1)^2 - n^2)} \quad (B11)$$

Substitution of Equation B11 into B10 and subsequent integration yielded

$$J_k = -\frac{2}{a\pi} \sum_{n=k}^{N-1} (I_{n+1}(u) - I_n(u)) \times \frac{((n+1)^2 - k^2)^{1/2} - (n^2 - k^2)^{1/2}}{(2n+1)} \quad (B12)$$

A transformation to the original coordinate system yielded

$$J_k = -\frac{2}{a\pi} \sum_{n=k}^{N-1} A_{kn} (I_{n+1}(X) - I_n(X)) \quad (B13)$$

where,

$$A_{kn} = \frac{((n+1)^2 - k^2)^{1/2} - (n^2 - k^2)^{1/2}}{(2n+1)} \quad (B14)$$

Equation B14 was further simplified to yield

$$J_k = - \frac{2}{a\pi} \sum_{n=k}^N B_{kn} I_n \quad (\text{B15})$$

where,

$$B_{kn} = - A_{kn} \quad \text{for} \quad n = k$$

and (B16)

$$B_{kn} = A_{k,n-1} - A_{kn} \quad \text{for} \quad n \geq k+1$$

Other methods for numerical solution of Equation B5 are also available. Pearce (132b) suggested a procedure similar to the Nestor and Olsen method. Maldonado, et al. (53) described a method which yielded more reliable radial emission coefficients when the measured lateral intensity distribution showed irregular fluctuations, especially in regions where $I(X)$ changed gradually with lateral position X . However, this procedure was computationally more complex than the Nestor and Olsen method described above. Maldonado and Olsen (54) generalized the method of reference 53 to include asymmetric sources and applied it to those which possessed a mirror plane of symmetry. Olsen, et al. (55) later extended this application to optically thin plasma cross-sectional geometries of arbitrary shape.

Discussions on the errors associated with numerical methods may be found elsewhere (133,134) and will not be reiterated here. It is worth noting, however, that these

methods generally suffer when the error level on the measured $I(X)$ profile values is significant because the numerical solution procedure for obtaining $J(R)$ values greatly magnifies these errors.

Data Approximation Methods

In 1966, Cremers and Birkebak (50) described a data approximation scheme for solution of Equation B3 or B5 which was faster than conventional numerical techniques and could readily be adapted to computer analysis. The basic assumption of this method was that the lateral intensity distribution function could be approximated by an n -th degree polynomial of the form

$$I(X) = C_0 + C_1X + C_2X^2 + \dots + C_nX^n \quad (\text{B17})$$

with the corresponding derivative function

$$I'(X) = C_1 + 2C_2X + 3C_3X^2 + \dots + nC_nX^{n-1} \quad (\text{B18})$$

When Equation B18 was substituted into Equation B5 the following expression for the radial distribution function was obtained

$$J(R) = -\frac{1}{\pi} \int_R^{R_B} \frac{(C_1 + 2C_2X + \dots + nC_nX^{n-1})}{(X^2 - R^2)^{1/2}} dX \quad (\text{B19})$$

An analytical solution of Equation B19 was possible when the polynomial coefficients were determined by least-squares techniques and the equation was separated into "n" component integrals.

Cremers and Birkebak cautioned that fitting the entire curve to a single polynomial resulted in peculiar radial profiles which precluded this approach because of the many poor fits that resulted. Consequently, they suggested subdividing the profiles into m zones and fitting an n-th degree polynomial to the form

$$I_k(X) = {}_k C_0 + \sum_{i=1}^n {}_k C_i X^i, \quad \text{for } k = 1, 2, \dots, m \quad (\text{B20})$$

to each zone. To assure smooth transitions from zone to zone, the polynomial fits overlapped into the adjacent zones. When the differential form of Equation B20 was substituted into Equation B5 an integrable expression was obtained.

If the integrant of Equation B5 is defined as

$$S_k = - I'_k(X) / ((X^2 - R^2)^{1/2}) \quad (\text{B21})$$

a closer examination of the actual integrations indicated by this equation may be carried out. For $I(X)$ divided into m zones and for a given R contained within a zone k such that

$$R_{k-1} \leq R \leq R_k \quad (\text{B22})$$

the radial intensity is given by

$$J(R) = {}_k F_0(R) + F_1(R) \quad (B23)$$

where, ${}_k F_0(R)$ and $F_1(R)$ are defined by

$${}_k F_0(R) = \int_R^{R_k} S_k \, dX \quad (B24)$$

and

$$F_1(R) = \sum_{i=k+1}^m \int_{R_{i-1}}^{R_i} S_i \, dX \quad \text{for } k < m$$

$$= 0 \quad \text{for } k = m \quad (B25)$$

The subdivision of the $I(X)$ profile employed in these calculations is schematically represented in Figure B-3. It should be noted that the zones were counted from the center where $R_0=0$ to the outer radius of the source where $R_m=R_B$.

Cremers and Birkebak made an additional refinement on the form of the assumed polynomial in Equation B20 because of the nature of the slope at $R = 0$. When Equation B20 was differentiated the following form was obtained

$$I'_k(X) = {}_k C_1 + \sum_{i=2}^n ({}_k C_i) i X^{i-1} \quad (B26)$$

and it was noted that $I'_k(X) \neq 0$ at $X = 0$. Consequently, the profile did not possess the desired zero slope at the

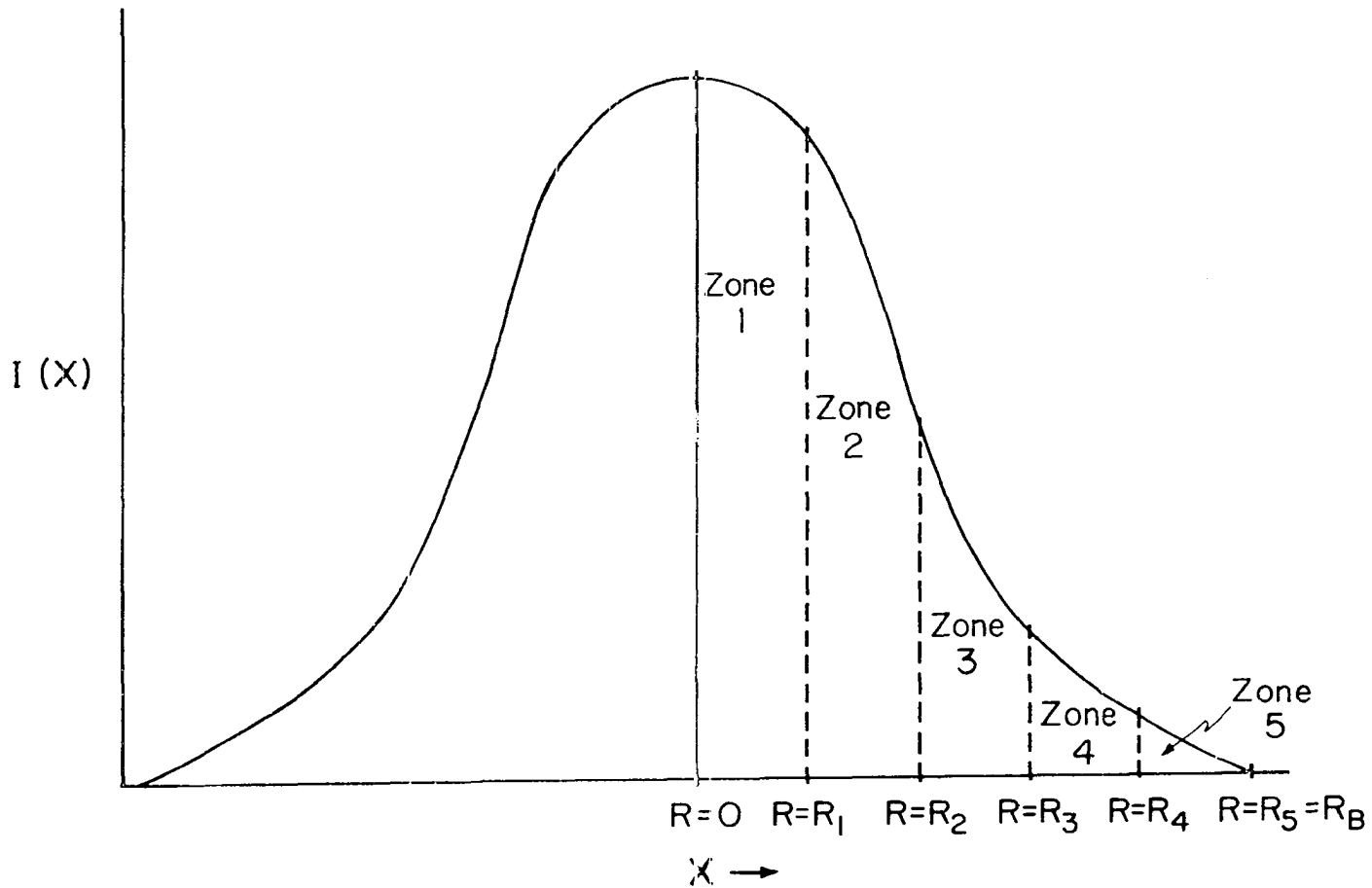


Figure B-3. Schematic representation of five zone subdivision of the $I(X)$ profile (bell-type curve case)

center that a circularly symmetric distribution should have. To avert this problem, Cremers and Birkebak (50) suggested that a polynomial in X^2 which possesses the desired zero slope at $X = 0$, be employed for the inner-most zone, i.e.,

$$I_1(X) = {}_1C_0 + \sum_{i=1}^n {}_1C_i X^{2i} \quad (B27)$$

Therefore, solutions of Equation B5 which utilize the zone dependency of Equations B20 or B27 were considered in this dissertation research.

Cremers and Birkebak also suggested that (1) subdivision of the $I(X)$ profile into five zones and (2) 4-th degree polynomial least-squares fitting of the data, were sufficient for most cases encountered in physical systems. The following discussions of the actual integration procedures employed here have been restricted to these suggestions.

Method of integration for zones 2-5

Examination of Equation B23 revealed that it was necessary to evaluate the integrals ${}_kF_0(R)$ and $F_1(R)$. Substitution of the 4-th degree polynomial of the form given by Equation B20 into Equation B24 yielded

$${}_kF_0(R) = -\frac{1}{\pi} \left(\int_R^{R_k} \frac{{}_kC_1}{G(X,R)} dX + 2 \int_R^{R_k} \frac{{}_kC_2 X}{G(X,R)} dX + 3 \int_R^{R_k} \frac{{}_kC_3 X^2}{G(X,R)} dX + 4 \int_R^{R_k} \frac{{}_kC_4 X^3}{G(X,R)} dX \right) \quad (B28)$$

where, $n = 4$ and

$$G(X,R) = (X^2 - R^2)^{1/2} \quad (\text{B29})$$

Solutions for the integrals in Equation B28 may be found in most integral tables, e.g., (135). Upon integration of Equation B28 the following form was obtained

$$\begin{aligned} k^F_o(R) = & -\frac{1}{\pi} \left[k^C_1 \ln(X + G(X,R)) + 2 k^C_2 G(X,R) \right. \\ & + \frac{3}{2} k^C_3 (X G(X,R) + R^2 \ln(X + G(X,R))) \\ & \left. + 4 k^C_4 (G^3(X,R)/3 + R^2 G(X,R)) \right] \Big|_R^{R_k} \quad (\text{B30}) \end{aligned}$$

Evaluation of Equation B30 at the limits (R to R_k) and combining terms yielded

$$\begin{aligned} k^F_o(R) = & -\frac{1}{\pi} \left(k^C_1 \ln\left(\frac{R_k + G(R_k,R)}{R}\right) + 2 k^C_2 G(R_k,R) \right. \\ & + \frac{3}{2} k^C_3 (R_k G(R_k,R) + R^2 \ln\left(\frac{R_k + G(R_k,R)}{R}\right)) \\ & \left. + 4 k^C_4 (G^3(R_k,R)/3 + R^2 G(R_k,R)) \right) \quad (\text{B31}) \end{aligned}$$

where, the following relations were used

$$(R_k^2 - R^2)^{1/2} = G(R_k,R)$$

$$\ln(X + G(X,R)) = \ln(R_k + G(R_k,R)) \quad \text{for} \quad X = R_k$$

$$(R^2 - R^2)^{1/2} = 0 = G(R,R)$$

and

$$\ln(X + G(X,R)) = \ln(R) \quad \text{for} \quad X = R$$

For a given R such that $R_4 \leq R \leq R_5$, ${}_5F_0(R)$ was the only integral that required evaluation. However, when k was less than m, Equation B25 indicated that $F_1(R)$ also had to be evaluated. This set of summed integrals possessed solutions identical to those of Equation B30 except that the limits were replaced by the appropriate values from B25, i.e.,

$$\begin{aligned} F_1(R) = & \sum_{i=k+1}^5 \left(-\frac{1}{\pi} \right) \left({}_iC_1 \ln(R_i + G(R_i,R)) \right. \\ & + 2 {}_iC_2 G(R_i,R) + \frac{3}{2} {}_iC_3 (R_i G(R_i,R) \\ & + R^2 \ln(R_i + G(R_i,R))) + 4 {}_iC_4 (G^3(R_i,R)/3 \\ & + R^2 G(R_i,R)) - ({}_iC_1 \ln(R_{i-1} + G(R_{i-1},R)) \\ & + 2 {}_iC_2 G(R_{i-1},R) + \frac{3}{2} {}_iC_3 (R_{i-1} G(R_{i-1},R) \\ & + R^2 \ln(R_{i-1} + G(R_{i-1},R))) \\ & \left. + 4 {}_iC_4 (G^3(R_{i-1},R)/3 + R^2 G(R_{i-1},R)) \right) \quad (B32) \end{aligned}$$

It should be noted that when the integrals were summed from zone to zone, the predetermined least-squares polynomial

coefficients changed smoothly to the zone under consideration because of the overlapping of the fits into adjacent zones.

Method of integration for zone 1

From the previous discussion of the desired behavior of $I(X)$ in the neighborhood of $X = 0$ ($I'(X=0) = 0$) it was apparent that a polynomial of the form of Equation B27 was required for values of R when $0 \leq R < R_1$, i.e., R was confined to zone 1. Differentiation, expansion, and substitution of Equation B27 into B24 yielded

$$\begin{aligned}
 {}_1F_0(R) = & \left(-\frac{2}{\pi}\right) \left(\int_R^{R_1} \frac{{}_1C_1 X}{G(X,R)} dX + 2 \int_R^{R_1} \frac{{}_1C_2 X^3}{G(X,R)} dX \right. \\
 & \left. + 3 \int_R^{R_1} \frac{{}_1C_3 X^5}{G(X,R)} dX + 4 \int_R^{R_1} \frac{{}_1C_4 X^7}{G(X,R)} dX \right) \quad (B33)
 \end{aligned}$$

where, $n = 4$ and the notation of Equation B29 was used. When the integration was performed and the limits were evaluated, ${}_1F_0(R)$ was given by

$$\begin{aligned}
 {}_1F_0(R) = & \left(-\frac{2}{\pi}\right) \left({}_1C_1 G(R_1,R) + 2 {}_1C_2 (G^3(R_1,R)/3 \right. \\
 & + R^2 G(R_1,R)) + 3 {}_1C_3 (R^4 G(R_1,R) \\
 & + \frac{2}{3} R^2 G^3(R_1,R) + \frac{1}{5} G^5(R_1,R)) \\
 & + 4 {}_1C_4 (R^6 G(R_1,R) + R^4 G^3(R_1,R) \\
 & \left. + \frac{3}{5} R^2 G^5(R_1,R) + \frac{1}{7} G^7(R_1,R)) \right) \quad (B34)
 \end{aligned}$$

Because the other zones (2-5) were not affected by the change in the zone 1 equation for $I(X)$, $F_1(R)$ was evaluated in precisely the same manner established in Equation B32.

Other data approximation methods are also available for solution of the Abel integral equation (B3) or its inverted form (B5). Freeman and Katz (56) suggested a curve-fitting procedure in which a single polynomial was fitted to the $I(X)$ profile data. However, Cremers and Birkebak (50) cautioned that this method yielded peculiar line profiles when it was applied to arc data. Barr (57) suggested a method similar to that of Cremers and Birkebak which employed polynomials determined by least-squares techniques that yielded the best fit of the data over five-point intervals centered about each data point.

Error analysis

When Equation B3 was solved for the lateral displacement $X = 0$, the following form was obtained

$$I(X=0) = 2 \int_0^{R_B} J(R) dR \quad (B35)$$

Therefore, the area under the radial intensity profile was predicted to equal the lateral intensity at zero displacement from the plasma axis. When test data were employed (50,53), the agreement was better than 1% while for experimental data

it was ~ 1 to 5% for bell-type profiles and ~ 5 to 15% for toroidal curves.

Equations B31, B32, and B34 were readily amenable to differential error treatments (81) so that the computational uncertainties in the radial intensities obtained could be calculated. The radial intensity defined by these equations was a function of the polynomial coefficients, ${}_1C_j$, and the radial position R . When the uncertainty in R was assumed to be negligible, a maximum differential error treatment yielded

$$\Delta J(R)_k \approx \sum_{j=1}^4 \left\{ \left| \frac{\partial {}_k F_0(R)}{\partial {}_k C_j} \right| \Delta {}_k C_j + \sum_{i=k+1}^5 \left| \frac{\partial F_1(R)}{\partial {}_i C_j} \right| \Delta {}_i C_j \right\} \quad (\text{B36})$$

where, the subscript k denoted the profile zone. For zone 1 the uncertainty, $\Delta J(R)_1$ was obtained by combining Equation B36 with the expressions for ${}_1 F_0(R)$ and $F_1(R)$, Equations B34 and B32, respectively. For the other zones ($2 \leq k \leq 5$) Equation B36 was combined with Equations B31 and B32 to yield the appropriate $\Delta J(R)_k$ values. The $\Delta J(R)_k$ values so obtained represented approximations to the maximum random calculation error in the corresponding $J(R)_k$ values for each zone. Systematic errors such as those encountered when measuring lateral intensities were accounted for by other means, e.g., added to the random error estimates.

The uncertainties in the coefficients ($\Delta_1 C_j$) were obtained from the error analysis techniques incorporated within the polynomial fitting method employed (reference 81, Chapter 8).

APPENDIX C:

ATOMIC PARTITION FUNCTION AND SAHA-EGGERT'S
ELECTRON DENSITY CALCULATIONS

To a first approximation, partition functions appear to be easily calculated by summing over all energy levels of the element of interest which are below the ionization limit; this would be accomplished with the expression (36)

$$z^{z-1}(T) = \sum_n g_n \exp\left(-\frac{E_n}{kT}\right) \quad (C1)$$

where, $z-1$ is the ionization stage and g_n is the statistical weight of the level, n , with energy E_n at temperature T . An immediate problem is encountered when attempts are made to apply the above procedure to the calculation of atomic partition functions namely, even the most complete listing of atomic energy levels (136) contains only a fraction of those predicted for a given element. If the missing levels are reasonably high in energy, few problems will be experienced for temperatures below 7000 K. However, the calculated values may be seriously in error at higher temperatures or, for elements for which the missing levels are at relatively low energies. Also, when the ionization limit (E_1^{z-1}) of the species is approached, the sum in Equation C1 diverges because the number of discrete levels is unbounded while the

corresponding energies (except for levels which autoionize; 36, p. 140) are restricted to values less than E_1^{Z-1} .

Several methods for overcoming these difficulties have been reported (31, pp. 231-258). All these theories share the premise that there exists a finite maximum principal quantum number n^* (sometimes referred to as the "effective" quantum number) and, accurate partition function values are obtained only when all energy levels for values of n below n^* are considered in the calculation. The effective quantum number (n^*) and the corresponding energy (E_{n^*}) are functions of temperature, electron number density, ion densities, and the effective nuclear charge of the species. Therefore, the summation in Equation C1 must be truncated at the reduced ionization limit (RIL), $E_1^{Z-1} - \Delta E_1^{Z-1}$ where, ΔE_1^{Z-1} is the ionization lowering for the species in question (36). In this manner, only those energy levels less than or equal to the RIL value are counted. This truncation precludes the possibility of counting a single level twice, once in a bound state and once in a free state.

The energies of the levels near the ionization limit which are sufficiently hydrogen-like, are given by the Rydberg formula (36)

$$E_1^{Z-1} - E_{n\ell}^{Z-1} = \frac{z^2 E_H}{n^2} \quad (C2)$$

where, E_H is the ionization energy of atomic hydrogen ($109,679 \text{ cm}^{-1}$) and $n \geq 4$. The statistical weight of the level

$E_{n\ell}^{z-1}$, is given by $g_n = 2n^2$. When the term value, $-E_H/(n^*)^2$, is combined with Equation C2, the effective principal quantum number is given by

$$n^* = \left(\frac{z^2 E_H}{\Delta\epsilon} \right)^{1/2} \quad (C3)$$

where, $\Delta\epsilon = E_i^{z-1} - E_{n\ell}^{z-1}$. The Ritz formula (117) may then be written as

$$n^* = n - \alpha - \frac{z^2}{n^2} \beta \quad (C4)$$

where, $z = 1$ for neutral atoms, $z = 2$ for singly charged ions, $z = 3$ for doubly charged ions, etc., and α, β are series parameters. Drawin and Felenbok (31) suggested that Equation C4 be used to complete each spectral series that was considered in the partition function calculation. Generally, the last two members observed in the series were used to evaluate α and β , which were subsequently employed with Equation C4 to calculate the remaining members of the series. In the case where a spectral series was predicted but for which no members were observed, an alternate series as closely related as possible was substituted and its degeneracy approximately increased to account for the unobserved terms. This method is reasonably accurate for elements with simple energy level schemes, however, its application to complex systems is overly elaborate. An alternate approach was reported by Griem (36)

and was applied to plasma simulation calculations by Barnett (137). This method for calculating atomic partition functions employed only those levels from reasonably complete configurations for which all states with principal quantum numbers less than a maximum value were observed. In this approach, the effective quantum number was defined by

$$n^* = n_{\max} \leq \left(\frac{z^2 E_H}{E_1^{z-1}} \right)^{1/2} \quad (C5)$$

where, hydrogen-like character was assumed, Only those levels E_n with $n \leq n_{\max}$ contributed to the partition function calculation. The procedure involved two steps: (1) selection of n' , the highest usable principal quantum number for the species, and (2) addition of a correction factor (from n' to n_{\max}) with hydrogen-like character assumed but still accounting for multiplicity differences. The complete partition function was then approximately given by (36)

$$z^{z-1}(T) \approx \sum_{n=1}^{n'} g_n \exp\left(-\frac{E_n}{kT}\right) + (2S_1+1)(2L_1+1) \\ \times \sum_{n=n'+1}^{n_{\max}} 2n^2 \exp\left(-\frac{E_1^{z-1} - (z^2 E_H/n^2)}{kT}\right) \quad (C6)$$

where, the first summation was made over those levels which were included in the complete or nearly complete configurations and, the second summation was the correction term. In

the second summation, S_1 and L_1 were the spin and orbital quantum numbers of the parent configuration, i.e., the ground state of the next higher ionization stage z . The degeneracies in the first summation were given by $g_n = 2J_n + 1$ where, J_n was the orbital angular momentum quantum number for the (discrete) level E_n and, the index n referred to all relevant quantum numbers (36).

Barnett (137) demonstrated that the Ritz completion method and Griem's method yielded parallel trends in partition function calculations for reasonable temperatures (below 15,000 K). Therefore, because Griem's method was computationally simpler, Equation C6 was employed to calculate the neutral atom ($z = 1$) partition functions of several elements for subsequent use in Saha-Eggert's electron density studies for this dissertation research. The correction term was generally not needed for singly charged and higher ionization stages because the missing levels were high in energy for the elements considered. The value of n' for each element was determined in the following manner: (1) all observed spectral series were tabulated (136) with the corresponding maximum observed n values (n_{\max}); (2) a weighted maximum principal quantum number, n_w , was calculated according to the total degeneracy of each series term ($n_w = (2S+1)(2L+1)(n_{\max})$); (3) a weighted average maximum principal quantum number was defined by

$$n_{wa} = \frac{1}{N_d} \sum_{i=1}^N (n_w)_i \quad (C7)$$

where, N_d = sum of the degeneracies of the observed spectral terms,

$$N_d = \sum_{j=1}^N (n_{max})_j \quad (C8)$$

and, N = number of observed spectral terms; (4) n' was taken as the largest integer satisfying the inequality $n' \leq n_{wa}$; and (5) the correction was begun at $n'' = (n'+1)$ where, n'' was the smallest integer which satisfied the condition, $n_{wa} \leq n''$. Griem (36) concluded that the best procedure for selecting n' was neither clearly established nor extremely critical because the last terms of the correction sum tend to dominate its contribution to the partition function calculation. The approach outlined here was reasonable because the maximum principal quantum numbers of the observed levels were weighted according to the degeneracy of the spectral term of the series to which they belonged (n_{max} values) and, the correction for missing levels was begun above a weighted average of these n_{max} values. The partition function values calculated by this procedure were in reasonable agreement with those reported by Drawin and Felenbok (31) and those calculated by Barnett (137) for temperatures below 10,000 K.

Use of the Saha-Eggert's Electron
Density Program

A FORTRAN IV computer program was written to perform the radial Saha-Eggert's electron density calculations and a complete listing of the source statements is included as C337EDNS. This program employed the partition function values which were calculated by the procedure discussed above. The data card requirements for this program are listed in Table C-1.

Table C-1. Data card requirements for C337EDNS

Type #	# Cards	Columns	Variable Name	Format	Remarks
1	1	1- 5	NSETS	I5	Number of data sets; one data set per Saha element
2	500 (max)	1- 8 11-20 21-30 31-40 41-50	TSYM TTEST QTEST(1,i) QTEST(2,i) QTEST(3,i)	2A4 F10.0 F10.0 F10.0 F10.0	Element identifier of partition function arrays Temperature array for partition functions Partition function array for neutral atom species Partition function array for first ion species Partition function array for second ion species
3	1/set	1- 5	NRUNS	I5	Number of runs in a given data set
4	1/run	1-70 71-75	XIDENT NUMAQP	35A2 I5	Data set identification label Number of transition probability sources (5 max)
5	1/run	1-10 11-20 21-30 31-40 41-50	WAVEA WAVEI GATOM GION EQATOM	F10.0 F10.0 F10.0 F10.0 F10.0	Wavelength of atomic line (Angstrom units) Wavelength of ionic line (Angstrom units) Degeneracy of atomic line emitting level Degeneracy of ionic line emitting level Excitation energy of atomic line (cm ⁻¹ units)

Table C-1. (Continued)

Type #	# Cards	Columns	Variable Name	Format	Remarks
		51-60	EQION	F10.0	Excitation energy of ionic line (cm^{-1} units)
6a	1/run	1-50	A(1,j)	5F10.0	Transition probability array for atomic line (5 max)
6b	1/run		A(2,j)		Same as 6a except for ionic line
7	1/run	1-10	XIP	F10.0	Ionization energy of atomic species (cm^{-1} units)
		11-20	DELXIP	F10.0	Ionization energy lowering
8	1/run	1- 5	NR	I5	Number of radial positions
9	NR/run	1-10	TR	F10.0	Radial temperature array
		11-20	R	F10.0	Corresponding radial position array
10a	NR/run	1-10	XI(i,1)	F10.0	Radial intensity array for atomic line
		21-30	DELIR(i,1)	F10.4	Corresponding relative uncertainty array (%)
10b	NR/run		XI(i,2)		Same as 10a except for ionic line
			DELIR(i,2)		Same as 10a except for ionic line


```

51  IF (TSYM(1) .EQ. CHECKT) GO TO 6
52  CONTINUE
53  ITEST=I-1
54  READ(5,99) NRUNS
55  FORMAT(I5)
56  DO 999 ILDDF=1, NRUNS
57  READ(5,101) XIDENT, NUMAQP
58  FORMAT(35A2, I5)
59  READ(5,102) WAVEA, WAVEI, GATOM, GION, EQATOM, EGIION
60  FORMAT(6F10.0)
61  DO 200 I=1, 2
62  FORMAT(SF10.0)
63  READ(5,201) (A(I,J), J=1, NUMAQP)
64  READ(5,103) XIP, DELXIP
65  FORMAT(2F10.0)
66  READ(5,104) NR
67  FORMAT(I5)
68  DO 10 I=1, NR
69  FORMAT(2F10.0)
70  READ(5,105) TR(I), R(I)
71  DO 9 J=1, ITEST
72  IF (ABS(TR(I))-TEST(J)) .GT. 5.0) GO TO 9
73  QZERO(I)=QTEST(1,J)
74  QPLUS(I)=QTEST(2,J)
75  GO TO 10
76  CONTINUE
77  CONTINUE
78  DO 20 J=1, 2
79  FORMAT(F10.0, 10X, F10.0)
80  READ(5,106) XI(I,J), DELIR(I,J)
81  DC 25 I=1, NR
82  SUMDEN(I)=0.0
83  SUMRAT(I)=0.0
84  SUMS(I)=0.0
85  DO 998 IDEX=1, NUMAQP
86  AION=A(1, IDEX)
87  AION=A(2, IDEX)
88  DO 30 I=1, NR
89  EFAC=EGATOM-EGION-XIP+DELXIP
90  EFAC=EFAC/0.69505
91  ERRFAC=(1.50-(EFAC/TR(I)))*100.0
92  EXP=2.71828*(EFAC/TR(I))
93  TTERM=TR(I)*1.5
94  RATIO=(XI(I,1))*WAVEA*GION*AION)/((XI(I,2))*WAVEI*GATOM*AATOM)
95  EXPFAC=(EGION-EGATOM)/0.69505
96  EXPN=2.71828*(EXPFAC/TR(I))
97  ZRATIO=QPLUS(I)/QZERO(I)
98  EIP=- (XIP-DELXIP)
99  100

```

	EIP=EIP/0.69505	101
	EXPIP=2.71828**((EIP/TR(I)))	102
	SSTAR=4.8296E15*TTERM*ZRATIO*EXPIP	103
	RATION(I)=EXPN*ZRATIO/RATIO	104
	EDENS(I)=4.8296E15*RATIO*TTERM*EXP	105
	ERR1=200.+(DELIR(I,1)**2)+(DELIR(I,2)**2)+ERRFAC	106
	S(I)=SQRT(ERR1*EDENS(I)*EDENS(I))	107
	S(I)=S(I)/EDENS(I)	108
	SUMDEN(I)=SUMDEN(I)+EDENS(I)	109
	SUMRAT(I)=SUMRAT(I)+RATION(I)	110
30	SUMS(I)=SUMS(I)+S(I)	111
	WRITE(6,1000) XIDENT	112
1000	FORMAT(1H1,T10,'ELECTRON DENSITY CALCULATION; IDENT= ',35A2)	113
	WRITE(6,1001) WAVEA,GATOM,EQATOM,AATOM	114
1001	FORMAT(/////T15,'ATOM LINE DATA: WAVELENGTH = ',F10.4,2X,'GQ = '	115
1	,F10.4,2X,'EQ = ',F10.4,2X,'AQP = ',F10.4)	116
	WRITE(6,1002) WAVEI,GION,EQION,AION	117
1002	FORMAT(//,T15,'ION LINE DATA: WAVELENGTH = ',F10.4,2X,'GQ = ',F10	118
1	.4,2X,'EQ = ',F10.4,2X,'AQP = ',F10.4)	119
	WRITE(6,1003) XIP,DELXIP	120
1003	FORMAT(/////T15,'IONIZATION POTENTIAL = ',F10.3,2X,'LOWERING OF I	121
1	ONIZATION PCTENTIAL = ',F10.4)	122
	WRITE(6,1004)	123
1004	FORMAT(/////T10,'RADIUS',T20,'TEMPERATURE',T35,'ION LINE INT',T55	124
1	, 'ATOM LINE INT',T75,'ELECTRON DENSITY',T95,'ION/ATOM RATIO',T110,	125
2	'DELTA NE, PERCENT')	126
	DO 40 N=1,NR	127
1005	FORMAT(T5,F10.4,T20,F10.4,T35,E12.5,T55,E12.5,T75,E12.5,T95,E12.5,	128
1	T110,E12.5)	129
40	WRITE(6,1005) R(N),TR(N),XI(N,2),XI(N,1),EDENS(N),RATION(N),S(N)	130
998	CONTINUE	131
	WRITE(6,1006)	132
1006	FORMAT(1H1,//,T10,'AVERAGE VALUES')	133
	WRITE(6,1004)	134
	DO 50 N=1,NR	135
1007	FORMAT(T5,F10.4,T20,F10.4,T35,E12.5,T55,E12.5,T75,E12.5,T95,E12.5,	136
1	T110,E12.5)	137
	SUMDEN(N)=SUMDEN(N)/NUMAQP	138
	SUMRAT(N)=SUMRAT(N)/NUMAQP	139
	SUMS(N)=SUMS(N)/NUMAQP	140
50	WRITE(6,1007) R(N),TR(N),XI(N,2),XI(N,1),SUMDEN(N),SUMRAT(N),SUMS(141
1	N)	142
999	CONTINUE	143
	STOP	144
	END	145

APPENDIX D:

CONVOLUTION AND H_{β} ELECTRON DENSITY CALCULATIONS

We consider the convolution integral for the "folding" of lorentzian and gaussian line profiles (61,93)

$$I^F(\Delta\lambda^*) = \int_{-\infty}^{+\infty} I^G(\Delta\lambda) I^L(\Delta\lambda^* - \Delta\lambda) d(\Delta\lambda) \quad (D1)$$

where, $I^G(\Delta\lambda)$ = gaussian profile, $I^L(\Delta\lambda)$ = lorentzian profile, and $I^F(\Delta\lambda)$ = folded line profile. Equation D1 mathematically expresses the effect of superimposition of the "smearing" function I^L on the gaussian line profile I^G . Each gaussian intensity contribution $I^G(\Delta\lambda)$ at displacement $\Delta\lambda$ from the unperturbed line center is smeared out over all other positions of the profile by the lorentzian broadening function centered at $\Delta\lambda$. The contribution of this smeared intensity to the I^F profile at a distance $\Delta\lambda^*$ from the unperturbed line center is given by the product of the gaussian at $\Delta\lambda$, $I^G(\Delta\lambda)$, with the lorentzian centered at $\Delta\lambda$, i.e., $I^L(\Delta\lambda^* - \Delta\lambda)$. The resulting folded intensity at the point $\Delta\lambda^*$ from the unperturbed line center is obtained by integration over all intensities contributing at $\Delta\lambda^*$.

The total area under the line envelope remains constant so it is convenient to normalize

$$\int_{-\infty}^{+\infty} I^G(\Delta\lambda) d(\Delta\lambda) = \int_{-\infty}^{+\infty} I^L(\Delta\lambda) d(\Delta\lambda) = 1 \quad (D2)$$

and, consequently

$$\int_{-\infty}^{+\infty} I^F(\Delta\lambda) d(\Delta\lambda) = 1 \quad (D3)$$

Because convolution is commutative, either the gaussian or the lorentzian profile may be considered to be the smearing function; this is shown as follows. First, we define

$$\Delta\lambda' = \Delta\lambda^* - \Delta\lambda \quad (D4)$$

then,

$$\Delta\lambda = \Delta\lambda^* - \Delta\lambda'$$

and

$$d(\Delta\lambda') = d(\Delta\lambda^*) - d(\Delta\lambda) \quad (D5)$$

but,

$$d(\Delta\lambda^*) = 0 \quad (D6)$$

thus,

$$d(\Delta\lambda') = - d(\Delta\lambda) \quad (D7)$$

The change in the integration limits is given by

$$\Delta\lambda = -\infty \implies \Delta\lambda' = +\infty$$

and

$$\Delta\lambda = +\infty \implies \Delta\lambda' = -\infty \quad (D8)$$

Combining Equation D1 with the variable transformations given by Equations D5, D7, and D8 yields

$$I^F(\Delta\lambda^*) = - \int_{+\infty}^{-\infty} I^G(\Delta\lambda^* - \Delta\lambda') I^L(\Delta\lambda') d(\Delta\lambda') \quad (D9)$$

but, the $\Delta\lambda'$ variable is only an integration dummy so this equation may be written

$$I^F(\Delta\lambda^*) = \int_{-\infty}^{+\infty} I^L(\Delta\lambda) I^G(\Delta\lambda^* - \Delta\lambda) d(\Delta\lambda) \quad (D10)$$

where the relationship

$$- \int_{+\infty}^{-\infty} = \int_{-\infty}^{+\infty}$$

has been used.

A FORTRAN IV computer program was written to perform the convolution calculations described in Chapter II of this dissertation and a complete listing of the source statements is included as C337CONV. The Cal-Comp plotting facility described in Appendix A was (optionally) employed to produce plots of the H_β Stark profiles folded with Doppler and instrument contributions, which were obtained from this program. This was accomplished in the PLOT subroutine, which made use of the SIMPLOTTER program library described in Appendix A. The PLOT subroutine and the CALL PLOT

statement in the main program should be removed for installations where SIMPLOTTER is not available; the plotting capability will be lost if this is done.

The user input variables for this program are defined at the beginning of the C337CONV listing. The card input of Stark profile data was designed to accommodate the format employed in the Stark profile tabulations of Vidal et al. (98). Either the instrument broadening profiles which were read from data cards (ICONV = 1) or, internally generated Doppler profiles for the temperatures employed in the calculations of reference 98 (ICONV = 0) could be employed as smearing functions. The broadening profile could be symmetric (ISYMBP = 0) for which only intensities at positive displacements from the center were required or, it could be asymmetric (ISYMBP = 1) for which complete profile data were required.

Because the comment cards included in the C337CONV listing are generally self-explanatory, only a brief description of the program operation will be presented here. First, the number of data sets (NSETS) was read where one data set was associated with each instrument broadening profile employed. The value of the primary DO loop variable (NUMSET) ranged from 1 to NSETS. Second, the appropriate number of runs (NRUNS) was read for the NUMSET value where NRUNS corresponded to the number of different electron density (n_e) values associated with the data set. Third, the relevant

instrument profile variables and the profile itself were read from data cards. Fourth, the variables associated with the run were input from data cards. Fifth, the reduced wavelength scaling factor defined by (98)

$$\text{DENOM} = 1.25 \times 10^{-9} n_e^{2/3} \quad (\text{D11})$$

was calculated for the electron density run. The wavelength displacements and half-widths of the instrument profile were divided by this scaling factor to yield reduced values and the instrument profile was area normalized. Sixth, the appropriate area normalized reduced Stark profile data (98) for positive displacements were read from data cards for the electron density run. Seventh, the convolution integration calculations were performed and the resulting folded profiles were area normalized. Finally, the half-widths of the folded profiles were determined by appropriate interpolation methods (98).

Within the convolution calculation section of the program, the ratio of the reduced instrument profile half-width to that of the appropriate reduced Stark profile, i.e., $\Delta\lambda_{\frac{1}{2}}^G / \Delta\lambda_{\frac{1}{2}}^S$ was calculated to determine the "narrowest" of the two profiles. When this ratio was 1.5 or greater, the convolution was integrated with respect to the "narrow" Stark profile (see Equation D10) but, for values less than 1.5 it was performed with respect to the gaussian-like instrument

profile (Equation D1). The instrument profile displacement axis was divided into 100 parts for the integration calculations and the corresponding intensity values were obtained by interpolation (98) between the original data points.

Before the empirical "narrowness" test was devised the convolution integration had been carried out exclusively over the reduced Stark profile displacement variable and very serious errors in calculated $I^F(\Delta\lambda^*)$ values were subsequently obtained, because integration over the wide reduced Stark profiles often obscured the effect of the narrower reduced instrument broadening profile. When this test was incorporated into the program the fine structure of these profiles was not lost and, consequently, the accuracy of the convolution calculation was significantly improved.

The convolution calculation was carried out over successive four-point segments from the negative to the positive integral limits; these limits were determined from the Stark and instrument broadening profiles employed in these calculations. The appropriate $I^G \cdot I^S$ products from Equation D1 or D10 were calculated for each segment and the area of that segment was determined which the DCSIQU function or the RLFOTH and RLDOPM subroutines. These routines were obtained from the International Mathematical and Statistical Libraries (IMSL) subroutine library (138) which was available at the ISU Computations Center.

The half-widths, profile maximum intensity values, and profile center intensities obtained here agreed within 1-3% with the corresponding values from Vidal et al. (98) when these H_{β} Stark and Doppler profile data were used to test the convolution method developed in this dissertation research. The accuracy of this method was better than 0.1% for pure Doppler-Doppler test convolutions; the folded profile half-widths and intensity values could be directly calculated for these data (93).

The contents of the data cards required for operation of the C337CONV program are listed in Table D-1.

H_{β} Electron Density Program

The FORTRAN IV computer program which was written to perform the electron density calculations from Stark broadening measurements on the H_{β} line (C337BROD) is listed after the convolution program. Electron densities were calculated in this program with the iterative approximation procedure outlined in Chapter II of this dissertation. The comment cards at the beginning of the listing of C337BROD define all input variables necessary for the operation of this program. The ALFA array in lines 33 to 38 of this program contained the reduced half-widths ($\alpha'_{\frac{1}{2}}$), which were calculated for the H_{β} line with the spectroscopic equipment employed in this investigation. These values were obtained with the convolution

program discussed above (C337CONV) and are shown in Figure 2 (Chapter IV) of this dissertation. Table D-2 outlines the contents of the data cards required for operation of C337BROD.

Table D-1. Data card requirements for C337CONV

Type #	# Cards	Columns	Variable Name	Format	Remarks
1	1	1- 5	NSETS	I5	Number of data sets
2	1/set	1- 5	NRUNS	I5	Number of runs for a given data set
3	1/set	1- 5	NPOINT	I5	Number of points in the instrument profile array
		6-10	ICONV	I5	Doppler/instrument profile convolution selection
		11-15	ISYMBP	I5	Symmetric/asymmetric instrument profile switch
		16-20	IPLOT	I5	Plot option switch
4	NPOINT /set	1-10	WAVE	F10.0	Wavelength displacement array of instrument profile (Angstrom units)
		11-22	PRFINT	E12.5	Corresponding instrument profile intensity array
5	1/run	1-60	TITLE	15A4	Experiment label for run calculations
		61-68	HLINE	2A4	Name of hydrogen line corresponding to ILINE value
6	1/run	1- 5	ISKIP	I5	Option to print calculation iterations (normally 0, <u>i.e.</u> , not printed)
		6-10	ILINE	I5	Number corresponding to H _β , H _γ , or H _δ convolution
		11-15	NTLOW	I5	Beginning NT value for convolutions (see comment cards and reference 98)
		16-20	NTUP	I5	Ending NT value
		21-32	DENS	E12.5	Electron density for the run
		36-55	LDENS	5A4	Graph label for plot identification

Table D-1. (Continued)

Type #	# Cards	Columns	Variable Name	Format	Remarks
7	1/run	1- 5	NALPHA	I5	Number of Stark profile data points
		6-10	NCONV	I5	Number of convolutions
		11-15	ISYMCP	I5	Symmetric/asymmetric Stark profiles to be convoluted with instrument broadening profile
		15-20	IPUNCH	I5	Option to punch convoluted (folded) profiles
		21-25	IREAD	I5	Option to input profile data from disk file (see comment cards)
		26-30	IPROFL	I5	Option to apply asymptotic wing formula in convolution calculation (see comment cards)
8	NAPHA /run	1-10	ALPHA	F10.0	Reduced displacement array for Stark profiles
		11-70	STARK	5E12.5	Stark profile intensity arrays for temperatures from NTLOW to NTUP (see comment cards and reference 98)


```

C      ISYMBP=0. SYMMETRIC BROADENING PROFILE; READ IN FROM ZERO          51
C      DISPLACEMENT TO PRFINT(NPOINT): PROGRAM GENERATES                52
C      LEFT (NEGATIVE DISPLACEMENT) PORTION OF PROFILE                 53
C      =1, NOT SYMMETRIC; READ IN COMPLETE PROFILE INCLUDING             54
C      NEGATIVE DISPLACEMENT INTENSITIES                                55
C      IPLDT=0. NO PLOTS GENERATED                                       56
C      =1, BROADENING, STARK/DOPPLER, AND CONVOLVED PROFILES PLOTTED    57
C      IREAD=0. INPUT PROFILE DATA ON PUNCHED CARDS                     58
C      =1, INPUT PROFILE DATA READ IN FROM FILE, CPS07.A0986.CONV       59
C      (REQUIRES ADDITIONAL FILE READ JCL AND UTILITY PL/1             60
C      PROGRAM TO EDIT FILE DATA IN CARD IMAGE)                          61
C      WAVEL(I)=DISPLACEMENT ARRAY (ANGSTROMS) OF INSTRUMENT PROFILE    62
C      PRFINT(I)=CORRESPONDING INTENSITY ARRAY                            63
C                                                                           64
C      DOUBLE PRECISION T(12),P(8)                                        65
C      DIMENSION C(5),S(5),A(2),B(2),XF(6),LDENS(5),DINC(200)           66
C      DIMENSION TEMP(5),TITLE(15),HLINE(2),WAVE(3),ALPHA(100),STARK(100,  67
C      15),DEL(3,5),HWORK( 50),ALPHAD(3,5),X( 6),XPONET( 6),FX( 6)       68
C      DIMENSION APROF(100),STARKL(100,3),CONV(100,5),AREA(5)           69
C      DIMENSION XINTRP(100),YINTRP(100),ALEFT(5),ARIGHT(5),HMAXL(5),HMAX  70
C      1R(5),XMID(100),YMID(100),SHALF(5)                                71
C      DIMENSION WAVEL(100),PRFINT(100),XWAVEL(100),XPROFL(100)         72
C      DATA TEMP/2500.,5000.,10000.,20000.,40000./,WAVE/4861.33,4340.46,4  73
C      1101.73/                                                            74
C                                                                           75
C      READ IN NUMBER OF DATA SETS                                       76
C                                                                           77
C      READ(5,1) NSETS                                                    78
C      1 FORMAT(I5)                                                       79
C      DO 9999 NUMSET=1,NSETS                                             80
C                                                                           81
C      READ IN NUMBER OF RUNS FOR THE DATA SET                           82
C                                                                           83
C      READ(5,100) NRUNS                                                  84
C      100 FORMAT(I5)                                                     85
C                                                                           86
C      READ IN INSTRUMENT BROADENING PROFILE FOR THE DATA SET           87
C                                                                           88
C      READ(5,1000) NPOINT,ICONV,ISYMBP,IPLDT                            89
C      1000 FORMAT(4I5)                                                    90
C      DO 1010 I=1,NPOINT                                                  91
C      1001 FORMAT(F10.0,E12.5)                                           92
C      1010 READ(5,1001) WAVEL(I),PRFINT(I)                                93
C      DO 9999 NUMRUN=1,NRUNS                                             94
C                                                                           95
C      READ IN INFORMATION CARDS FOR A RUN WITHIN THE DATA SET          96
C                                                                           97
C      READ(5,101) TITLE,HLINE                                             98
C      101 FORMAT(15A4,2A4)                                                99
C      READ(5,102) ISKIP,ILINE,NTLOW,NTUP,DENS,LDENS                      100

```

```

102 FORMAT(4I5,E12.5,3X,5A4)
WRITE(6,200) TITLE
200 FORMAT(1H1, //T10,15A4)
WRITE(6,201) HLINE, WAVE(ILINE), DENS
201 FORMAT(//,T20,2A4,5X,F7.2,2X,'ANGSTROMS',5X,'ELECTRON DENSITY = ',
1E11.4)
C
C CALCULATE DISPLACEMENT SCALING FACTOR AND HALF-WIDTHS OF DOPPLER
C BROADENING PROFILE (ICNV=0 USES INTERNAL DOPPLER BROADENING
C PROFILE AT TEMPERATURE SPECIFIED BY NT UP AND NTLOW)
C
DENOM=1.25E-9*(DENS**0.6666667)
WRITE(6,50) DENOM
50 FORMAT(/,T20,'1.25E-09*(NE**(2/3))= ',E12.5)
WRITE(6,55)
55 FORMAT(///,T10,'GAUSSIAN PROFILE HALF-WIDTHS')
WRITE(6,60)
60 FORMAT(/,T5,'TEMP',T20,'LAMDEL(1,T)',T35,'LAMDEL(2,T)',T50,'LAMDEL
1(3,T)',T65,'ALFDEL(1,T)',T80,'ALFDEL(2,T)',T95,'ALFDEL(3,T)')
DO 5 I=1,5
DEL(1,I)=0.001733* SQRT(TEMP(I))
DEL(2,I)=0.001548* SQRT(TEMP(I))
DEL(3,I)=0.001462* SQRT(TEMP(I))
ALPHAD(1,I)=DEL(1,I)/DENOM
ALPHAD(2,I)=DEL(2,I)/DENOM
5 ALPHAD(3,I)=DEL(3,I)/DENOM
DO 70 I=1,5
65 FORMAT(T1,7(4X,E11.4))
70 WRITE(6,65) TEMP(I),(DEL(J,I),J=1,3),(ALPHAD(K,I),K=1,3)
C
C READ IN PROFILE DATA TO BE CONVOLUTED WITH THE BROADENING PROFILE
C
READ(5,103) NALPHA,NCONV,ISYMBP,IPUNCH,IREAD,IPROFL
103 FORMAT(6I5)
DO 10 I=1,NALPHA
104 FORMAT(F10.0,SE12.5)
IF(IREAD.EQ.0) GO TO 8
READ(9,104) ALPHA(I),(STARK(I,J),J=1,5)
GO TO 10
8 READ(5,104) ALPHA(I),(STARK(I,J),J=1,5)
10 CONTINUE
C
C COMPLETE AND AREA NORMALIZE THE BROADENING PROFILE
C
IF(ISYMBP.EQ.1) GO TO 1030
DO 1020 I=1,NPOINT
J=NPOINT+1-I
XWAVEL(I)=-WAVEL(J)/DENOM
1020 XPROFL(I)=PRFINT(J)*DENOM
XWAVEL(NPOINT)=WAVEL(1)

```

```

101
102
103
104
105
106
107
108
109
110
111
112
113
114
115
116
117
118
119
120
121
122
123
124
125
126
127
128
129
130
131
132
133
134
135
136
137
138
139
140
141
142
143
144
145
146
147
148
149
150

```

	DO 1025 I=2,NPOINT	151
	J=NPOINT-1+I	152
	XWAVEL(J)=WAVEL(I)/DENOM	153
1025	XPROFL(J)=PRFINT(I)*DENOM	154
	NPTS=2*NPOINT-1	155
	GO TO 1040	156
1030	NPTS=NPOINT	157
	DO 1035 I=1,NPTS	158
	XWAVEL(I)=WAVEL(I)/DENOM	159
1035	XPROFL(I)=PRFINT(I)*DENOM	160
1040	AREAIN=0.00	161
	BMAX=0.00	162
	JCHK=(NPTS/2)+1	163
	DO 1050 I=1,NPTS,3	164
	NL=I	165
	NU=NL+3	166
	IF(NU.GE.NPTS) NU=NPTS	167
	N=0	168
	DO 1045 J=NL,NU	169
	N=N+1	170
	X(N)=XWAVEL(J)	171
	XF(N)=XWAVEL(J)	172
	IF(XWAVEL(J).EQ.0.00) JCHK=J	173
	IF(XPROFL(J).LT.BMAX) GO TO 1045	174
	BMAX=XPROFL(J)	175
	JLOW=J-1	176
	JUP=J+1	177
1045	FX(N)=XPROFL(J)	178
	IER=0	179
	NUMBER=4	180
	NTEST=NU-NL+1	181
	IF(NTEST.LT.4) NUMBER=NTEST	182
	AINSTR=DCS1QU(FX,X,NUMBER,HWORK,IER)	183
	IF(IER.NE.129) GO TO 1049	184
	WRITE(6,1046) IER,NL,(X(M),M=1,NUMBER),(FX(M),M=1,NUMBER)	185
1046	FORMAT(/,T10,'*****FLAG, IER= ',I3,2X,'FOR INITIAL SEGMENT VALUE',	186
	1I4,/,T15,'X(1)---X(N) = ',4(2X,E11.4),/,T15,'FX(1)---FX(N) = ',4(2X	187
	2,E11.4))	188
	DO 1500 M=1,12	189
1500	T(M)=0.00	190
	DO 1501 M=1,2	191
	A(M)=0.00	192
1501	B(M)=0.00	193
	DO 1502 M=1,8	194
1502	P(M)=0.00	195
	DO 1503 M=1,5	196
	C(M)=0.00	197
1503	S(M)=0.00	198
	RSQ=100.0	199
	MD=2	200

	IER=0	201
	ID=0	202
	IF(NUMBER.EQ.2) MD=1	203
	IF(NUMBER.EQ.1) GO TO 1050	204
	CALL RLFOTH(X,FX,NUMBER,RSQ,MD, ID,P,C,S,A,B,IER)	205
	IF(IER.EQ.129) GO TO 1050	206
	IF(IER.EQ.130) GO TO 1050	207
	CALL RLDOPM(C, ID,A,B,T)	208
	FUP=XF(NUMBER)	209
	FLOW=XF(1)	210
	FU2=FUP*FUP	211
	FL2=FLOW*FLOW	212
	FU3=FU2*FUP	213
	FL3=FL2*FLOW	214
	AINSTR=9999.	215
	IF(ID.EQ.1) C(3)=0.00	216
	AINSTR=(C(1)*((FUP-FLOW)))+((C(2)/2.0)*(FU2-FL2))+((C(3)/3.0)*(FU3-FL3))	217
	WRITE(6,1510) AINSTR	218
1510	FORMAT(/,T10,'POLYNOMIAL APPROXIMATION TO AREA USED: AINSTR= ',E11.4)	219
1049	AREAIN=AREAIN+AINSTR	220
1050	CONTINUE	221
	BMAX=BMAX/AREAIN	222
	DO 1060 I=1,NPTS	223
1060	XPROFL(I)=XPROFL(I)/AREAIN	224
	ISHAPE=0	225
	IF(BMAX.GT.XPROFL(JCHK)) ISHAPE=1	226
	HALFR=0.00	227
	CALL HMAX(XWAVEL,XPROFL,NPTS,0,0,0,JLOW,JUP,BMAX,0,0,HALFR,0,0,ISHAPE)	228
	BHALF=HALFR	229
	BMAX=BMAX	230
	WRITE(6,1061) BMAX,BHALF,AREAIN	231
1061	FORMAT(////,T25,'AREA AND DISPLACEMENT NORMALIZED INSTRUMENT BROADENING PROFILE',/,T35,'MAX INTENSITY = ',E12.5,2X,'HALF-WIDTH = ',E12.5,2X,'AREA BEFORE NORMALIZATION = ',1X,E12.5)	232
	WRITE(6,1062)	233
1062	FORMAT(///,T10,'ALPHA',T25,'INTENSITY')	234
	DO 1070 I=1,NPTS	235
1065	FORMAT(T10,E11.4,T25,E11.4)	236
1070	WRITE(6,1065) XWAVEL(I),XPROFL(I)	237
	WRITE(6,150)	238
150	FORMAT(/,T10,'INPUT DATA')	239
	WRITE(6,151)	240
151	FORMAT(/,T2,'ALPHA',T20,'STARK(2500)',T40,'STARK(5000)',T60,'STARK(10000)',T80,'STARK(20000)',T100,'STARK(40000)')	241
	DO 15 I=1,NALPHA	242
152	FORMAT(T2,E11.4,T20,E11.4,T40,E11.4,T60,E11.4,T80,E11.4,T100,E11.4)	243
	1)	244
		245
		246
		247
		248
		249
		250

	15	WRITE(6,152) ALPHA(I),(STARK(I,J),J=1,5)	251
C			252
C		COMPLETE PROFILES TO BE CONVOLUTED WITH THE BROADENING PROFILE	253
C			254
		DO 19 I=1,5	255
		HMAXL(I)=0.0	256
	19	HMAXR(I)=0.00	257
		IF(ISYMCP.EQ.1) GO TO 1900	258
		DO 20 I=1,NALPHA	259
		J=NALPHA+1-I	260
		APROF(I)=-ALPHA(J)	261
		DO 20 K=1,5	262
	20	STARKL(I,K)=STARK(J,K)	263
		APROF(NALPHA)=ALPHA(I)	264
		DO 25 I=2,NALPHA	265
		J=NALPHA-I+1	266
		APROF(J)=ALPHA(I)	267
		DO 25 K=1,5	268
	25	STARKL(J,K)=STARK(I,K)	269
		NALPHA=2*NALPHA-1	270
		GO TO 1950	271
	1900	DO 1910 I=1,NALPHA	272
		APROF(I)=ALPHA(I)	273
		DO 1910 J=1,5	274
	1910	STARKL(I,J)=STARK(I,J)	275
	1950	NCONV=NALPHA	276
		DO 1995 NT=1,5	277
		SHALF(NT)=0.00	278
		IF(NT.LT.NTLJW) GO TO 1995	279
		IF(NT.GT.NTUP) GO TO 1995	280
		JRCHK=(NALPHA/2)+1	281
		JLCHK=JRCHK	282
		DO 1990 I=1,NALPHA	283
		IF(APROF(I).GT.0.0) GO TO 1955	284
		IF(APROF(I).EQ.0.0) GO TO 1960	285
		IF(STARKL(I,NT).LT.HMAXL(NT)) GO TO 1990	286
		HMAXL(NT)=STARKL(I,NT)	287
		ILSLOW=I-1	288
		ILSUP=I+1	289
		GO TO 1990	290
	1955	IF(STARKL(I,NT).LE.HMAXR(NT)) GO TO 1990	291
		HMAXR(NT)=STARKL(I,NT)	292
		IRSLOW=I-1	293
		IRSUP=I+1	294
		GO TO 1990	295
	1960	JRCHK=I	296
		JLCHK=I	297
		IF(STARKL(I,NT).GT.HMAXR(NT)) GO TO 1970	298
		IF(STARKL(I,NT).LT.HMAXL(NT)) GO TO 1990	299
		HMAXL(NT)=STARKL(I,NT)	300

```

      ILSLOW=I-1
      ILSUP=I+1
      GO TO 1990
1970 HMAXR(NT)=STARKL(I,NT)
      IRSLOW=I-1
      IRSUP=I+1
1990 CONTINUE
      SRMAX=HMAXR(NT)
      SLMAX=HMAXL(NT)
      DO 1994 J=1,NALPHA
1994 XINTRP(J)=APROF(J)
      YINTRP(J)=STARKL(J,NT)
      HALFR=0.0
      HALFL=0.00
      ISHAPE=0
      IF(SRMAX.GT.YINTRP(JRCHK)) ISHAPE=1
      IF(SLMAX.GT.YINTRP(JLCHK)) ISHAPE=1
      CALL HMAX(XINTRP,YINTRP,NALPHA,1,ILSLOW,ILSUP,IRSLOW,IRSUP,SRMAX,S
1 LMAX,HALFR,HALFL,ISHAPE)
      SHALF(NT)=(HALFR-HALFL)/2.00
      HMAXR(NT)=SRMAX
      HMAXL(NT)=SLMAX
1995 CONTINUE
      WRITE(6,2000)
2000 FORMAT(/,T10,'COMPLETE PROFILE DATA')
      WRITE(6,2001)
2001 FORMAT(/,T2,'ALFA',T20,'STARKL(2500)',T40,'STARKL(5000)',T60,'STA
1 RKL(10000)',T80,'STARKL(20000)',T100,'STARKL(40000)')
      DO 2015 I=1,NALPHA
2002 FORMAT(T2,E11.4,T20,E11.4,T40,E11.4,T60,E11.4,T80,E11.4,T100,E11.4
1 )
2015 WRITE(6,2002) APROF(I),(STARKL(I,J),J=1,5)
      WRITE(6,2003) (HMAXR(I),I=1,5),(HMAXL(J),J=1,5),(SHALF(K),K=1,5)
2003 FORMAT(/,T2,'RIGHT MAX INTENS',T20,E11.4,4(9X,E11.4),/,T3,'LEFT M
1 AX INTENS',T20,E11.4,4(9X,E11.4),/,T4,'AVE HALF-WIDTH',T20,E11.4,
24(9X,E11.4))
C
C   PERFORM THE CONVOLUTION CALCULATIONS
C
      DO 99 NT=1,5
      DO 2990 INUM=1,NALPHA
2990 YINTRP(INUM)=STARKL(INUM,NT)
      DO 99 J=1,NCONV
      CONV(J,NT)=0.00
      IF(NT.LT.NTLOW) GO TO 99
      IF(NT.GT.NTUP) GO TO 99
      IF(ICONV.EQ.1) GO TO 3000
      XUP=1.000/DENOM
      IF(NT.EQ.3) XUP=1.50/DENOM
      IF(NT.EQ.4) XUP=2.00/DENOM

```

```

301
302
303
304
305
306
307
308
309
310
311
312
313
314
315
316
317
318
319
320
321
322
323
324
325
326
327
328
329
330
331
332
333
334
335
336
337
338
339
340
341
342
343
344
345
346
347
348
349
350

```

	IF(NT.EQ.5) XUP=3.00/DENOM	351
	XLOW=-XUP	352
	RATIO=ALPHAD(ILINE,NT)/SHALF(NT)	353
	KEY=0	354
	IF(RATIO.GE.1.5) KEY=1	355
	GO TO 3010	356
3000	XUP=XWAVEL(NPTS)	357
	XLOW=XWAVEL(1)	358
	RATIO=BHALF/SHALF(NT)	359
	KEY=0	360
	IF(RATIO.GE.1.5) KEY=1	361
3010	XAINC=XUP/50.00	362
	XX=XLOW-XAINC	363
	DO 3020 M=1,100	364
	XX=XX+XAINC	365
3020	DINC(M)=XX	366
	NDET=100	367
	IF(KEY.EQ.1) NDET=NALPHA	368
	DO 98 K=1,NDET,3	369
	NL=K	370
	NU=NL+3	371
	IF(NU.GE.NDET) NU=NDET	372
	N=0	373
	DO 96 I=NL,NU	374
	N=N+1	375
	IF(KEY.EQ.1) X(N)=APROF(J)-APROF(I)	376
	IF(KEY.EQ.1) GO TO 3031	377
	X(N)=DINC(I)	378
	XXX=APROF(J)-X(N)	379
	IF(XXX.LT.APROF(1)) GO TO 3030	380
	IF(XXX.GT.APROF(NALPHA)) GO TO 3030	381
	POLYN=0.00	382
	CALL PLYNN(APROF,YINTRP,POLYN,XXX,NALPHA,6)	383
	SVALUE=POLYN	384
	GO TO 3031	385
3030	BXX=ABS(XXX)	386
	SVALUE=2.0*3.5261E-03*(BXX**(-2.5))	387
	IF(IPROFL.NE.0) SVALUE=0.	388
3031	IF(ICONV.EQ.1) GO TO 75	389
	XX2N=ABS(X(N))	390
	XPONET(N)=-0.69314718*(XX2N**2.)/(ALPHAD(ILINE,NT)**2.)	391
	XPTTEST=ABS(XPONET(N))	392
	IF(XPTTEST.GT.60) GO TO 72	393
	XPONET(N)=EXP(XPONET(N))/(1.77245*DEL(ILINE,NT))	394
	XPONET(N)=DENOM*XPONET(N)*SQRT(0.69314718)	395
	IF(KEY.EQ.1) SVALUE=STARKL(I,NT)	396
	FX(N)=SVALUE*XPONET(N)	397
	GO TO 86	398
72	XPONET(N)=0.0	399
	FX(N)=0.00	400

	GO TO 86	401
75	XXX=X(N)	402
	IF(KEY.EQ.1) SVALUE=STARKL(I,NT)	403
	IF(XXX.LT.XWAVEL(1)) GO TO 80	404
	IF(XXX.GT.XWAVEL(NPTS)) GO TO 80	405
	POLYN=0.00	406
	CALL PLYNN(XWAVEL,XPROFL,POLYN,XXX,NPTS,6)	407
	XPONET(N)=POLYN	408
	GO TO 85	409
80	XPONET(N)=0.00	410
85	FX(N)=SVALUE*XPONET(N)	411
86	CONTINUE	412
	XF(N)=DINC(I)	413
	IF(KEY.EQ.1) XF(N)=APROF(I)	414
	IF(KEY.EQ.1) X(N)=APROF(I)	415
96	CONTINUE	416
	IER=0	417
	NUMBER=4	418
	NTEST=NU-NL+1	419
	IF(NTEST.LT.4) NUMBER=NTEST	420
	CTEST=DCS1QU(FX,X,NUMBER,HWORX,IER)	421
	IF(ISKIP.EQ.0) GO TO 997	422
995	FORMAT(T50,'CTEST= ',E11.4,2X,'FOR J= ',I3,2X,'K= ',I3)	423
	WRITE(6,996) CTEST,J,K	424
997	IF(IER.NE.129) GO TO 97	425
	WRITE(6,105) IER,J,K	426
105	FORMAT (T10,'***FLAG***,IER= ',I5,2X,'RETURNED FOR CONVOLUTION	427
1	NUMBER ',I5,5X,'SUBSET K VALUE = ',I3)	428
	WRITE(6,106) APROF(J),NT	429
106	FORMAT(T15,'ALFA(J)= ',E12.5,2X,'NT = ',I3)	430
	DO 600 M=1,12	431
600	T(M)=0.00	432
	DO 601 M=1,2	433
	A(M)=0.00	434
601	B(M)=0.00	435
	DO 602 M=1,8	436
602	P(M)=0.00	437
	DO 603 M=1,5	438
	C(M)=0.00	439
603	S(M)=0.00	440
	RSQ=100.0	441
	MD=2	442
	IER=0	443
	ID=0	444
	IF(NUMBER.EQ.1) GO TO 98	445
	IF(NUMBER.EQ.2) MD=1	446
	DIF=0.0	447
	DO 608 M=2,NUMBER	448
	L=M-1	449
608	DIF=DIF+(FX(M)-FX(L))**2	450

	XNMBR=NUMBER	451
	DIF=SQRT(DIF)/XNMBR	452
	AVE=0.0	453
	DO 609 M=1,NUMBER	454
609	AVE=AVE+FX(M)	455
	AVE=AVE/XNMBR	456
	AVTEST=0.001*AVE	457
	IF(DIF.GT.AVTEST) GO TO 604	458
	CTEST=AVE*(X(NUMBER)-X(1))	459
	GO TO 611	460
604	CONTINUE	461
	CALL RLFOTH(X,FX,NUMBER,RSQ,ND,ID,P,C,S,A,B,IER)	462
	IF(IER.EQ.129) GO TO 98	463
	IF(IER.EQ.130) GO TO 98	464
	CALL RLDOPM(C, ID, A, B, T)	465
	FUP=XF(NUMBER)	466
	FLOW=XF(1)	467
	FU2=FUP*FUP	468
	FL2=FLOW*FLOW	469
	FU3=FU2*FUP	470
	FL3=FL2*FLOW	471
	CTEST=9999.	472
	IF(ID.EQ.1) C(3)=0.00	473
	CTEST=((C(1))*(FUP-FLOW))+((C(2)/2.0)*(FU2-FL2))+((C(3)/3.0)*(FU3-FL3))	474
	WRITE(6,610) CTEST, ID	475
610	FORMAT (T10, 'POLYNOMIAL APPROXIMATION TO AREA USED: CTEST= ',E11	476
	1.4,2X, 'DEGREE= ',I3)	477
	GO TO 97	478
611	WRITE(6,615) CTEST	479
615	FORMAT (T10, 'FX(N) VALUES NEARLY CONSTANT: SQUARE APPROXIMATION	480
	1 TO AREA; CTEST= ',E12.5)	481
	97 CONV(J,NT)=CONV(J,NT)+CTEST	482
	98 CONTINUE	483
	99 CONTINUE	484
		485
		486
	DETERMINE AREA OF CONVOLVED PROFILES	487
		488
	DO 501 NT=1,5	489
	AREA(NT)=0.00	490
	HMAXL(NT)=0.00	491
	HMAXR(NT)=0.00	492
	ALEFT(NT)=0.00	493
	ARIGHT(NT)=0.00	494
	DO 500 I=1,NCONV,3	495
	NL=I	496
	NU=NL+3	497
	IF(NU.GE.NCONV) NU=NCONV	498
	N=0	499
	DO 495 J=NL,NU	500

C
C
C

	N=N+1	501
	XF(N)=APROF(J)	502
	X(N)=APROF(J)	503
C		504
C	DETERMINE FIRST APPROXIMATIONS TO RIGHT AND LEFT PROFILE	505
C	MAXIMUMS USING TABULATED (UNNORMALIZED) CONVOLUTION RESULTS	506
C	AREA NORMALIZATION AFTER STATEMENT 501	507
		508
	IF(APROF(J).GT.0.00) GO TO 450	509
	IF(APROF(J).EQ.0.00) GO TO 460	510
	IF(CONV(J,NT).LT.HMAXL(NT)) GO TO 495	511
	HMAXL(NT)=CONV(J,NT)	512
	LJLOW=J-1	513
	LJUP=J+1	514
	GO TO 495	515
450	IF(CONV(J,NT).LE.HMAXR(NT)) GO TO 495	516
	HMAXR(NT)=CONV(J,NT)	517
	JRLOW=J-1	518
	JRUP=J+1	519
	GO TO 495	520
460	IF(CONV(J,NT).GT.HMAXR(NT)) GO TO 470	521
	IF(CONV(J,NT).LT.HMAXL(NT)) GO TO 495	522
	HMAXL(NT)=CONV(J,NT)	523
	LJLOW=J-1	524
	LJUP=J+1	525
	GO TO 495	526
470	HMAXR(NT)=CONV(J,NT)	527
	JRLOW=J-1	528
	JRUP=J+1	529
495	FX(N)=CONV(J,NT)	530
	IER=0	531
	NUMBER=4	532
	NTEST=NU-NL+1	533
	IF(NTEST.LT.4) NUMBER=NTEST	534
	ATEST=DCS1QU(FX,X,NUMBER,HWORX,IER)	535
	IF(IER.NE.129) GO TO 497	536
	WRITE(6,204) NL,NU,NT	537
204	FORMAT (T10,'*****FLAG, IER:=129 RETURNED FOR ATEST WITH NL= ',I3	538
	1,2X,'NU= ',I3,2X,'NT= ',I3)	539
	DO 700 M=1,12	540
700	T(M)=0.00	541
	DO 701 M=1,2	542
	A(M)=0.00	543
701	B(M)=0.00	544
	DO 702 M=1,8	545
702	P(M)=0.00	546
	DO 703 M=1,5	547
	C(M)=0.00	548
703	S(M)=0.00	549
	RSQ=100.0	550

	MD=2	551
	IER=0	552
	ID=0	553
	IF(NUMBER.EQ.1) GO TO 500	554
	IF(NUMBER.EQ.2) MD=1	555
	DIF=0.00	556
	DO 708 M=2,NUMBER	557
	L=M-1	558
708	DIF=DIF+(FX(M)-FX(L))**2	559
	XNMBR=NUMBER	560
	DIF=SQRT(DIF)/XNMBR	561
	AVE=0.00	562
	DO 709 M=1,NUMBER	563
709	AVE=AVE+FX(M)	564
	AVE=AVE/XNMBR	565
	AVTEST=0.001*AVE	566
	IF(DIF.GT.AVTEST) GO TO 704	567
	AATEST=AVE*(X(NUMBER)-X(1))	568
	GO TO 711	569
704	CONTINUE	570
	CALL RLFOTH(X,FX,NUMBER,RSQ,MD,ID,P,C,S,A,B,IER)	571
	IF(IER.EQ.129) GO TO 500	572
	IF(IER.EQ.130) GO TO 500	573
	CALL RLDOPM(C,ID,A,B,T)	574
	FUP=XF(NUMBER)	575
	FLOW=XF(1)	576
	FU2=FUP*FUP	577
	FL2=FLOW*FLOW	578
	FU3=FU2*FUP	579
	FL3=FL2*FLOW	580
	AATEST=9999.	581
	IF(ID.EQ.1) C(3)=0.0	582
	AATEST=((C(1)*(FUP-FLOW))+((C(2)/2.0)*(FU2-FL2))+((C(3)/3.0)*(FU3-FL	583
	13))	584
	WRITE(6,710) ATEST	585
710	FORMAT (T10,'POLYNOMIAL APPROXIMATION TO AREA USED: ATEST= ',E11	586
	1.4)	587
	GO TO 497	588
711	WRITE(6,715) ATEST	589
715	FORMAT (T10,'FX(N) VALUES NEARLY CONST: SQUARE APPROX TO AREA:	590
	1 ATEST= ',E12.5)	591
497	AREA(NT)=AREA(NT)+ATEST	592
500	CONTINUE	593
501	CONTINUE	594
C		595
C	AREA NORMALIZE CONVOLVED PROFILES AND MAX INTENSITY VALUES	596
C		597
	DO 502 NT=1.5	598
	IF(NT.LT.NTLOW) GO TO 502	599
	IF(NT.GT.NTUP) GO TO 502	600

	HMAXL(NT)=HMAXL(NT)/AREA(NT)	601
	HMAXR(NT)=HMAXR(NT)/AREA(NT)	602
502	CONTINUE	603
	WRITE(6,203)	604
203	FORMAT(1H1,/,T20,'AREA NORMALIZED CONVOLUTION RESULTS')	605
	IF(ICONV.EQ.0) WRITE(6,403)	606
	IF(ICONV.EQ.1) WRITE(6,402)	607
402	FORMAT(T30,'INSTRUMENT PROFILE CONVOLUTION')	608
403	FORMAT(T30,'DOPPLER CONVOLUTION (INTERNALLY GENERATED DOPPLER PROF	609
	1('LES'))	610
	IF(IPUNCH.EQ.1) WRITE(7,110) HLINE,WAVE(ILINE),DENS	611
110	FORMAT(2A4,2X,F7,2,2X,'ANGSTROMS',2X,'ELEC DENS = ',E13.6)	612
	WRITE(6,202) (TEMP(I),I=1,5)	613
202	FORMAT(/,T13,'ALPHA',T25,F6.0,' K',T40,F6.0,' K',T55,F6.0,' K',T7	614
	10,F6.0,' K',T85,F6.0,' K')	615
	IF(IPUNCH.EQ.1) WRITE(7,210)	616
210	FORMAT('DELTA ALPHA FOLLOWED BY CONVOLVED PROFILES; 2500,5000,1000	617
	10,20000, & 40000')	618
	DO 199 J=1,NCONV	619
	DO 198 K=1,5	620
	IF(K.LT.NTLOW) GO TO 198	621
	IF(K.GT.NTUP) GO TO 198	622
	CONV(J,K)=CONV(J,K)/AREA(K)	623
198	CONTINUE	624
	IF(IPUNCH.NE.1) GO TO 199	625
109	FORMAT(F10,6,5E12.5)	626
	WRITE(7,109) APROF(J),(CONV(J,M),M=1,5)	627
107	FORMAT(T8,E11,4,T21,5(4X,E11,4))	628
199	WRITE(6,107) APROF(J),(CONV(J,L),L=1,5)	629
C		630
C	CALCULATE THE HALF-WIDTH BY USING HALF-MAX INTENSITY VALUES	631
C	FOR BOTH RIGHT AND LEFT SIDES OF THE COMPLETE PROFILE.	632
C	THE MAX INTENSITY VALUE FOR EACH HALF IS DETERMINED BY USING	633
C	THE INTERPOLATING SUBROUTINE, PLYNN.	634
C	THE RESPECTIVE HALF-WIDTHS FOR EACH SIDE ARE THEN DETERMINED BY	635
C	REVERSING THE INTENSITY AND DISPLACEMENT ARRAYS AND INTERPOLATING	636
C	A VALUE WITH PLYNN	637
C		638
	DO 299 I=1,5	639
	IF(I.LT.NTLOW) GO TO 299	640
	IF(I.GT.NTUP) GO TO 299	641
	JRCHK=(NCONV/2)+1	642
	JLCHK=JRCHK	643
	DO 249 J=1,NCONV	644
	XMID(J)=APROF(J)	645
	IF(APROF(J).EQ.0.00) JRCHK=J	646
	JLCHK=JRCHK	647
249	YMID(J)=CONV(J,I)	648
	CRMAX=HMAXR(I)	649
	CLMAX=HMAXL(I)	650

```

        HALFR=0.00
        HALFL=0.00
        ISHAPE=0
        IF(CRMAX.GT.YMID(JRCHK)) ISHAPE=1
        IF(CLMAX.GT.YMID(JLCHK)) ISHAPE=1
        CALL HMAX(XMID,YMID,NCONV,1,LJLOW,LJUP,JRLOW,JRUP,CRMAX,CLMAX,HALFR
1R,HALFL,ISHAPE)
        ALEFT(I)=HALFL
        ARIGHT(I)=HALFR
        HMAXR(I)=CRMAX
        HMAXL(I)=CLMAX
299 CONTINUE
396 FORMAT(/,T3,'RIGHT MAX INTENS',T21,5(4X,E11.4))
397 FORMAT(T4,'LEFT MAX INTENS',T21,5(4X,E11.4))
398 FORMAT(/,T3,'RIGHT HALF-WIDTH',T21,5(4X,E11.4))
399 FORMAT(T4,'LEFT HALF-WIDTH',T21,5(4X,E11.4))
        WRITE(6,396) (HMAXR(N1),N1=1,5)
        WRITE(6,397) (HMAXL(N2),N2=1,5)
        WRITE(6,398) (ARIGHT(I1),I1=1,5)
        WRITE(6,399) (ALEFT(I2),I2=1,5)
        WRITE(6,510) (AREA(NN),NN=1,5)
510 FORMAT(/,T3,'AREA(1)-AREA(5)',T22,5(3X,E12.5))
        IF(IPLUT.NE.1) GO TO 9999
        CALL PLOT(APROF,STARKL,CONV,XWAVEL,XPROFL,NTUP,NTLOW,ALPHAD,ICONV,
1NPTS,NALPHA,NCONV,ILINE,LDENS)
9999 CONTINUE
        STOP
        END
        SUBROUTINE HMAX(X,Y,N,ISYM,ILLOW,ILUP,IRLOW,IRUP,YRMAX,YLMAX,HALFR
1,HALFL,ISHAPE)
        DIMENSION X(100),Y(100),XH(51),YH(51)
        SUBROUTINE TO DETERMINE HALF-WIDTHS FOR RIGHT AND (OPTIONALLY)
        LEFT PROFILES
        ISYM=0, SYMMETRIC PROFILE SO ONLY CALCULATE RIGHT HALF-WIDTH
        NE 0, DETERMINE BOTH RIGHT AND LEFT HALF-WIDTHS
        NHALF=N/2
        IF(ISYM.EQ.0) GO TO 2000
        NPLUS=NHALF+1
        IF(ISHAPE.EQ.1) NPLUS=ILLOW+1
        DO 1010 I=1,NPLUS
        XH(I)=Y(I)
1010 YH(I)=X(I)
        XINC=(X(ILUP)-X(ILLOW))/100.0
        XXX=X(ILLOW)-XINC
        DO 1020 J=1,100
        XXX=XXX+XINC

```

651
652
653
654
655
656
657
658
659
660
661
662
663
664
665
666
667
668
669
670
671
672
673
674
675
676
677
678
679
680
681
682
683
684
685
686
687
688
689
690
691
692
693
694
695
696
697
698
699
700

C
C
C
C
C
C
C

	POLYN=0.00	701
	CALL PLYNN(X,Y,POLYN,XXX,N,6)	702
	IF(POLYN.GT.YLMAX) YLMAX=POLYN	703
1020	CONTINUE	704
	POLYN=0.00	705
	XXX=YLMAX/2.00	706
	CALL PLYNN(XH,YH,POLYN,XXX,NPLUS,4)	707
	HALFL=POLYN	708
2000	J2=0	709
	J4=0	710
	IF(ISHAPE.EQ.1) NHALF=IRLOW+1	711
	DO 2030 J3=NHALF,N	712
	J4=N-J3+NHALF	713
	J2=J2+1	714
	XH(J2)=Y(J4)	715
2030	YH(J2)=X(J4)	716
	XINC=(X(IRUP)-X(IRLOW))/100.0	717
	XXX=X(IRLOW)-XINC	718
	DO 2040 JS=1,100	719
	XXX=XXX+XINC	720
	POLYN=0.00	721
	CALL PLYNN(X,Y,POLYN,XXX,N,6)	722
	IF(POLYN.GT.YRMAX) YRMAX=POLYN	723
2040	CONTINUE	724
	POLYN=0.00	725
	XXX=YRMAX/2.00	726
	CALL PLYNN(XH,YH,POLYN,XXX,J2,4)	727
	HALFR=POLYN	728
	RETURN	729
	END	730
	SUBROUTINE PLYNN(X,Y,POLYN,XXX,NUMX,NPOLY)	731
	DIMENSION X(100),Y(100)	732
		733
	N POINT POLYNOMIAL INTERPOLATING SUBROUTINE	734
		735
	TO INTERPOLATE A VALUE FOR XXX THE NPOLY NEAREST KNOWN POINTS ARE	736
	SELECTED AND AN INTERPOLATING POLYNOMIAL OF DEGREE NPOLY-1 IS	737
	FITTED TO THESE POINTS	738
	X AND Y ARE THE ARRAYS OF NUMX KNOWN POINTS ON THE CURVE	739
	THE RESULT IS POLYN	740
		741
		742
101	POLYN=0.0	743
	NM=(NPOLY+1)/2	744
	NM1=NM+1	745
	NUP=NUMX+NM1-NPOLY	746
	DO 102 J=NM1,NUP	747
	IF(XXX.LE.X(J)) GO TO 104	748
102	CONTINUE	749
	J=NUP	750
104	L=J-NM	

```

LLL=L+NPOLY-1
DO 106 K=L,LLL
TERM=1.0
DO 105 M=L,LLL
IF(K.EQ.M) GO TO 105
TERM=TERM*(XXX-X(M))/(X(K)-X(M))
105 CONTINUE
TERM=Y(K)*TERM
106 POLYN=POLYN+TERM
RETURN
END
SUBROUTINE PLOT(APROF,STARKL,CONV,XWAVEL,XPROFL,NTUP,NTLOW,ALPHAD,
1 ICONV,NPTS,NALPHA,NCONV,ILINE,LDENS)
DIMENSION LBP(5),LSDP(5),LCP(5),LT1(5),LT2(5),LT3(5),LT4(5),LT5(5)
1,LINE1(5),LINE2(5),LINE3(5),APROF(100),STARKL(100,5),CONV(100,5),X
2WAVEL(100),XPROFL(100),ALPHAD(3,5),LDENS(5),JPROF(100,5),X1(100),
3X2(100),Y1(100),Y2(100),LBLT(5)
DATA LBP/'BROA',DENI,'NG P',RJFI,'LE',LSDP/'STAR',K-DO,'P
1PLE',R PR,'OF',LCP/'CONV',DLVE,'D',PROF,'ILE',LT1/'T
2EMP',2500,'K',LT2/'TEMP',5000,'K',
3',LT3/'TEMP',1000,'K',LT4/'TEMP',
4'2000,'K',LTS/'TEMP',4000,'K',
DATA LINE1/'H-BE',TA,'4861',.33,'A',LINE2/'H-GA',MMA
1,'4340',.46,'A',LINE3/'H-DE',LTA,'4101',.73,'A'
IF(ICONV.EQ.1) GO TO 100
DO 10 I=1,5
DO 10 J=1,NALPHA
A2=APROF(J)*APROF(J)
XPNT=-0.96314718*A2/(ALPHAD(ILINE,I)**2)
XPTEST=ABS(XPNT)
IF(XPTEST.GT.4.5) GO TO 9
DPROF(J,I)=(SQRT(0.69314718))*(EXP(XPNT))/(1.77245*ALPHAD(ILINE,I)
1)
GO TO 10
9 DPROF(J,I)=0.00
10 CONTINUE
NPTS=NALPHA
100 DO 9999 NT=NTLOW,NTUP
DO 110 I=1,NALPHA
X1(I)=APROF(I)
IF(ICONV.EQ.1) GO TO 110
XWAVEL(I)=APROF(I)
XPROFL(I)=DPROF(I,NT)
110 Y1(I)=STARKL(I,NT)
DO 120 I=1,NCONV
X2(I)=APROF(I)
120 Y2(I)=CONV(I,NT)
CALL GRAPH(NPTS,XWAVEL,XPROFL,0.7,8.0,10.0,0.0,0.0,0.0,'ALPHA (NORMAL
1 IZED);','AREA NORM INTENSITY;',CONVOLUTION PROFILES',LDENS)
IF(ILINE.EQ.3) GO TO 300

```

751
752
753
754
755
756
757
758
759
760
761
762
763
764
765
766
767
768
769
770
771
772
773
774
775
776
777
778
779
780
781
782
783
784
785
786
787
788
789
790
791
792
793
794
795
796
797
798
799
800

	IF(ILINE.EQ.2) GO TO 200	801
	IF(ILINE.EQ.1) GO TO 125	802
1000	FORMAT(/,T10,'*****FLAG***** ERROR: ILINE NOT SPECIFIED CORRECT	803
	ILY; NO PLOTS GENERATED')	804
	WRITE(6,1000)	805
	RETURN	806
125	CALL GRAPHS(NPTS,XWAVEL,XPROFL,0,107,LINE1)	807
	IF(NT.EQ.5) GO TO 148	808
	IF(NT.EQ.4) GO TO 146	809
	IF(NT.EQ.3) GO TO 144	810
	IF(NT.EQ.2) GO TO 142	811
	IF(NT.EQ.1) GO TO 140	812
1010	FORMAT(/,T10,'*****FLAG***** ERROR IN NTLOW OR NTUP')	813
	WRITE(6,1010)	814
	RETURN	815
140	DO 141 N=1,5	816
141	LBLT(N)=LT1(N)	817
	GO TO 150	818
142	DO 143 N=1,5	819
143	LBLT(N)=LT2(N)	820
	GO TO 150	821
144	DO 145 N=1,5	822
145	LBLT(N)=LT3(N)	823
	GO TO 150	824
146	DO 147 N=1,5	825
147	LBLT(N)=LT4(N)	826
	GO TO 150	827
148	DO 149 N=1,5	828
149	LBLT(N)=LT5(N)	829
150	CALL GRAPHS(NPTS,XWAVEL,XPROFL,0,107,LBLT)	830
	CALL GRAPHS(NPTS,XWAVEL,XPROFL,1,107,LBP)	831
	CALL GRAPHS(NALPHA,X1,Y1,2,107,LSDP)	832
	CALL GRAPHS(NCONV,X2,Y2,3,107,LCP)	833
	GO TO 9999	834
200	CALL GRAPHS(NPTS,XWAVEL,XPROFL,0,107,LINE2)	835
	IF(NT.EQ.5) GO TO 248	836
	IF(NT.EQ.4) GO TO 246	837
	IF(NT.EQ.3) GO TO 244	838
	IF(NT.EQ.2) GO TO 242	839
	IF(NT.EQ.1) GO TO 240	840
2000	FORMAT(/,T10,'*****FLAG***** ERROR IN NTLOW OR NTUP')	841
	WRITE(6,2000)	842
	RETURN	843
240	DO 241 N=1,5	844
241	LBLT(N)=LT1(N)	845
	GO TO 250	846
242	DO 243 N=1,5	847
243	LBLT(N)=LT2(N)	848
	GO TO 250	849
244	DO 245 N=1,5	850

245	LBLT(N)=LT3(N)	851
	GO TO 250	852
246	DO 247 N=1,5	853
247	LBLT(N)=LT4(N)	854
	GO TO 250	855
248	DO 249 N=1,5	856
249	LBLT(N)=LT5(N)	857
250	CALL GRAPHS(NPTS,XWAVEL,XPROFL,0,107,LBLT)	858
	CALL GRAPHS(NPTS,XWAVEL,XPROFL,1,107,LBP)	859
	CALL GRAPHS(NALPHA,X1,Y1,2,107,LSDP)	860
	CALL GRAPHS(NCONV,X2,Y2,3,107,LCP)	861
	GO TO 9999	862
300	CALL GRAPHS(NPTS,XWAVEL,XPROFL,0,107,LINE3)	863
	IF(NT.EQ.5) GO TO 348	864
	IF(NT.EQ.4) GO TO 346	865
	IF(NT.EQ.3) GO TO 344	866
	IF(NT.EQ.2) GO TO 342	867
	IF(NT.EQ.1) GO TO 340	868
3000	FORMAT(/,T10,'*****FLAG***** ERROR IN NTLOW OR NTUP*')	869
	WRITE(6,3000)	870
	RETURN	871
340	DO 341 N=1,5	872
341	LBLT(N)=LT1(N)	873
	GO TO 350	874
342	DO 343 N=1,5	875
343	LBLT(N)=LT2(N)	876
	GO TO 350	877
344	DO 345 N=1,5	878
345	LBLT(N)=LT3(N)	879
	GO TO 350	880
346	DO 347 N=1,5	881
347	LBLT(N)=LT4(N)	882
	GO TO 350	883
348	DO 349 N=1,5	884
349	LBLT(N)=LT5(N)	885
350	CALL GRAPHS(NPTS,XWAVEL,XPROFL,0,107,LBLT)	886
	CALL GRAPHS(NPTS,XWAVEL,XPROFL,1,107,LBP)	887
	CALL GRAPHS(NALPHA,X1,Y1,2,107,LSDP)	888
	CALL GRAPHS(NCONV,X2,Y2,3,107,LCP)	889
9999	CONTINUE	890
	RETURN	891
	END	892

Table D-2. Data card requirements for C337BROD

Type #	# Cards	Columns	Variable Name	Format	Remarks
1	1	1- 5	NSETS	I5	Number of data sets
2	1/set	1- 5	NRUNS	I5	Number of runs within data set
3	1/run	1-60 61-68	TITLE HLINE	15A4 2A4	Experiment label Name of hydrogen line
4	1/run	1- 5 6-10	ILINE NRAD	I5 I5	Line identification number Number of positions for electron density calculations
5	NRAD /run	1-10 11-20 21-30	RAD TRAD HALF	F10.0 F10.0 F10.0	Radial position array Corresponding radial temperature array Corresponding radial half-width array

IT10,15A4,/,T10,2A4,2X,F7.2)	51
K=0	52
DC 140 I=1,45,5	53
K=K+1	54
NUP=I+4	55
L=0	56
DC 140 J=I,NUP	57
L=L+1	58
140 ALFAD(K,L)=ALFA(J)	59
WRITE(6,2000) (TEMP(I),I=1,5)	60
2000 FORMAT(/,T25,'HALF-WIDTH DATA',/,T15,'ELECTRON DENS',T30,5(F15.0)	61
1)	62
DO 145 I=1,9	63
2001 FORMAT(T15,E11.4,T33,5(3X,E11.4))	64
145 WRITE(6,2001) DENS(I),(ALFAD(I,J),J=1,5)	65
DO 200 I=1,NRAD	66
150 FORMAT(3F10.0)	67
READ(5,150) RAD(I),TRAD(I),HALF(I)	68
DO 160 J=1,9	69
DO 155 K=1,5	70
XINTRP(K)=ALOG10(TEMP(K))	71
155 YINTRP(K)=ALFAD(J,K)	72
X(J)=ALOG10(DENS(J))	73
POLYN=0.00	74
XXX=ALOG10(TRAD(I))	75
CALL PLLYNN(XINTRP,YINTRP,POLYN,XXX,5,3)	76
Y(J)=POLYN	77
160 CONTINUE	78
ICOUNT=0	79
XXDENS=14.0	80
170 POLYN=0.00	81
ICOUNT=ICOUNT+1	82
CALL PLLYNN(X,Y,POLYN,XXDENS,9,2)	83
XXALFA=POLYN	84
CALDEN=7.9568E+12*((HALF(I)/XXALFA)**1.5)	85
CALDEN=ALOG10(CALDEN)	86
TEST=ABS(CALDEN-XXDENS)	87
IF(TEST.LE.0.00005) GO TO 180	88
IF(ICOUNT.GT.50) GO TO 190	89
XXDENS=CALDEN	90
GC TO 170	91
180 EDENS(I)=10.0**CALDEN	92
ALPHA(I)=XXALFA	93
GC TO 200	94
190 CALDEN=10.0**CALDEN	95
WRITE(6,195) RAD(I),TRAD(I),HALF(I),CALDEN,XXALFA	96
195 FORMAT(/,T15,'*****FLAG***** ELECTRON DENSITY ITERATION FAILED TO	97
ICCNVERGE WITHIN 50 ITERATIONS FOR:',/,T15,'RADIUS= ',E11.4,2X,'TEM	98
PERATURE= ',E11.4,2X,'FULL WIDTH HALF MAX INTENS= ',E11.4,/,T15,'L	99
AST CALCULATED DENSITY= ',E11.4,2X,'LAST INTERPOLATED REDUCED HALF	100

	4 WIDTH= ',E11.4)	101
	EDENS(I)=0.00	102
	ALPHA(I)=0.00	103
200	CONTINUE	104
	WRITE(6,1001)	105
1001	FORMAT(/////,T2,'RADIUS',T15,'TEMP (K)',T30,'FWHMI',T45,'ELEC DENS	106
	1',T60,'REDUCED HALF-WIDTH')	107
	DO 300 N=1,NRAD	108
1002	FORMAT(T2,E12.5,T15,E12.5,T28,4(3X,E12.5))	109
300	WRITE(6,1002) RAD(N),TRAD(N),HALF(N),EDENS(N),ALPHA(N)	110
9999	CONTINUE	111
	STOP	112
	END	113
	SUBROUTINE PLLYNN(X,Y,POLYN,XXX,NUMX,NPOLY)	114
	DIMENSION X(100),Y(100)	115
C		116
C	N POINT POLYNOMIAL INTERPOLATING SUBROUTINE	117
C		118
C	TC INTERPOLATE A VALUE FOR XXX THE NPOLY NEAREST KNOWN PCINTS ARE	119
C	SELECTED AND AN INTERPOLATING POLYNOMIAL OF DEGREE NPOLY-1 IS	120
C	FITTED TO THESE POINTS	121
C	X AND Y ARE THE ARRAYS OF NUMX KNOWN POINTS ON THE CURVE	122
C	THE RESULT IS POLYN	123
C		124
	101 POLYN=0.0	125
	NM=(NPOLY+1)/2	126
	NM1=NM+1	127
	NUP=NUMX+NM1-NPOLY	128
	DO 102 J=NM1,NUP	129
	IF(XXX.LE.X(J)) GO TO 104	130
102	CONTINUE	131
	J=NUP	132
104	L=J-NM	133
	LLL=L+NPOLY-1	134
	DO 106 K=L,LLL	135
	TERM=1.0	136
	DO 105 M=L,LLL	137
	IF(K.EQ.M) GO TO 105	138
	TERM=TERM*(XXX-X(M))/(X(K)-X(M))	139
105	CONTINUE	140
	TERM=Y(K)*TERM	141
106	POLYN=POLYN+TERM	142
	RETURN	143
	END	144